UNIVERSITY OF SOUTHAMPTON

UNCOVERING FEATURES OF CHEMICAL REACTION NETWORKS IN COMPLEX SYSTEMS

by

Duncan J. Parker

A thesis submitted for the degree of
Doctor of Philosophy

in the
Faculty of Natural and Environmental Sciences
Chemistry

April 2018

Supervisor: Professor George S. Attard

Word count ≈ 24530 words

UNIVERSITY OF SOUTHAMPTON

ABSTRACT

FACULTY OF NATURAL AND ENVIRONMENTAL SCIENCES
Chemistry

Doctor of Philosophy

UNCOVERING FEATURES OF CHEMICAL REACTION NETWORKS IN COMPLEX SYSTEMS

by Duncan J. Parker

This thesis introduces a comprehensive atlas of behaviour in the iron-catalysed Belousov-Zhabotinsky reaction across a wide parameter space, under both stirred and unstirred conditions, encompassing variations in the concentrations of sulfuric acid, malonic acid and sodium bromate. All stirred reactions were monitored by UV-vis spectroscopy enabling the definition of concentration-dependent transitions in behaviour including those to chaotic oscillation.

A programme was generated to quantify spirals observed in the unstirred reaction. This expanded on the work of Müller et al. by increasing the length of time that such spirals had been monitored. There was good agreement between their experimental results and those set out in this thesis, which shows the transition from normal spiral wave behaviour to a final steady state. The work on spiral waves also includes the first use of a statistical image-based method for identifying changes in chemical wave behaviour with time. Attempts were made at producing a model for the iron-catalysed Belousov-Zhabotinsky reaction using a swarm intelligence algorithm having identified key reactions involved in modifying the reaction behaviour based upon the Marburg-Budapest-Missoula model. A further comparison between this model for the cerium-catalysed reaction and the chemical component of the Kyoto Encyclopaedia of Genes and Genomes database demonstrated that study of such small scale systems is applicable to a larger scale biochemical network.

215 words

Contents

List of Figures

List of Tables

List of Algorithms

Declaration of Authorship

I, Duncan J. Parker , declare that the thesis entitled *UNCOVERING FEATURES OF CHEMICAL REACTION NETWORKS IN COMPLEX SYSTEMS* and the work presented in the thesis are both my own, and have been generated by me as the result of my own original research. I confirm that:

- this work was done wholly or mainly while in candidature for a research degree at this University;
- where any part of this thesis has previously been submitted for a degree or any other qualification at this University or any other institution, this has been clearly stated;
- where I have consulted the published work of others, this is always clearly attributed;
- where I have quoted from the work of others, the source is always given. With the exception of such quotations, this thesis is entirely my own work;
- I have acknowledged all main sources of help;
- where the thesis is based on work done by myself jointly with others, I have made clear exactly what was done by others and what I have contributed myself;
- none of this work has been published before submission

Signed:.....

Date:.....

Acknowledgements

First and foremost I would like to thank George Attard for being a great supervisor and friend throughout my time in Southampton for pushing me mentally and physically in everything whether it was academic or not. Clearly without him this would not have been possible. Also the Attard Group (plus former members) has always been a treat to work alongside with thanks to Jon Hunter, Marcus Dymond, Jamie Burrell, Ric Gillams, Rea Kapetanou, Alex Hartke, Jonny Watson, and a specific appreciation for the efforts of James Pugh and Ruben Green and Jessica Gusthart (also a great neighbour!) in undertaking their final year projects with us and contributing to the work that this thesis encompasses.

Besides the group I would like to thank my advisor Klaus-Peter Zauner, Dr Mauritz de Planque and their students for fascinating discussions regarding the more unconventional aspects of this research. Furthermore, I would like to acknowledge the support staff within Chemistry and around the University including the use of the IRIDIS High Performance Computing Facility, and associated support.

Thanks should be extended to the SSE cricket team and the one season of near-glory that we experienced. Indeed the whole of Levels 6 and 7, despite appearances have made the PhD far more bearable. I also thank my neighbours: Rich, Matt, Jess, Adam and Ellie for always being around and offering constant entertainment and food, and Ed for not being the worst housemate ever. A final special mention should go to Paul and Joe, the physics double act who got me involved in magic and the foundation of Bright Club, without whom I would probably have done far less but written far more.

And finally the rest of my friends and most importantly my family, who might not necessarily understand what I do but understand what it means. Thank you.

Abbreviations & Nomenclature

Abbreviations

Na-AOT	Dioctyl sulfosuccinate sodium salt
a.u.	Arbitrary units
BL	Bray-Liebhafsky
BR	Briggs-Raucher
BrEETRA	Bromoethenetricarboxylic acid
BrMA	Bromomalonic acid
BrMA	Bromotartronic acid
BZ	Belousov-Zhabotinsky
CHAPS	3-[(3-cholamidopropyl)dimethylammonio]-1- propanesulfonate
CHD	Cyclohexadione
CL	Chung-Lu
CMC	Critical micelle concentration
CSTR	Closed stirred tank reactor
CTAB	Cetyl trimethylammonium bromide
DFT	Discrete Fourier transform
DNA	Deoxyribose nucleic acid
ECS	Electronic and Computer Science
EEHTRA	Ethenehydroxytricarboxylic acid
EETA	Ethenetetracarboxylic acid
ER	Erdoös-Renyi

FFT	Fast Fourier transform
FKN	Field-Körös-Noyes
FT	Fourier transform
GTF	Györgyi-Turányi-Field
GWO	Grey wolf optimiser
HPLC	High performance liquid chromatography
HRP	Horseradish peroxidase
IP	Induction period
KEGG	Kyoto Encyclopedia of Genes and Genomes
MA	Malonic acid
MAMA	Malonyl malonate
MBM	Marburg-Budapest-Missoula
MBO	Minimal bromate oscillator
MOA	Mesoxalic acid
NAD+ / NADH	Nicotinamide adenine dinucleotide
OA	Oxalic acid
ODE	Ordinary differential equation
PDMS	Poly(dimethylsiloxane)
pNIPAAM	Poly(*N*-isopropylacrylamide)
RDS	Reduced-diffusion systems
SDS	Sodium dodecyl sulfate
SI	Swarm intelligence
SRP	Subgraph ratio profile
TA	Tartronic acid
TM	Transition metal
TX-100	Triton X-100
UV	Ultraviolet

Nomenclature

a	Spiral turn control parameter
A	Absorbance
b	Spiral pitch control parameter
χ	Concentration parameter for sulfuric acid and sodium bromate
C_s	Salt concentration
$\oslash$	Diameter
D	Diffusion coefficient(s)
Δ	Sampling time
E_a	Activation energy
ε	Molar absorption coefficient
η	Chirp decay constant
$F_s(\nu)$	Sampled Fourier transform
f	Oscillation frequency (in reciprocal seconds)
f_i	Initial chirp frequency (in reciprocal seconds)
f_Ω	Final chirp frequency (in reciprocal seconds)
f_0	Fundamental frequency
Γ	Image entropy-uniformity ratio
[G]	Gelatin w/v
$\Delta\ G$	Gibbs' free energy
I	Ionic strength of solution
I_p	Peak-to-peak intensity
k_B	Boltzmann's constant
K_{eq}	Equilibrium constant
k	Rate constant
k_s	Salting-out coefficient
λ	Wavelength of maximum absorption

Λ	Spiral pitch
l_{ij}	Edge connecting nodes i and j
l	Path length (in centimetres)
L	Average "shortest path" length
M	Image grey levels
N	Number of data points
n	Degree of connectivity
ν	Sampling frequency
N_{nodes}	Number of nodes
ϕ	Phase of sine wave
p_m	Probability of a grey level being populated
ψ	State variable set
R	Ideal gas constant
r	Spiral radius
$\hat{\rho}_o$	Erdem's correlation coefficient
T	Temperature (in Kelvin)
t_p	Oscillation period (in seconds)
θ	Spiral angle
t	Time (in seconds or minutes)
t_Ω	Length of chirp frequency sweep (in seconds)
w/v	Weight-by-volume
z	Ionic charge

Chapter 1

Introduction

The Belousov-Zhabotinsky (BZ) reactions are amongst the most commonly studied examples of non-linear chemical dynamics.[1–3] BZ-type reactions give rise to oscillations in the concentration of reactive chemical species through the metal catalysed oxidation of an organic substrate by acidified bromate.[3] There is a wealth of information regarding the features of such systems including the effects of different catalysts, substrates and conditions, yet with such a wide variety of behaviour there is a lack of unity between theories for the mechanisms of each system. Many choose to either reduce the systems to mathematical models or focus on the core of the overall system.[4]

There is general agreement that for a system to oscillate it must be far from thermodynamic equilibrium, contain at least one autocatalytic reaction step, and that this should be coupled to the rest of the reaction network through a feedback loop.[5,6] Mathematical considerations state that for oscillations to occur there has to be a series of attractors, inhibitors and feedback loops.[7] However, there is still a gap in our understanding of the chemistry of complex systems and consequently their emergence in nature.

1.1 Aims of the Work

In summary, the aims of this work were:

- Document the behaviour of the iron-catalysed BZ reaction across a wide range of concentrations under both a stirred and unstirred regime.
- Develop methods by which the progress of an unstirred reaction can be monitored with time.
- Quantify the behaviours observed in both regimes to classify the reaction and develop an atlas of the reaction.
- Explore the effect of macromolecular crowding on the reaction dynamics as well as modification of the reaction medium by use of surfactants or alternative organic substrates.
- Use network theory to deconstruct previous models of the reaction and explain the importance of certain chemical species within the mechanism.
- Compare the chemical reaction network present in a synthetic oscillator with those which appear naturally in biochemical systems.
- Correlate the simulated datasets to observed data for the iron(II)-catalysed reaction system.

1.2 The Structure of the Thesis

This thesis presents a comprehensive survey of initial conditions for the iron-catalysed BZ reaction in both a stirred and unstirred reactor that investigates the nature of the reaction and offers a further analysis from a network-based perspective with the ultimate end goal of constructing a generalised mechanism of the Belousov-Zhabotinsky reaction independent of catalyst.

As such this work is thus arranged in two parts: Part 1 reports the development of an atlas of the iron-catalysed Belousov-Zhabotinsky reaction under different conditions in which ***Chapter 2*** reports results from UV-Vis spectroscopy measurements monitoring the progress of the reaction under differing initial reagent conditions in a stirred batch reactor to produce a map of reaction dynamics, along with the approaches to signal analysis.
Chapter 3 is a study of the unstirred reaction system, again creating an atlas of behaviours with an emphasis on the development of spiral patterns. In all cases the reaction occurs under batch conditions, thereby enabling the aging of the solution to be observed.

Part 1 concludes with an investigation of alternative reaction media through the addition of surfactants as well as the use of gelling agents to mimic the crowded nature of the intracellular matrix.

Following from the laboratory studies, the second part of the thesis explores the networks of reactions that underpins the dynamics of the BZ reaction. ***Chapter 5*** is concerned with analysis of the cerium-catalysed network in relation to the iron(II)-catalysed system with simulations employed to understand the differences between the two, leading into a detailed analysis of the cerium-catalysed network in ***Chapter 6***, which compares the characteristics of this chemical oscillator with those of natural systems by monitoring the presence of network features and the distribution of nodes.

1.3 Review of the Literature

Since the discovery of the BZ reaction and the work of Prigogine in the 1970s and 80s there has been an explosion in the number of publications regarding Belousov-Zhabotinsky systems. Within these there exists a range of ideas, applications and analyses of the Belousov-Zhabotinsky reaction. As such, an exhaustive review of the literature is almost impossible and in many respects goes beyond the boundaries of this thesis. The following review of the literature presents a history of oscillating chemical reactions as well as the development of models of the BZ reaction. Furthermore, it highlights the biological relevance of such systems and therefore the motivation for their study in the current context.

1.4 Origins of Research into Oscillating Reactions

Oscillations have been routinely observed throughout the history of chemical science, for example the oxidation of phosphorus, the periodic dissolution of iron wire in nitric acid and the so-called "mercury beating heart".[8] This work stretches back as far as 1828 with Gustav Fechner's discovery of an oscillating current in an electrochemical cell.[6,9] However, these were typically heterogeneous processes.

Although it can be argued that the first observation of an oscillating system was by Fechner this is not truly a chemical system. Indeed, the observation by Raphael Liesegang in 1898 of alternating precipitation zones from diffusing and reacting pairs of inorganic salts (now commonly referred to as Liesegang rings or patterns) are probably the first true example of oscillations in a heterogeneous chemical medium. This was swiftly followed by the events mentioned above with Ostwald's periodic dissolution of chromium in acid being reported in 1899 and the Bredig and Weinmyar's dissolution of iron wire in nitric acid in 1903.[10,11]

Prior to the awareness of homogeneous oscillators there were models that purported some understanding of the phenomena. The cyclic interconversion of isomers had been discussed by Herniak and Lotka had already published work on the role of irreversible autocatalytic processes within oscillating chemical reactions.[8]

It was believed that liquid state systems could not exhibit such behaviour despite the assertion that there is fundamentally no difference between homogeneous and heterogeneous systems when it comes to behaviour; indeed the Lotka model of autocatalytic chemical processes had been proposed in 1909 yet was widely disregarded.[12,13] This was later followed up in 1920 by the proposal of another chemical system with two autocatalytic steps leading to the presence of undamped oscillations.

$$A + a \rightarrow 2a; \qquad a + b \rightarrow 2b; \qquad b \rightarrow . \tag{1.1}$$

However in 1921, the same year as Rayleigh demonstrated the periodic glow of phosphorus, the first genuine oscillatory reaction in a homogeneous chemical medium was discovered by Bray. This is the catalytic decomposition of hydrogen peroxide to oxygen and water by iodate and is now known as the Bray-Liebhafsky (BL) reaction, yet once again the notion of homogeneous oscillating chemical systems was largely ignored by the scientific community and would continue to be so until the 1960s despite mounting experimental and theoretical evidence.

1.4.1 Discovery of the Belousov-Zhabotinsky Reaction

In 1951, while searching for an *in vitro* model of the Krebs cycle Boris Belousov discovered experimentally that oscillations could indeed be produced in the liquid state, the original reaction mixture is shown in Table 1.1.

Species	**Concentration / M**
Cerium(IV) sulfate ($CeSO_4$)	0.04
Potassium bromate ($KBrO_3$)	0.10
Sulfuric acid (H_2SO_4)	0.80*
Citric acid ($C_6H_8O_7$)	0.87

TABLE 1.1: Boris Belousov's original reaction mixture. This recipe lead to the discovery of liquid state oscillations in the early 1960s (* concentration of sulfuric acid is approximate).[3]

Theories dependent on such systems also kept arising, including that by Alan Turing, in his work *The Chemical Basis of Morphogenesis*, which suggested oscillations in

reaction-diffusion systems could yield non-uniform patterns and drive embryonic development.[14] Further theoretical evidence came when Ilya Prigogine proved that oscillations could exist in far-from-equilibrium systems, which is a feature of the Belousov-Zhabotinsky, Bray-Liebhafsky and Briggs-Raucher (BR) oscillating systems.[15] Consensus finally shifted in 1962 when Anatol Zhabotinsky repeated the experiments of Belousov employing malonic acid as the organic substrate in place of citric acid so as to improve the contrast of the system, thereby proving the oscillations were genuine and a result of oscillations in [Ce(IV)] rather than the development of free bromine as had been reported by Belousov.[16]

1.5 Developing Models of the Belousov-Zhabotinsky Reaction

Oscillations arise in systems that are far from equilibrium and can easily pass between two regimes, in this case the reaction of the organic substrate and the autocatalytic bromic acid reaction.[8] Use of a further catalytic species (often a transition metal complex) allows for these oscillations to be followed through changes in colour or electrochemical potential. The chemical nature of the transition metal catalyst leads to an array of different oscillatory behaviours.[17,18] This thesis focuses predominantly on the Ce(III/IV) and Fe(II/III) systems although a wide range of catalysts have been used in the literature; discussion of which can be found later in Section 1.5.1. Alongside many others, an evident difference between these catalysts is easily seen in a stirred reactor: the cerium(IV)-catalysed reactions exhibit a long induction period prior to periodic oscillations whereas the iron(II)-catalysed systems yields oscillations almost instantaneously.[19] Various oscillatory phenomena are witnessed in both systems with numerous pattern and wave structures appearing in an unstirred reactor as well as bursting phenomena, mixed-mode oscillations, quasi-periodic oscillations, transient chaos and even long timescale oscillation rebirth in both stirred and unstirred systems.[20–24] Consequently to create a model capable of reproducing all of these behaviours is not without challenges.

1.5.1 Varying the Catalyst in Belousov-Zhabotinsky Reactions

Since its inception a wide variety of recipes for the Belousov-Zhabotinsky reaction have been used worldwide.[25] These systems are usually catalysed by transition metal ions with variations routinely utilising Ce(III/IV), Fe(II/III), Mn(II/III) and Ru(II/III) complexes. More rarely, researchers have used complexes of Co, Cu, Cr, Ag, Ni, and Os; each of these systems has its own distinct behaviours with the catalyst affecting frequency of oscillations and induction periods most dramatically, therefore making a generalised model harder to obtain.[3,17,26–30] The use of Co(II/III) has previously been

disputed due to its high standard potential of 1.8 V making BrO_3^- incapable of oxidising Co(II).[19,31] Catalysts for BZ reactions are generally classified as being either high or low reduction potential couples with each type offering different chemical mechanisms for the oxidation of the organic substrate.[32,33] However, it has been suggested as a general rule that ions of variable valence with a single electron transition and a standard redox potential in the range 0.9 - 1.6 V can act as catalysts in the BZ reaction.[19] There are 20 such ions listed in the 96th edition of the CRC Handbook of Chemistry and Physics, suggesting a broad range of potential catalysts for the system that are as yet unexplored, *e.g.* V(IV/V).[34] Although these conditions are necessary for the reaction they are not the only criteria.[35] While the standard potential of the Co(II/III) pair is deemed too high, the converse is true for an unbound Fe(III) ion, which with a standard potential of 0.77 V (under acidic conditions) is unable to directly oxidise the organic substrate; ferroin however has a standard potential of 1.06 V.[19,36,37]

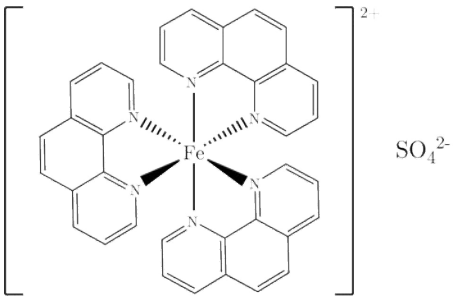

FIGURE 1.1: Structure of the ferroin, [Fe(*o*-phen)$_3$]SO_4, complex with sulfate counter-ion.

Complexes of ruthenium have similar redox potentials to those observed for complexed iron ions ($\sim$ 1.0 V).[19] Ferroin, [Fe(*o*-phen)$_3$]SO_4, was used as the catalyst for the reaction throughout this work and its structure can be seen in Figure 1.1, *o*-phen is the co-ordinated 1,10-phenanthroline ligand. As the catalyst oscillates between its oxidised and reduced states a blue-red colour change is observed enabling the reaction to be followed spectrophotometrically.

1.5.2 Varying the Substrate in Belousov-Zhabotinsky Reactions

The established recipe for the BZ reaction utilises malonic acid (MA) as the organic substrate, different to the original use of citric acid in Belousov's experiments, since it enables a greater contrast in the study of chemical waves. There are a wealth of oxidisable organic substrates which have potential for use in these reactions. Indeed there has been interest in exploring BZ-type reactions using a whole host of different substrates including bromomalonic acid,[38] 1,4-cyclohexadione,[39–43] oxalic acid[44,45], tartronic acid, mesoxalic acid,[45] resorcinol,[17] xylose[46] and aldosugars[47,48] among others.

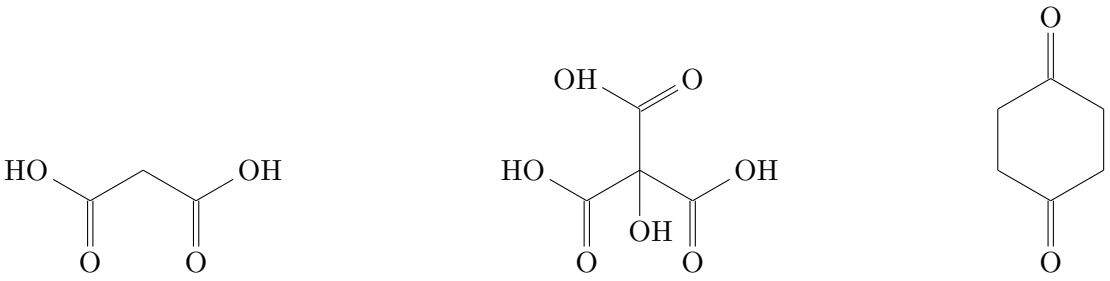

FIGURE 1.2: Common organic substrates in the Belousov-Zhabotinsky reaction include malonic Acid (left), citric acid (centre) and 1,4-cyclohexadione (right).

Bromomalonic acid is the most similar to malonic acid and it is known to lack the induction period seen in the classic cerium-catalysed reaction.

1.6 Anatol Zhabotinsky's Initial Experiments

In 1964 Anatol Zhabotinsky undertook the first experiments using malonic acid in place of citric acid to improve the optical contrast of the oscillations in the cerium(IV)-catalysed system.[16] Investigations searching for an inhibitory species identified Br^- as a key component of the feedback process since injections of Br^- at low concentrations suppressed oscillations and kept the catalyst in the reduced state; a point which has been well documented since.[3] This led to the first mechanistic model of the BZ reaction and followed the scheme set out in Figure 1.3. This shows the presence of two subsystems: (1) where brominated malonic acid derivatives produce Br^- and (2) the autocatalytic regime (bromous acid is the autocatalyst) producing Br_2.

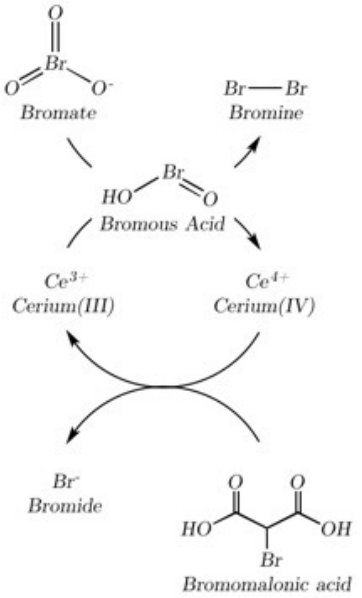

FIGURE 1.3: Anatol Zhabotinsky's original model of the reaction.

1.7 Field-Körös-Noyes (FKN) Mechanism and the Oregonator Model

Zhabotinsky's approach was an important step in the development of the model and was the best mechanism produced until 1972 when Field, Körös and Noyes created their model[4]. Where Zhabotinsky had proposed two subsystems the Field-Körös-Noyes model suggested three separate stages, these were: (1) bromination of malonic acid, (2) the oxidation of MA acid and (3) the oxidation of bromomalonic acid. This mechanism further probes the steps in the negative feedback loop, suggesting that the first step is the generation of Br^- by reaction of Ce(IV) with bromomalonic acid (BrMA). This mechanism also highlights bromous acid ($HBrO_2$) as the autocatalyst.

$$\begin{gathered}
BrO_3{}^- + 2\,Br^- + 3\,H^+ \longrightarrow 3\,HOBr \\
BrO_3{}^- + HBrO_2 + 3\,H^+ + 2\,Ce^{3+} \longrightarrow 2\,HBrO_2 + H_2O + 2\,Ce^{4+} \\
BrO_3{}^- + 5\,H^+ + 4\,Ce^{3+} \longrightarrow HOBr + 2\,H_2O + 4\,Ce^{4+} \\
10\,Ce^{4+} + MA + BrMA + 2\,H_2O + 2\,HOBr \longrightarrow 10\,Ce^{3+} + 3\,Br^- + 6\,CO_2 + 13\,H^+
\end{gathered} \tag{1.2}$$

As well as these conclusions the model also demonstrates there is a critical value for $[Br^-]$ as the reactions producing Br_2 and BrMA are incapable of proceeding simultaneously. Since the reaction of $HBrO_2$ and Br_2 is very rapid there can never be a significant quantity of both species simultaneously, in turn this reaction mechanism became known as "bromide controlled".[3] Equation 1.3 defines the critical $[Br^-]$, above this value the $HBrO_2$ is quickly reduced by Br^- while below this value it is possible for $[HBrO_2]$ to increase exponentially[4]. In Equation 1.3 the k_5 corresponds to the rate constant for the reaction of $HBrO_2$ with acidified $BrO_3{}^-$ while k_2 is the rate constant for the reaction of $HBrO_2$ with Br^-, see Equation 1.4 and Table 1.2.

$$[Br^-]_{crit} = \left(\frac{k_5}{k_2}\right)[BrO_3{}^-] \tag{1.3}$$

Where this is fundamentally a mechanistic approach it is obviously possible to express the system as a series of ordinary differential equations (ODEs). A simplified mathematical form of the mechanism was produced and called the Oregonator (Equation 1.4). These three equations are still the basis of many models today showing the utility of this approach and how well it represents the oscillations of the cerium(IV)-catalysed Belousov-Zhabotinsky reaction.[18,49,50]

$$\begin{aligned} \frac{\partial X}{\partial t} &= k_1 AY - k_2 XY + k_3 AX - 2k_4 X^2 \\ \frac{\partial Y}{\partial t} &= -k_1 AY - k_2 XY + \frac{1}{2} k_c f BZ \\ \frac{\partial Z}{\partial t} &= 2k_3 AX - k_c BZ \end{aligned} \tag{1.4}$$

Where X = $HBrO_2$, Y = Br^-, Z = Oxidised catalyst, A = $BrO_3{}^-$, B = Organic substrate, and P = Brominated species. f is a stoichiometric factor based on the initial concentration of bromate. These are in accordance with the Field-Korös-Noyes mechanism upon which the Oregonator model is based. Table 1.2 lists the values for each of the rate constants in the model.

Rate constant	**Value**
k_1	2 $mol^{-3}dm^9s^{-1}$
k_2	10^6 $mol^{-2}dm^6s^{-1}$
k_3	10 $mol^{-2}dm^6s^{-1}$
k_4	2000 $mol^{-1}dm^3s^{-1}$
k_5 (k_c)	1 $mol^{-1}dm^3s^{-1}$

TABLE 1.2: Values for the rate constants in the Oregonator model at 293.15 K.

1.7.1 Minimal bromate oscillator (MBO)

The Belousov-Zhabotinsky reactions are fundamentally the oxidation of an organic substrate by acidified bromate, however, it is possible to produce what is termed a minimal bromate oscillator wherein there is no organic substrate but oscillations are still present through the oxidation of cerium(III) ions by bromate.[51] Table 1.3 below details the simplified mechanism set out for this and it shall become clear that these steps remain at the core of the later mechanisms set out in the the following sections.[52]

1.8 Györgyi-Turányi-Field (GTF) Mechanism

The Györgyi-Turányi-Field (GTF) mechanism brought together all prior experimental and theoretical work on the cerium(IV)-catalysed BZ reaction.[50] This was originally proposed in 1990 but simplified in 1993 to yield a network of 42 reactions containing 22 different reactive species, which was further simplified to a three variable model akin to the Oregonator but with better agreement to experimental observations.[53] Work by

Reaction	k_1 **(Forward)**	k_{-1} **(Reverse)**
$BrO_3^- + Br^- + 2\,H^+ \rightleftharpoons HBrO_2 + HOBr$	2.1 $M^{-3}s^{-1}$	1 $\times 10^{-4}$ $M^{-1}s^{-1}$
$HBrO_2 + Br^- + H^+ \rightleftharpoons 2\,HOBr$	2 $\times 10^{9}$ $M^{-2}s^{-1}$	5 $\times 10^{-5}$ $M^{-1}s^{-1}$
$HOBr + Br^- + H^+ \rightleftharpoons Br_2 + H_2O$	8 $\times 10^{9}$ $M^{-2}s^{-1}$	110 s^{-1}
$BrO_3^- + HBrO_2 + H^+ \rightleftharpoons 2\,BrO_2^\bullet + H_2O$	1 $\times 10^{4}$ $M^{-2}s^{-1}$	2 $\times 10^{7}$ $M^{-1}s^{-1}$
$Ce^{3+} + BrO_2^\bullet + H^+ \rightleftharpoons Ce^{4+} + HBrO_2$	6.5 $\times 10^{5}$ $M^{-2}s^{-1}$	2.4 $\times 10^{7}$ $M^{-1}s^{-1}$
$Ce^{4+} + BrO_2^\bullet + H_2O \rightleftharpoons Ce^{3+} + BrO_3^- + 2\,H^+$	9.6 $M^{-1}s^{-1}$	1.3 $\times 10^{-4}$ $M^{-3}s^{-1}$
$2\,HBrO_2 \rightleftharpoons BrO_3^- + HOBr + H^+$	4 $\times 10^{7}$ $M^{-1}s^{-1}$	2.1 $\times 10^{-10}$ $M^{-2}s^{-1}$

TABLE 1.3: Simplified mechanism for the oxidation of Ce(III) by bromate. The minimal bromate oscillator is the basis of nearly all models of the BZ reaction.

Försterling and Noszticzius had identified a secondary negative feedback loop within the system caused by the presence of malonyl radicals and their reactions in what was termed the Radicalator model.[54,55] The GTF model re-examined this by suggesting that the organic free radicals actually disproportionate rather than undergoing recombination.

1.9 Marburg-Budapest-Missoula Model

Using HPLC analysis of full BZ systems a comprehensive set of reactions has been suggested for the cerium(IV)-catalysed system in what is termed the Marburg-Budapest-Missoula (MBM) model, the equations for which can be found in Appendix E.[50] This model contains both the original Oregonator and the Radicalator negative feedback loops and thus corroborates the theory of disproportionation. It is noted that the group highlighted key differences between the iron(II)-catalysed and cerium(IV)-catalysed systems most notably that products such as ethanetetracarboxylic acid (ETA) and malonyl malonate (MAMA) are not formed, suggesting that the malonic acid is not oxidised by ferroin.[56]

1.10 Models of the Iron-Catalysed Reaction

The literature concerning the BZ reaction has a vast array of models that accurately depict the oscillatory nature of the reaction, with the Oregonator model being the most commonly used. However this was first developed to understand the cerium(IV)-catalysed system and it has been known for over 30 years that the iron(II)-catalysed follows a different reaction pathway whose dynamics cannot be modelled in the same way.[56,57] Attempts have been made to predict other reactive species and reactions[18,38] as well as better understand the reaction network[58–60] and phenomena that arise within these systems.[20] Ultimately though, this limited knowledge of the mechanistic details of the ferroin based reaction creates a problem since in order to create an atlas of the reaction it is necessary to have a method that will enable prediction of the oscillatory behaviour under any conditions.

1.11 Features of the Unstirred Belousov-Zhabotinsky Reaction

All the models mentioned above predominantly refer to, or are based experimentally, on the stirred BZ system. The unstirred Belousov-Zhabotinsky reaction exhibits a far greater range of dynamic behaviours than the stirred system with reaction-diffusion mediated pattern formation and wave propagation. This leads to difficulties in marrying the stirred and unstirred systems together since the convective process of stirring has been removed. Increasing the depth of the reacting solution results in patterns transitioning from a chaotic appearance to ordered beyond a depth of 2 mm; potentially caused by the increased availability of surface O_2.[18] Identifying the presence of features that can give an understanding of the sensitivity to initial conditions, as well as those that are preserved from the stirred to unstirred systems, are integral to understanding the formation of complex networks all the way down to microscale (and crowded) systems. This is of specific interest to biological chemistry since biological systems are evidently unstirred and in crowded environments and so studies of the Belousov-Zhabotinsky reaction with reduced dimensionality provides an insight into how a complex chemical system (and as such its reaction network) develops with time.

1.12 Biological Relevance of the Belousov-Zhabotinsky reaction

As stated in Section 1.4.1, Belousov's initial aim was to create a model of the Krebs (or citric acid) cycle. The cycle is shown in Figure 1.4 and since then the BZ reaction

has been applied to numerous biological scenarios ranging from cardiac fibrilation to fungal growth and circadian clocks due to the development of complexity theory within the biological sciences.[61,62]

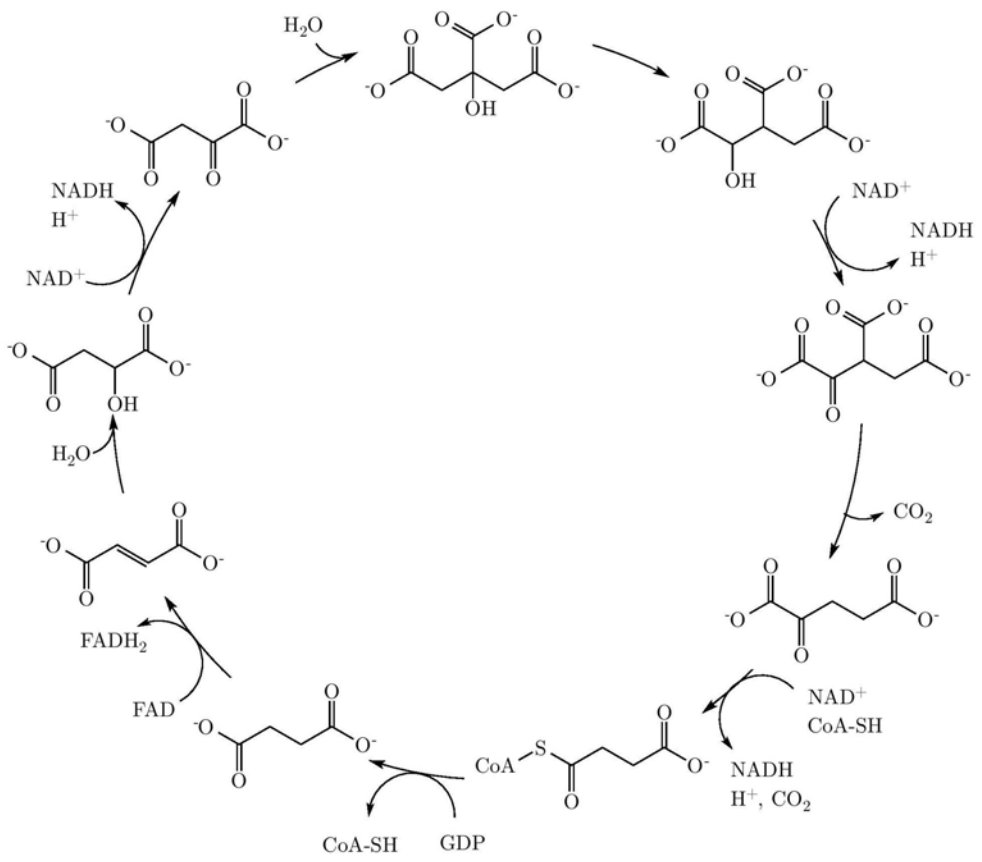

FIGURE 1.4: The Krebs cycle, also known as the citric acid cycle. Belousov was initially inspired to find an in vitro mimic of the cycle resulting in his discovery.

The Krebs cycle occurs in the mitochondria of eukaryotic cells and within the intracellular fluid of prokaryotes.[63,64] While non-linearity is something of the norm in chemistry, feedback loops are far less common and are a fundamental aspect of biological oscillators. Inhibitory feedback loops in combination with reaction rates that span orders of magnitude are routine in biochemical systems; this is akin to the early models of the BZ reaction.[7,65]

The observations made of the chemical medium and the biological phenomena are so closely related that it has been suggested that simply studying the Belousov-Zhabotinsky reaction can be as useful as studying the real world situation.[66] This has raised interesting questions about the extent to which the reaction can model biological processes since the physical behaviour and mathematical dynamics of the two chemical and biological match so well.[62]

1.12.1 Further Considerations of Biochemical Systems

Biochemical oscillators rely upon diffusion of chemical species through the highly crowded intracellular environment, a fact that is commonly disregarded in the field of molecular biology.[67] Since such complex cycles and networks can be produced there is an implication that either molecular crowding holds the necessary reactive species in place or there is an efficiency inherent within such networks enabling them to become ubiquitous in the natural world. Evolution of the Krebs cycle is believed to have occurred multiple times and therefore adds weight to the efficiency theory.[64,68,69]

1.13 Summary

If there is to be a greater understanding of the way in which complex reaction systems have formed in nature, a deeper study of how designed chemical oscillators and networks behave under a variety of initial conditions and environments. An atlas of the iron-catalysed BZ reaction in a stirred and unstirred reaction provides a reference point for further studies as well as a comparison for modified reaction media, including in gel-based systems. The subsequent half looks into the chemical networks observed in the reaction and how this relates to those seen in true biochemical systems, expanding the knowledge of how complex chemical and biochemical reaction networks form.

Developing an Atlas of the Iron-catalysed Belousov-Zhabotinsky Reaction

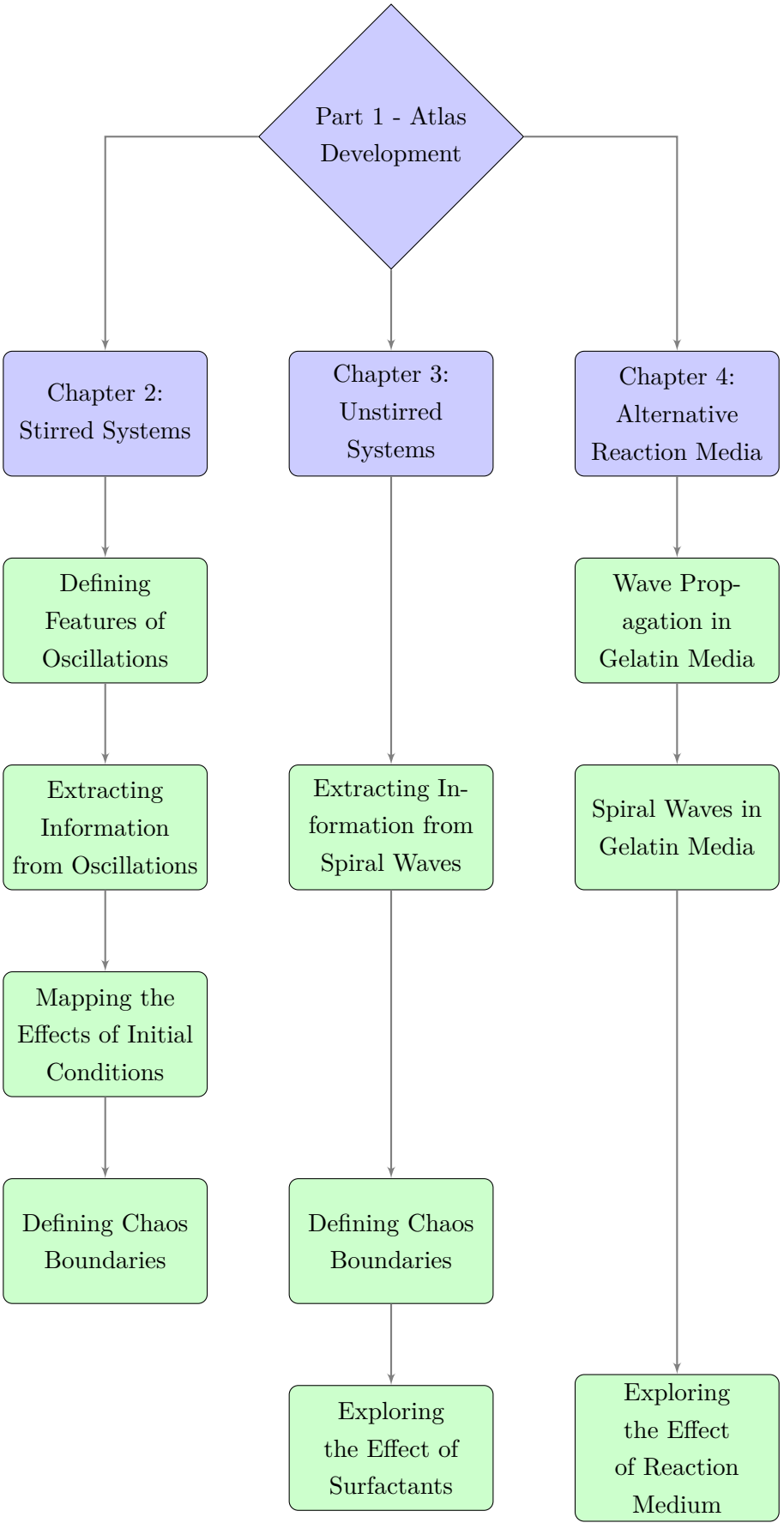
Part 1 - Atlas Development
Chapter 2: Stirred Systems
Chapter 3: Unstirred Systems
Chapter 4: Alternative Reaction Media
Defining Features of Oscillations
Extracting Information from Oscillations
Mapping the Effects of Initial Conditions
Defining Chaos Boundaries
Extracting Information from Spiral Waves
Defining Chaos Boundaries
Exploring the Effect of Surfactants
Wave Propagation in Gelatin Media
Spiral Waves in Gelatin Media
Exploring the Effect of Reaction Medium

Chapter 2

Mapping the Dynamics of the Stirred Belousov-Zhabotinsky Reaction

The effect of varying initial reagent conditions is explored through absorbance plots using UV-Vis spectroscopy. By fitting a logarithmic function to the average frequency as well as use of Fourier transforms an atlas of the stirred reaction dynamics at different initial conditions is created.

2.1 Introduction

Mapping dynamics of a complex reaction system with respect to the concentrations of initial reagents enables categorisation and prediction of behaviour. While there are a number of known recipes that will produce oscillations there is no single map of the dynamics of the stirred BZ reaction incorporating features such as the range over which oscillations occur, systematic changes in dynamic properties, and the emergence of atypical behaviour.[25]

Sensitivity to initial conditions is an intrinsic property of chaotic systems including the BZ reaction.[2] This leads to the appearance of a vast array of dynamical behaviours such as changes in oscillation frequency and amplitude with time as well as aperiodic oscillation and steps in amplitude; a wide range of other behaviours have also been reported for other chemical oscillators, such as the induction period reported for the cerium-catalysed reaction.[3,21,70–72]

2.2 Features of Chemical Oscillations in the Stirred Belousov-Zhabotinsky Reaction

This thesis sought to quantify the behaviours observed in a stirred batch regime to classify the reaction and develop an atlas of the reaction. That aim was achieved by recording BZ reactions via UV-vis spectroscopy, monitoring the reduction/oxidation of ferroin at $\lambda = 512$ nm. As the reactions progress the absorbance of the solution at 512 nm varies as expected from the Beer-Lambert law for complex mixtures (Equation 2.1).

$$A_{512\text{nm},t} = l \cdot \sum_{n=1}^{N} \varepsilon_n c_{n,t} \tag{2.1}$$

where $A_{512\text{nm},t}$ is the absorbance of the solution at the wavelength of maximum absorption for ferroin at any time, t; l is the path length of the beam (in cm); $c_{n,t}$ is the concentration of a species, n, in solution with a molar extinction coefficient of ε_n. By monitoring the reaction by these means it was possible to generate a library of experimental traces such as in Figure 2.1. Further details on the experimental procedure can be found in Section 2.7.

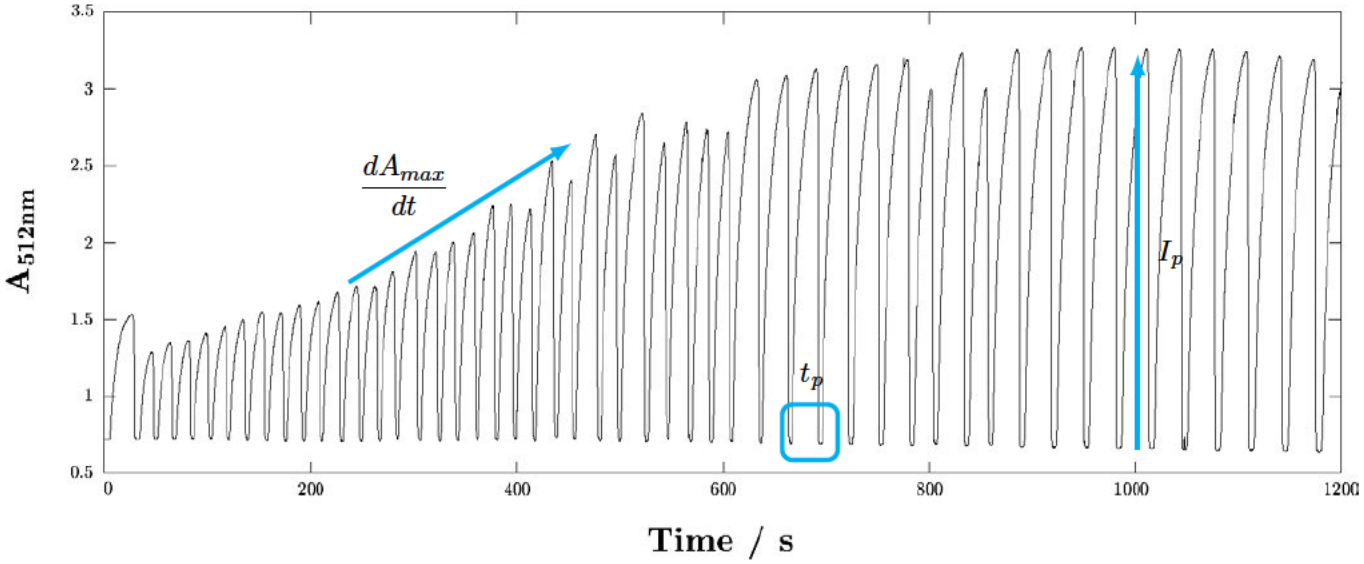

FIGURE 2.1: A typical time series absorbance plot for the iron(II)-catalysed BZ reaction illustrating the oscillation period, t_p, the peak-to-peak intensity, I_p, and the change in maximal absorbance, dA_{max}/dt. The absorbance was measured at $\lambda = 512$ nm for 1200 s with $[H_2SO_4] = 0.25$ M, $[BrO_3^-] = 0.10$ M, [MA] = 0.05 M and [ferroin] = 2.00 mM.

While it is possible to produce a matrix for the Beer-Lambert law to solve for the precise concentration of one species, the large (and to an extent unknown) number

of chemical intermediates present in the reaction system make this prohibitive, consequently the absolute absorbance values are of limited use. As an alternative, the following three criteria, highlighted in Figure 2.1, were determined to be the most effective for monitoring the progress of the reaction:

1. Peak intensity (I_p) - the peak to peak amplitude of the oscillation.
2. Change in amplitude with respect to time, $\frac{dA_{max}}{dt}$ - the rate at which the concentration of absorbing species varies with time.
3. Oscillation period, t_p, and thereby oscillation frequency.

Since the reactions all contain the same initial starting reagents, albeit in different concentrations, then these criteria each confer an individual signature for those initial conditions. In order to quantify these metrics the sharp minima in absorbance were identified programmatically with a high tolerance to noise.

Having identified oscillations by this method the amplitude was calculated as the peak-to-peak amplitude, *i.e.* the change between a minimum and the next maximum, labelled I_p in Figure 2.1. This metric avoided the need to attribute a baseline to any of the datasets and enabled direct comparison of experiments - while a baseline would be beneficial in analysis the changing concentration meant that the position of the minima were not always constant; a lower absorbance indicates a lower concentration of the reduced iron species and represents the furthest extent of the reaction cycle - the complex dynamics and competitive reactions within the system mean that this point is not always the same.

2.2.1 Frequency of Oscillations

Oscillation frequency in the stirred BZ reaction varies with time. Extracting the time of each minimum in the oscillation it was possible to calculate the time period, t_p, between each oscillation, giving the frequency as $\frac{1}{t_p}$ and therefore capable of being monitored with time. This change in frequency was modelled effectively as a chirp signal (Section 2.4.1), yet it was also possible to use the Fourier transform (Section 2.4.2) to calculate the fundamental frequencies that make up the oscillations in each dataset.

2.2.2 Chaotic Oscillations

While the above metrics are of utility in discussing typical periodic oscillations they are of equal benefit when exploring the chaotic and quasiperiodic oscillations observed in the BZ reactions, an example of which is shown in Figure 2.2. Such oscillations are characterisable by sudden changes in frequency and amplitude.

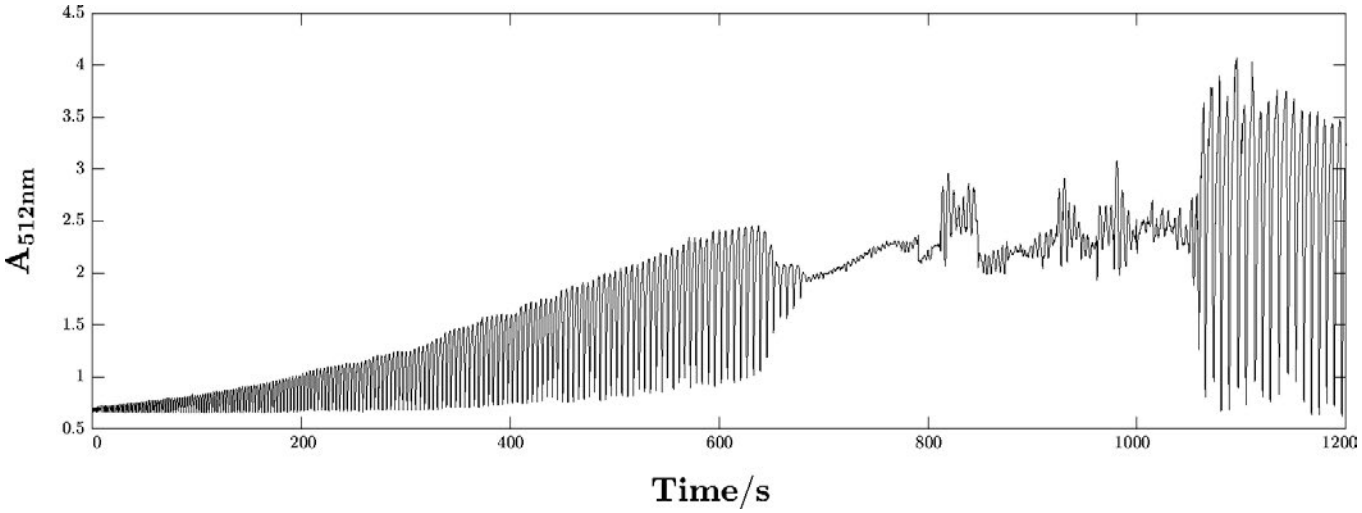

FIGURE 2.2: Presence of chaotic and quasiperiodic behaviour in a stirred BZ reaction observed by UV-vis spectroscopy at $\lambda = 512$ nm. Under certain initial conditions the oscillating system shifts to show chaotic or quasiperiodic oscillations, in this case the initial conditions were $[H_2SO_4] = 0.50$ M, $[BrO_3^-] = 0.50$ M, [MA] $= 0.25$ M and [ferroin] $= 2.00$ mM.

2.3 Visual Representation of Data

Work in this section was completed using data gathered by Jessica Gusthart.

The dynamics of Belousov-Zhabotinsky reactions are predominantly reliant on the concentration of the bromate ion, sulfuric acid and ferroin, however the latter was excluded from analysis since this was kept constant in all experiments. There was a weak dependence on the malonic acid concentration, therefore the three varying concentrations were visualised alongside any number of the metrics outlined previously. The primary visualisation method for reporting the results in this thesis is the use of ternary maps, although a two-dimensional representation was also applied to the definition of dynamical boundaries and later in unstirred systems.

2.3.1 Ternary Maps

A ternary diagram plots three variables that sum to a constant, in this case the sum of the initial molar percentages for the bromate ion, sulfuric acid and malonic acid on an equilateral triangle as per the method described by Biosa *et al.*[22]. Consequently, the three values sum to 100% with the molar percentage for each species being equal to 100% at the vertices of the triangle and 0% at an adjoining vertex. By plotting various compositions onto a two dimensional graph makes this a convenient approach to plotting higher dimensional data.

The points on the grid are calculated from Cartesian coordinates as follows: if a = 100% is placed at (x, y) = (0,0) and b = 100% at (1,0) then c = 100% is found at $\left(\frac{1}{2}, \frac{\sqrt{3}}{2}\right)$. Any point can then be calculated as being at $\left(\frac{2b+c}{2(a+b+c)}, \frac{\sqrt{3}c}{2(a+b+c)}\right)$.

Ternary maps were created by adapting freely available code (`https://uk.mathworks.com/matlabcentral/fileexchange/2299-alchemyst-ternplot`) and proved highly effective in demonstrating the effect of each initial reagent on the dynamic behaviours. The adapted code is included in Appendix A.1

2.4 Frequency

Having monitored the reaction by UV-vis spectroscopy the oscillations observed were quantifiable by their frequency. However, there are a couple of ways in which to analyse these frequencies. Firstly, the oscillations could be simplified and modelled as a chirp sequence. Secondly, a more representative atlas could be generated by extracting the frequency of oscillations from the time domain data through the use of Fourier transforms.

2.4.1 Oscillations as a Chirp Signal

As the reaction system progresses towards a steady state under batch conditions there is an accompanying decrease in oscillation frequency, $f(t)$, where $f(t)$ is defined relative to the oscillation period at each time point, t, according to Equation 2.2.

$$f(t) = \frac{1}{t_p} \tag{2.2}$$

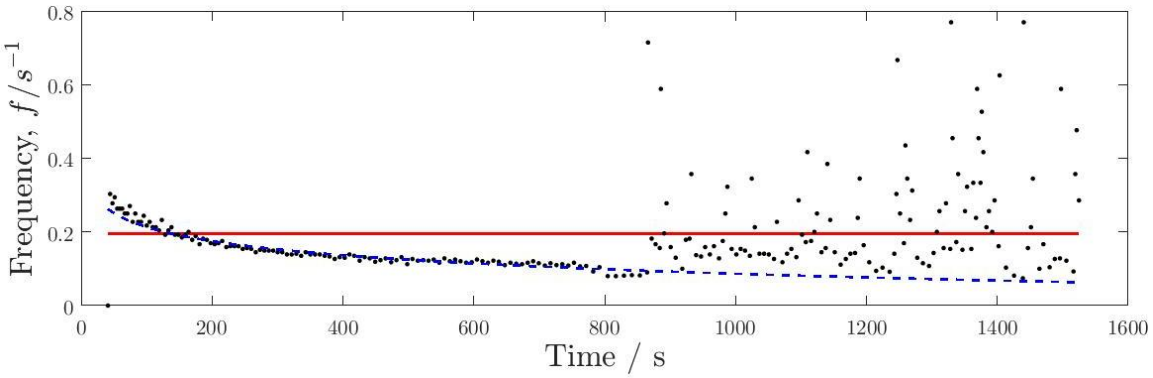

FIGURE 2.3: Fitting a simple logarithmic equation of the form $-a \ln x + b$ to a chaotic dataset. The dashed blue line indicates the fit to data excluding the chaotic oscillations. The solid red line uses the complete dataset. In both cases the condition $a \geq 0$ was imposed. The absorbance was measured at λ = 512 nm with initial conditions of[H_2SO_4] = 0.50 M, [BrO_3^-] = 0.40 M, [MA] = 0.20 M and [ferroin] = 2.00 mM.

Initial attempts at fitting a simple logarithmic line to the frequency data show the impact of chaotic oscillations on modelling the reaction. For the example shown in Figure 2.3 the equation of the dashed blue line was $-0.055 \ln t + 0.467$, demonstrating that under normal periodic oscillations this method is effective.

As can be seen from the data in Figure 2.3 there is a decrease in oscillation frequency with time, which is a standard feature across aging BZ reactions in batch conditions. In acoustics, a variation in oscillation frequency with time is a defining feature of chirp signals. The observed decrease in the BZ reaction is not linear and such a decay is typically termed an exponential chirp signal since the frequency varies exponentially with time as in Equation 2.3. This afforded an alternative method by which the original absorbance-time data could be modelled, giving more information on the oscillations although still unable to account for the periods of chaotic oscillation.

$$f(t) = f_i \eta^t \tag{2.3}$$

f_i is the initial frequency of the oscillation and η controls the rate at which the oscillation reaches its final frequency,f_Ω, at time, t_Ω.

$$k = \left(\frac{f_\Omega}{f_i}\right)^{\frac{1}{t_\Omega}} \tag{2.4}$$

In the time domain the wave would have the form of the sinusoidal function given by Equation 2.5

$$x(t) = A(t) \sin\left[2\pi f_i \left(\frac{\eta^t - 1}{\ln \eta}\right) + \phi_0\right] + x_0 \tag{2.5}$$

where $A(t)$ is the amplitude of the wave as a function of time, since amplitude typically increases with time in the BZ reaction (Figure 2.1). Appendix B contains the calculated values of η and f_i from a range of initial reagent concentrations. Figure 2.4 shows that decay rate from the onset of oscillations is independent of initial conditions.

Modelling the stirred oscillations as chirp sequences greatly simplified the behaviour of the reaction. This method gave a reasonable approximation as to how the frequency of oscillation varied with time depending on the initial conditions and provided a significant depth to the atlas of reaction dynamics even if it largely ignores periods of chaos.

Therefore extracting the individual frequencies of the oscillations via Fourier transform as opposed to using a method that looked into the change in frequency completed the atlas of the stirred reaction since it provides a set of frequencies for each combination of initial reagents.

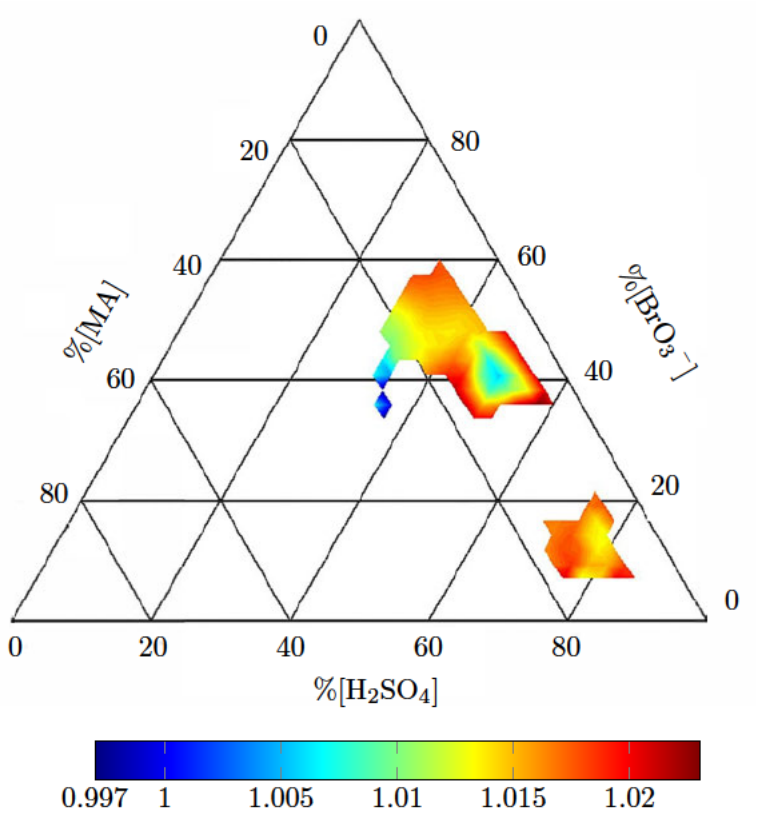

FIGURE 2.4: Ternary diagram of η values for the exponential chirp model. Mapping on the 3D parameter space demonstrates that the decay rate of oscillations, η, is largely independent of initial conditions; η ranges from 0.9970 - 1.0229.

2.4.2 Fourier Transforms

The Fourier transform (FT) extracts the frequency components from a time-domain signal. The oscillations produced by the BZ reaction are a function of at least three differential equations as per the Oregonator model, the structure of which cannot be easily captured by a simple sine wave as demonstrated above. Thus obtaining the FT of absorbance data for the stirred system established the range of frequencies that are observed in oscillating BZ media.

The general equation for a Fourier transform of a continuous time-domain signal, $f(t)$, is given by Equation 2.6

$$F(\nu) = \int_{-\infty}^{+\infty} f(t) \cdot e^{-2\pi i \nu t} \quad dt \tag{2.6}$$

where ν is the chosen frequency and t is the time in seconds. However, UV-vis spectroscopy yielded a discrete sampled sequence where the sampling frequency, ν_s is given as the inverse of the sampling time, Δ. A modified version of the Fourier transform equation (Equation 2.7) accounts for sampling.

$$F_s(\nu) = \int_{-\infty}^{+\infty} f(t) \cdot e^{-2\pi i \nu t} \quad dt \simeq \Delta \sum_{n=-\infty}^{+\infty} [f(t) \cdot e^{-2\pi i \nu t}]_{t=n\Delta} \tag{2.7}$$

The Fourier transform of a sampled sequence, denoted $F_s(\nu)$, is dependent on the normalised frequency, $\frac{\nu}{\nu_s}$. The Poisson sum formula (Equation 2.8) demonstrates how $F_s(\nu)$ is related to $F(\nu)$. It becomes clear that $F_s(\nu)$ is the sum of shifted versions of the continuous signal Fourier transform and hence is also a continuous function of frequency.

$$F_s(\nu) = \nu_s \sum_{k=-\infty}^{+\infty} F(\nu - k\nu_s) \tag{2.8}$$

For a sequence with only N data points $F_s(\nu)$ takes the form seen in Equation 2.9. Henceforth non-periodic sequences are considered to be periodic with length N.

$$F_s(\nu) = \nu_s \sum_{t=0}^{N-1} f(t) \cdot e^{-2\pi i t \Delta} \tag{2.9}$$

The discrete Fourier transform (DFT) evaluates the function at frequencies between 0 and $\left(\nu_s - \frac{\nu_s}{N}\right)$ and produces the final frequency spectrum. The step in frequency is $\frac{1}{t_\Omega}$ where t_Ω is the total length of the time series in seconds. Equation 2.9) accurately computes the Fourier transform but requires $\sim N^2$ complex multiplications. A more computationally efficient method is the fast Fourier transform (FFT), formulated in 1965 by J. W. Cooley and J. W. Tukey, which drastically reduces the number of computations required through use of a radix algorithm.[73,74]

This is more effective as for a sequence of length 2^n, where n is an integer, a radix-2 algorithm will successively halve the length of the sequence prior to solution. In the case of the radix-2 method the number of computations required is reduced from N^2 to just $N \log_2 N$, *i.e.* if $N = 1024$ then just 10,240 calculations are required as opposed to 1,048,576.

The FFT was computed for 95 datasets across the range of concentrations presented in Section 2.7 in Table 2.1. Appendix C contains a table of fundamental frequencies observed in stirred Belousov-Zhabotinsky experiments as calculated by DFT. A fundamental frequency is the lowest frequency of a periodic waveform and demonstrate the major frequency component within the reaction oscillations. Where oscillations occur in a periodic fashion the fundamental frequency will appear in the Fourier transform along with its harmonics, the integer multiples of the fundamental frequency. An example is shown in Figure 2.5.

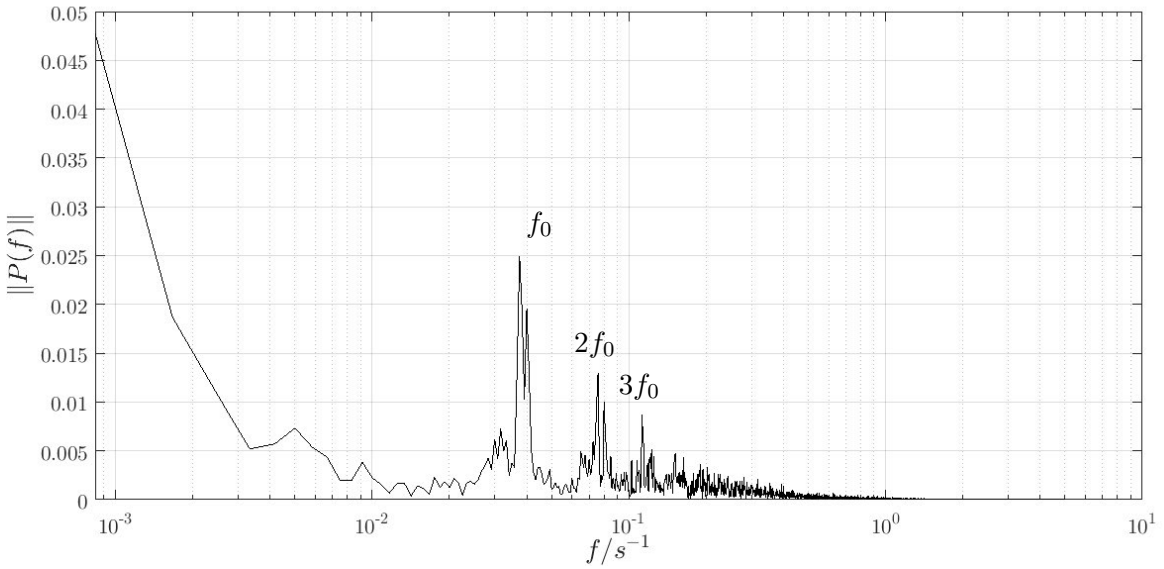

FIGURE 2.5: Fourier transform of periodic data. Periodic oscillations were analysed by Fourier transform in order to extract frequency components. Using $[H_2SO_4]$ = 0.80 M, $[BrO_3^-]$ = 0.05 M, [MA] = 0.20 M and [ferroin] = 2.00 mM, it was possible to see the presence of harmonic frequencies.

In the BZ reaction, two factors alter the appearance of the Fourier transform meaning that they tend to produce more complex signals. Firstly, the decreasing frequency of the oscillations with time, and secondly, the presence of quasi-periodicity and chaotic oscillations mean that more than one frequency makes up the signal as seen in Figure 2.6. As such the spectra obtained are not able to be easily deconstructed but if each frequency component were isolated and its amplitude recovered then the signal could be rebuilt.

An alternative method of exploring the chemical reaction network is to view it as a system made up of Markov processes. In such a view it is possible to argue that the next step in the chemical reaction is solely dependent on the system at that discrete moment in time and the direction based on a series of probabilities. From this perspective the system can be set up as a series of decisions through which information can flow. The method has been successfully applied to a variety of chemical systems including the theoretical "Brusselator" model.[75] However, there is an issue in that with the lack of knowledge on the overall reaction mechanism for the BZ reactions the system cannot be effectively modelled in this way. By monitoring flow in the network using a Markov chain analysis it could be possible to identify structure however this was beyond the scope of the thesis, interesting reviews of such ideas have been published by Lambiotte *et al.* and Bacik *et al.*.[76,77]

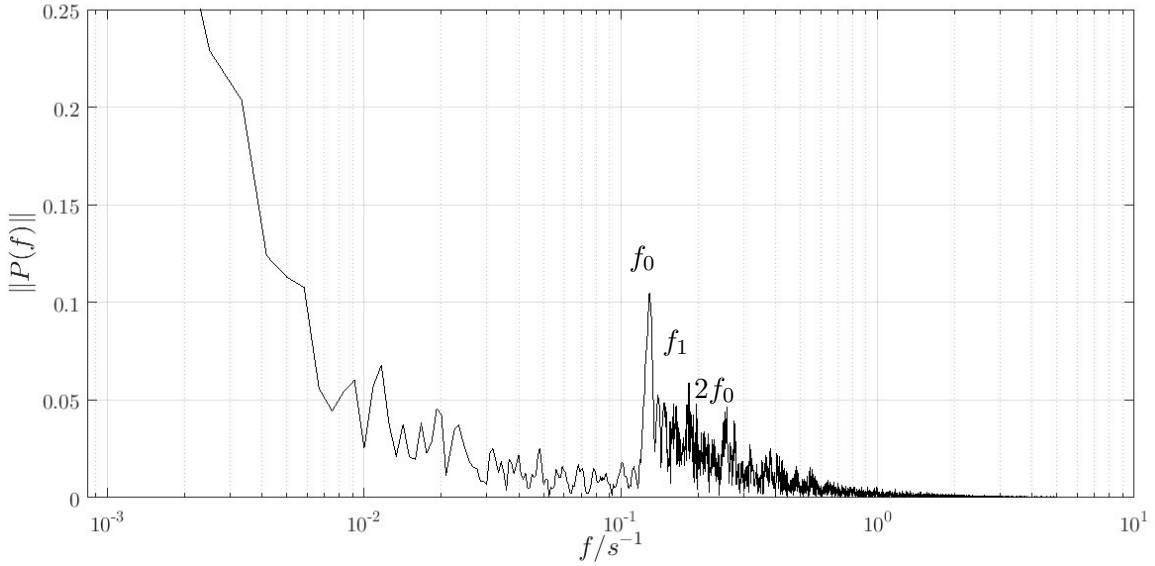

FIGURE 2.6: Fourier transform of aperiodic data. By using $[H_2SO_4]$ = 0.50 M, $[BrO_3^-]$ = 0.50 M, [MA] = 0.25 M and [ferroin] = 2.00 mM a more complex Fourier transform is observed with multiple frequencies and their harmonics arising, demonstrating the presence of chaotic and quasiperiodic oscillations.

By plotting the fundamental frequencies of the reaction a better understanding of the parameter space in which the reaction is undertaken was achieved (Figure 2.7). The spectra yielded information regarding the major frequency component of the oscillations - a dependence on $[BrO_3^-]$ was observed but none was seen for [MA]. As expected an increase in $[H_2SO_4]$ resulted in a further increase in oscillation frequency.

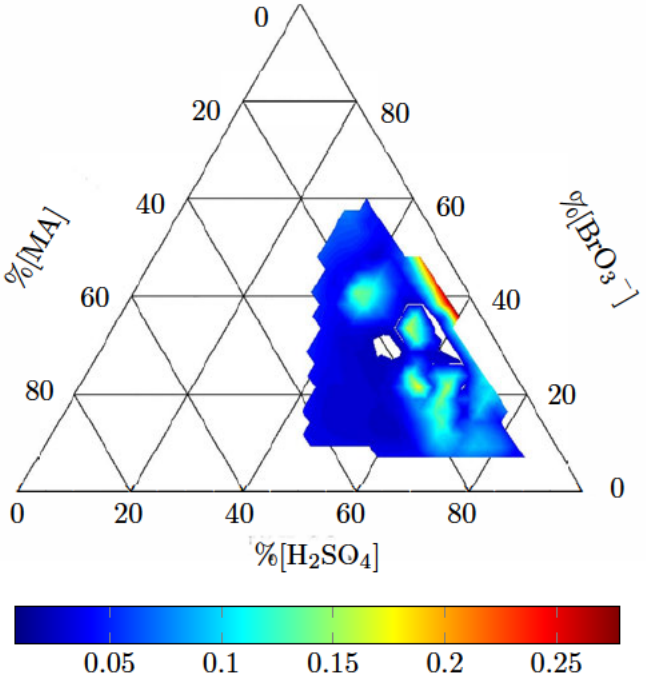

FIGURE 2.7: Ternary diagram of fundamental frequencies. Plotting the fundamental frequencies of the oscillations, including chaotic datasets, against initial conditions shows that the highest frequencies were observed with high concentrations of sulfuric acid and sodium bromate.

2.5 Effects of High Sulfuric Acid Concentration

Typically increasing the concentration of sulfuric acid results in a faster frequency of oscillation as observed in Section 2.4.2, however, a concentration of $[H_2SO_4]$ greater than 1.00 M is linked to an inhibition of the reaction.[56] Simulations produced in CoPaSi, a software package designed for biochemical networks simulation[78], using the MBM model set out by Hegedűs *et al.*[50] suggested that an inhibitory effect is observed when $[H^+] \geq$ 1.00 M, this is likely due to the overexpression of certain reactions that would result in either too much or too little bromide being produced.

In this report the iron(II)-catalysed Belousov-Zhabotinsky reaction had only been discussed for $[H_2SO_4] \leq 0.80$ M, however, a reduction in the rate of the reaction has previously been reported for the iron(II) system at higher concentrations.[56]

At $[H_2SO_4] \geq 1.00$ M there is an increasing loss of order and inhibition of the conventional fast oscillations. Despite this there appears an underlying oscillation with a frequency of $\approx 0.004\,s^{-1}$ observed in experiments where the acid concentration ranged from 1.00 M to 2.00 M (Figure 2.8 and Figure 2.9). This suggests that there is a very slow underlying oscillatory mechanism that allows the reaction to proceed even when faster oscillations have ceased or are unfavourable. It is plausible that such mechanisms are components of networks within the larger reaction network that are turned on or off

dependent on the overall concentrations in the system, a similar mechanism may well be responsible for the presence of oscillatory rebirth in reactions lasting 24 hours.[24]

It has been postulated that the inhibition of fast oscillations is a result of malonic acid not being directly oxidised when $[H_2SO_4] \geq 1.00$ M as a potential consequence of a substitution of a phenanthroline ligand for two HSO_4^- ions within the ferroin complex.[79] Nonetheless, a ferriin reduction can still occur and has been linked to the hypothetical oxidation of OH^- ions to $OH^\bullet$.[80,81] This process is unlikely in such an acidic medium and the following reaction was put forward by Hegedüs *et al.*[56]:

$$[Fe(phen)_3]^{3+} + H_2O \rightleftharpoons [Fe(phen)_3]^{2+} + H^+ + OH^\bullet \tag{2.10}$$

Equation 2.10 provides an explanation as to why a decrease in the rate of reaction would be expected with an increase in acid concentration. With an ever increasing acid concentration the equilibrium position is likely to be shifted in favour of ferriin and water and as such after the initial oxidation the reverse reaction becomes unfavourable. Furthermore this is mechanistically feasible in the given reaction conditions.

2.6 Chaos

The BZ reaction is an inherently chaotic system as a consequence of the sensitivity to initial conditions. Under certain concentrations of initial reagents the oscillations in the stirred system shift from a periodic profile to a chaotic or quasiperiodic profile, as previously stated in Section 2.2.2. As these oscillations are a core feature of the reaction it is possible to map the point at which the chemical system will exhibit such behaviour.

2.6.1 Defining Boundaries on Dynamic Behaviours

An alternative to the ternary diagram is to plot data on two dimensional axes by plotting [MA] against a secondary parameter, $\chi = \sqrt{[H_2SO_4][BrO_3^-]}\,/\,\mathrm{M}$. This parameter has been used in other research of the Belousov-Zhabotinsky reaction, specifically as an aid in studying spirals in unstirred BZ media. The use of the parameter is justified as a means of identifying boundaries in dynamic behaviour since it relates to the initiation of the reaction through formation of the autocatalyst, $HBrO_2$. The limited effect of [MA] on the dynamics of the reaction further enable its use for comparing data in a two-dimensional space.

Systems that pass through a period of chaotic behaviour show drastic changes in the amplitude of the signal as a consequence of the reaction pathway altering. During periodic oscillation the absorbance minima remain relatively constant. As predicted

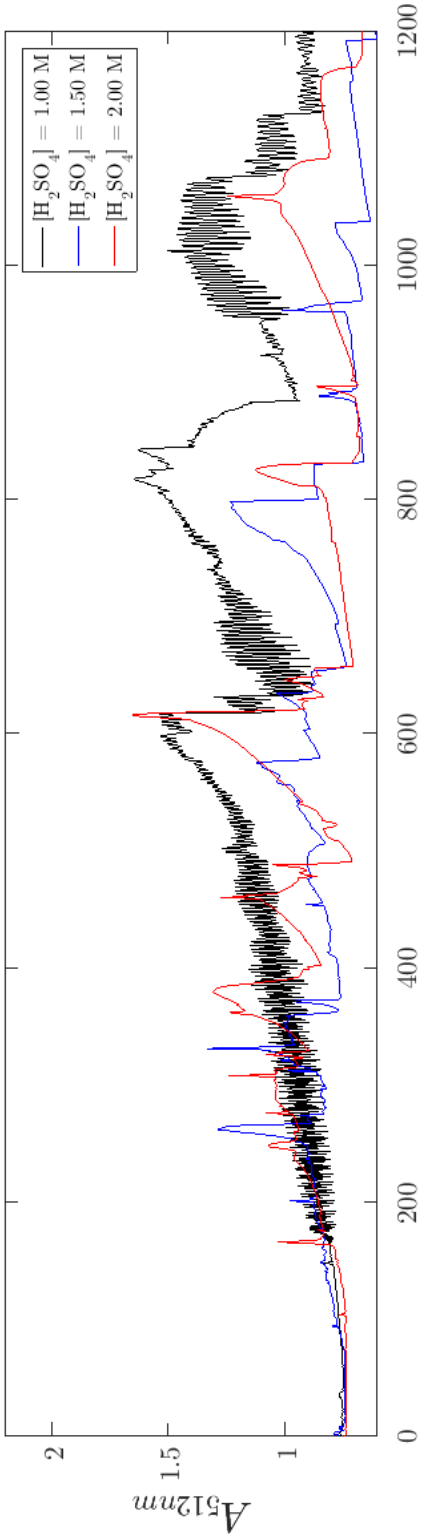

FIGURE 2.8: Comparison of the dynamics of the Belousov-Zhabotinsky reaction at high acid concentration, *i.e.* 1.00 M $\leq [H_2SO_4] \leq$ 2.00 M.

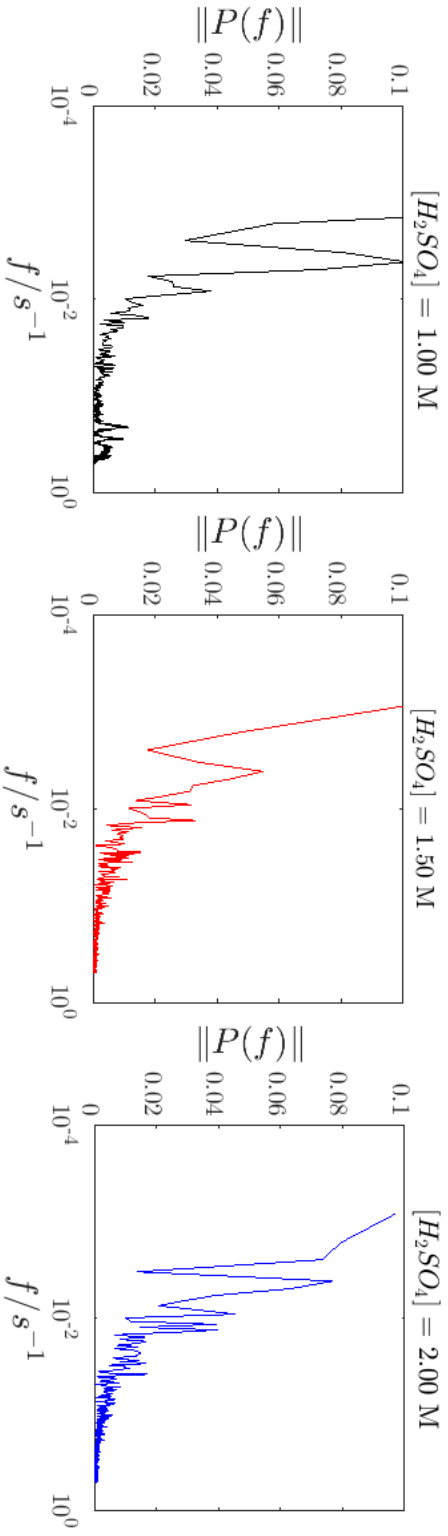

FIGURE 2.9: Fourier transforms for a range of high sulfuric acid concentrations. There remains an underlying frequency at $\approx 0.004\,s^{-1}$ for each reaction. In all cases the other reagent concentrations were fixed at $[BrO_3^-]$ = 0.20 M, [MA] = 0.10 M and [ferroin] = 2.00 mM.

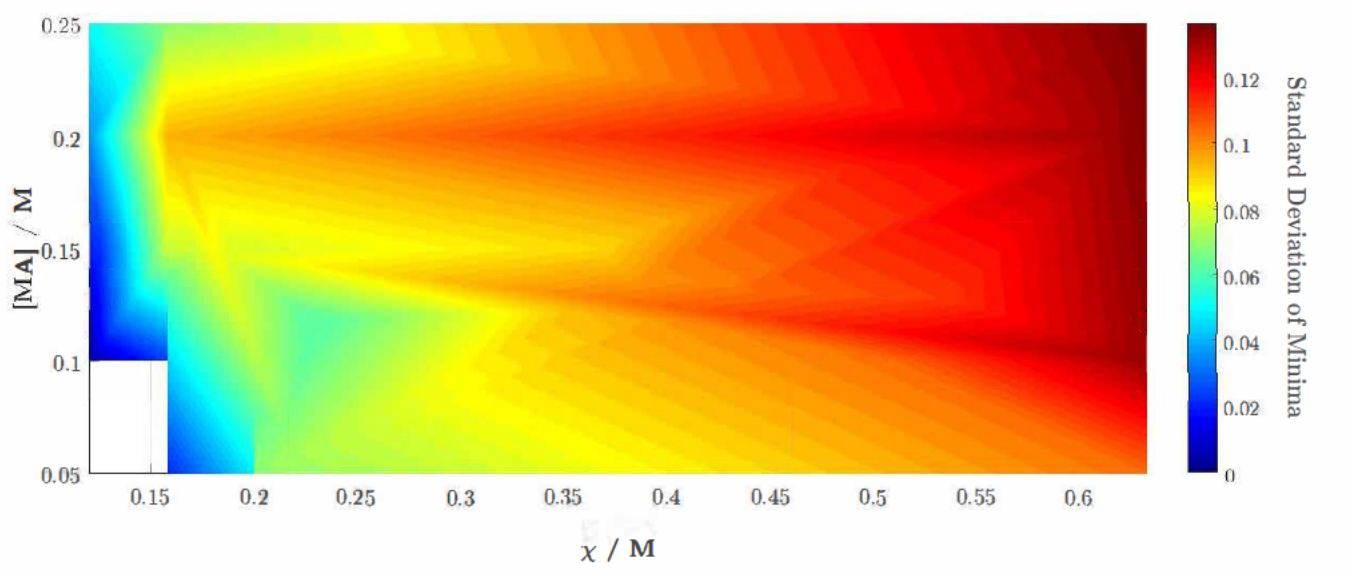

FIGURE 2.10: Mapping the standard deviation of the absorbance minima across a range of initial conditions suggests a transition to chaotic behaviour at higher values of χ. Fluctuation in the baseline absorbance, *i.e.* the point of complete catalyst oxidation, is indicative of a transition away from stable oscillations.

by application of the Beer-Lambert law, the absorbance minima varied as the reaction pathway transitioned towards a chaotic regime.

A change in the position of the absorbance minima accompanied a transition to chaos; by monitoring the variation in the position of the absorbance minima suggested a transition to chaos beyond a boundary at $\chi > 0.30\,\mathrm{M}$. Transitions were most likely to occur at the highest χ values (Figure 2.10).

Monitoring the overall number of peaks observed in a 20 minute period also offered a qualitative boundary at which oscillations were more likely to tend towards chaotic behaviour. By plotting the number of peaks on a map of concentrations (Figure 2.11) it became apparent that as χ increased more oscillations were observed. This result is expected from the theory but there are also clear points of transition as the system reaches oscillation frequencies of $0.125\ \mathrm{s}^{-1}$, around $\chi = 0.35\,\mathrm{M}$, corroborating the results seen in Figure 2.10.

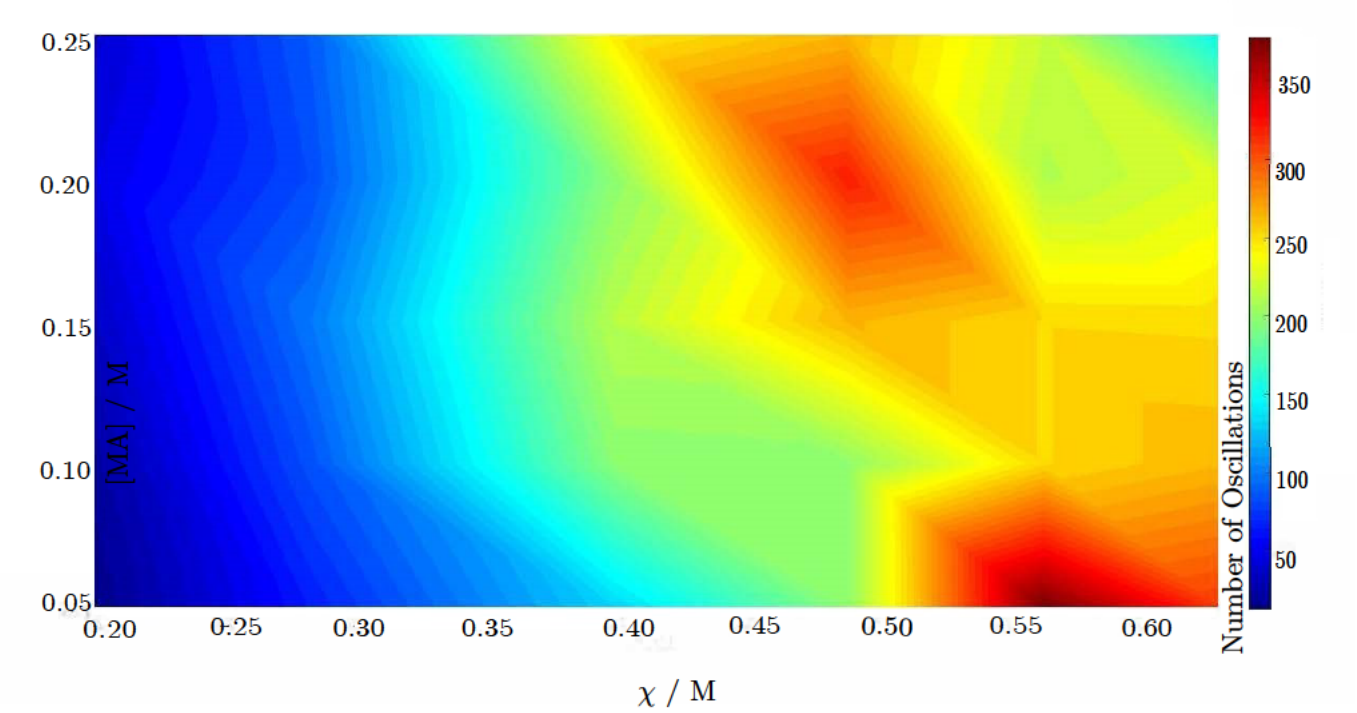

FIGURE 2.11: Surface plot capturing the transition to chaotic behaviour in the stirred Belousov-Zhabotinsky reaction. Monitoring the total number of oscillations observed in 20 minutes in the stirred Belousov-Zhabotinsky reaction using $[H_2SO_4] = 0.80$ M. A transition to chaotic behaviour is observed as the average oscillation frequency passes 0.125 s^{-1} (150 oscillations over 20 minutes).

These rather rudimentary measures are further supported by two artefacts of the analysis method, namely that oscillations faster than 1.4 seconds in length are not registered, nor are oscillations that have minima greater than $A_{512nm} = 1.00$. Therefore experiments that featured a time period seemingly absent of oscillations was likely to be chaotic, and the longer the gap the more chaotic the system was likely to be. Figure 2.12 shows the length of any gap in seconds, to prevent reporting slow oscillating systems as chaotic any experiments featuring fewer than 30 oscillations were ignored. Again, it becomes clear that as the value of χ increased the system became more chaotic with the transition seemingly occurring at a similar position to that in Figure 2.11, increasing the malonic acid concentration does not play a role in creating a chaotic regime yet from this it appears that a higher initial concentration sustains the chaotic regime for a longer time interval.

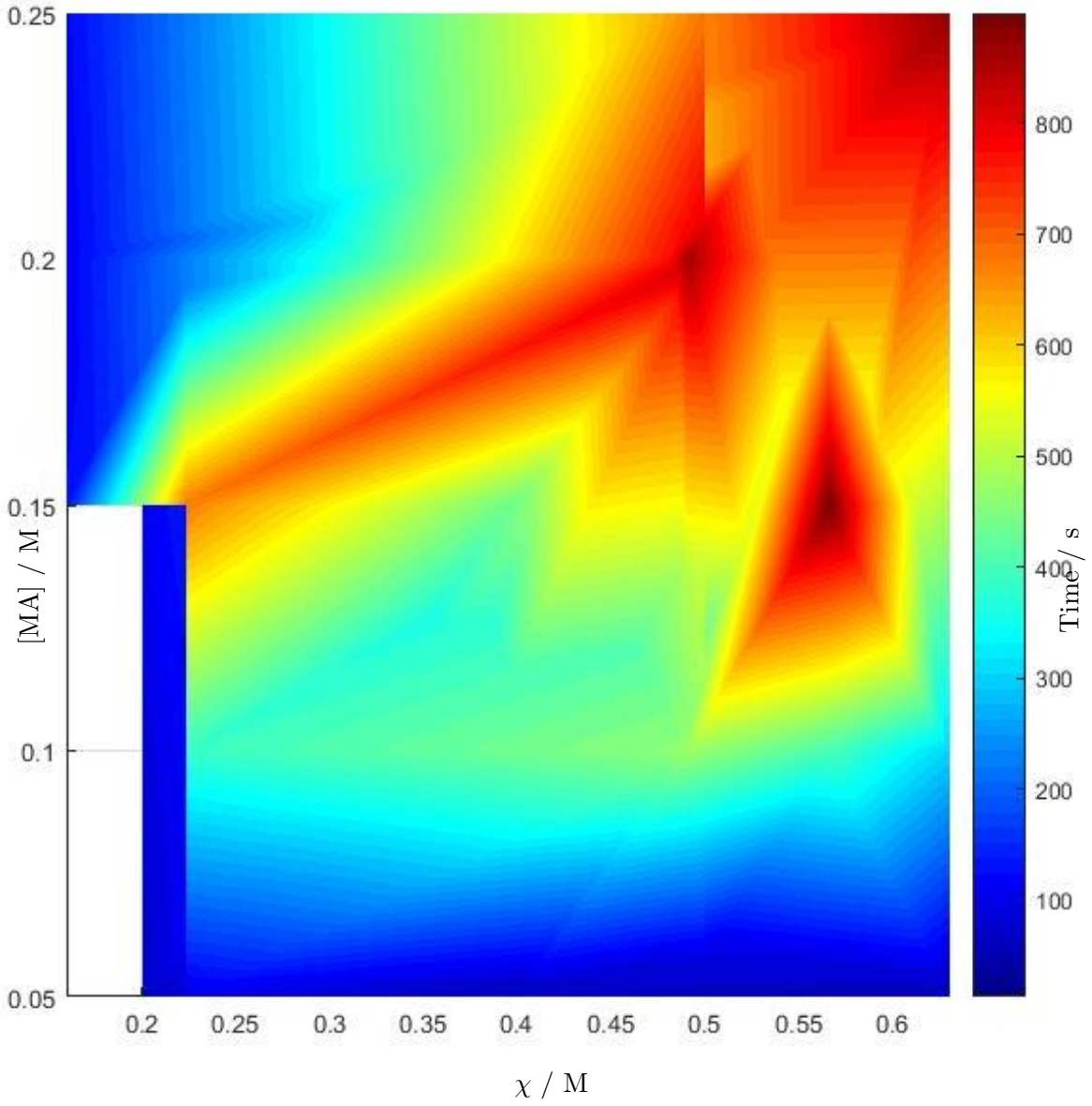

FIGURE 2.12: A surface plot of the timescale over which chaotic oscillations were observed in 20 minutes in the stirred Belousov-Zhabotinsky reaction. Taken across a range of concentrations however any spectra with fewer than 30 oscillations were discarded.

2.7 Experimental

2.7.1 UV-Vis Experiments

UV-Vis spectroscopy monitored changes in absorbance as the reactions progressed. In the reduced state ferroin has wavelength of maximum absorption (λ) $\approx$ 512 nm and so following the dynamics of the reaction across a range of initial conditions at a fixed

temperature was routine.[82] All measurements were made on a well stirred system using a Cary 100 UV-Vis spectrometer (Varian Technologies, UK), and a fixed temperature at 25 °C. Each experimental run varied the initial conditions to cover the parameter space given inTable 2.1. Data was collected for 1200 s at a sampling frequency of 10 s^{-1}.

Species	**Concentrations studied / M**
Sulfuric Acid	0.25, 0.50, 0.80
Sodium bromate	0.05, 0.10, 0.20, 0.30, 0.40, 0.50
Malonic acid	0.05, 0.10, 0.15, 0.20, 0.25
ferroin	0.002

TABLE 2.1: Concentration ranges studied in initial mapping experiments.

The algorithm in Appendix A enabled the automatic production of ternary diagrams for each of the metrics outlined in Section 2.2, representing a comprehensive overview of the information attainable from any stirred Belousov-Zhabotinsky system.

2.7.1.1 Peak-Picking and Chirp Analysis

Absorbance of all samples had been recorded by UV-Vis spectroscopy with 0.1 s intervals using a 512 nm excitation wavelength. In order to minimise the effect of noise analysis was performed using longer time intervals. Datasets with fast and/or chaotic oscillations or were noisy resulted in a wide variation in the number of peaks identified by the peak-picking algorithm. A sampling interval of 0.7 s yielded the minimum error across a range of datasets meaning the minimum recordable oscillation period was 1.4 seconds, which is an acceptable time frame for even the fastest of periodic oscillations. Any oscillations faster than this likely featured in a chaotic regime and therefore enabled the definition of such behaviour by the apparent absence of oscillations (Section 2.6.1).

2.7.2 $H_2SO_4 \geq 1.00$ M Experiments

Solutions were made up to a total volume of 2 mL containing final concentrations of [MA] = 0.10 M, [ferroin] = 2.00×10^{-3} M and [$NaBrO_3$] = 0.20 M. The final concentrations of sulfuric acid ranged from 1.00 M to 3.00 M. In all cases sodium bromate was added to the solution last and reactions were continuously stirred for 30 s prior to monitoring at 25 °C. A 512 nm wavelength was used as in previous experiments and reactions were monitored for 20 minutes.

2.8 Conclusions

In this chapter the link between $[H_2SO_4]$, $[NaBrO_3]$ and the oscillation frequency has been mapped using the fundamental frequency of the oscillations. Furthermore the shift in dynamics brought about by increasing sulfuric acid concentration has been presented along with evidence that although fast oscillations cease, a slower underlying oscillation ($f_0 \approx 0.004\,s^{-1}$) is still present. By mapping the frequency, amplitude and induction period of the stirred Belousov-Zhabotinsky reaction a clearer picture of the range of behaviours possible emerges. With this in mind it is evident that even a very simple initial system can exhibit many layers of behaviour, *i.e.* a complex network of reactions with known function under constrained conditions may have the potential to exhibit remarkably different behaviour if the initial conditions are suitably altered. Subsequent chapters explore the effect of having no convective forcing applied to the solution and whether similar definition is observed.

Chapter 3

Mapping the Unstirred Belousov-Zhabotinsky Reaction

Continuing the atlas of the BZ reaction by detailing the nature of the reaction in an unstirred system, this chapter largely focuses on the evolution of spiral waves with time and a discussion of statistical methods by which wave patterns can be monitored as the reaction progresses. Addition of surfactants to the reaction is also examined with regards to their effect on observed patterns in the unstirred system.

Parts of this work were undertaken in collaboration with Jessica Gusthart who obtained data regarding the effect of surfactants on the unstirred system.

3.1 Origin of Propagating Waves in the BZ reaction

First described in detail by Winfree propagating waves of oxidation are a notorious phenomenon of the reaction, travelling at velocities on the order of mm.min^{-1}. These waves are generated at so-called "pacemaker" sites and travel outwards until collision with a physical boundary, at which they disappear without reflection, or until the interaction of two opposing oxidation waves leads to their mutual annihilation. "Pacemakers" pulse at a frequency set by the initial conditions, if this frequency is greater than that of the oscillation in bulk solution then temporal oscillations are suppressed in an increasing area of concentric circles. Evidently this applies solely to continuous bands of oxidation however should a band be broken then the two ends will rotate around the discontinuity to form a spiral, further discussion of which is in Section 3.2.[84]

Leading edge of an oxidising band advances into a reducing region containing bromide above the critical threshold described in Section 1.7. In this leading edge bromous acid is created autocatalytically. This autocatalytic reaction process drives the wave

FIGURE 3.1: Pattern formation in the unstirred BZ reaction. Spiral waves and planar wavefronts are visible along with bubble formation in a reaction set up in a petri dish. Image colour has been enhanced for clarity.

faster than by diffusion alone, yet the velocity of wave propagation is inversely related to the surrounding bromide concentration.[84]

3.2 Pattern Formation and Spiral Waves

In the unstirred BZ reaction pattern formation typically occurs for a few hours and the duration is dependent on reactant concentrations, with low bromate and sulfuric acid concentrations resulting in longer lived patterns.[85] Figure 3.1 represents a typical example of pattern formation exhibited by the iron-catalysed BZ reaction.

There are numerous patterns observed in the BZ reaction including stationary patterns and "Turing" patterns. Alan Turing postulated the reaction-diffusion equation (Equation 3.1) as part of his seminal work "The Chemical Basis of Morphogenesis" in 1952 wherein he surmised that a system of chemicals reacting together and diffusing through a tissue could, despite initial homogeneity, develop a pattern or structure through random disturbance.[14].

$$\frac{\partial \Psi}{\partial t} = D\nabla^2\Psi + F(\Psi) \tag{3.1}$$

where Ψ is a set of state variables dependent on the temperature of the system, and concentration of each species in solution. Here D is a vector of diffusion coefficients for each species present.

Six different patterns in the form of fronts, spirals, targets, hexagons, stripes and dissipative solitons were proposed and now collectively termed "Turing patterns". These may arise depending on the pertubation of the chemical system and its initial state, all of which are generally reproducible in chemical cells.[86] Spatial heterogeneities provide the necessary perturbation in an excitable medium to produce patterns that oscillate periodically in time.[87]

Spiral waves are a specific set of spatio-temporal solutions of the reaction-diffusion equation in which convection effects are ignored.[88] Turing's initial paper outlined the presence of spirals as a singular pattern, however spirals are most commonly observed as rotating spiral waves in the BZ reaction, the mathematics of which was elucidated by Cohen *et al.*.[83,89]

A common feature in chemical and biological systems, spiral waves were first used in Wiener and Rosenbleuth's explanation of cardiac arrhythmia as an excitable medium in 1946.[90] They were later observed experimentally in the aggregation of *Dictyoselium discoideum* as well as the propagation of calcium ion release near the plasma membrane of *Xenopus laevis* oocytes.[91–94] The propagation of such spatio-temporal patterns make them capable of carrying information and inducing physiological responses in biological systems.[95] Understanding their formation and development in time therefore facilitates how they transmit information.

Although the BZ reaction was discovered in the 1950s it was not until the 1960s and 70s that spiral patterns in solution were being studied and formalised.[83,96] Spirals have since been observed in other oscillating chemical systems including the chlorite-iodide-malonic acid reaction suggesting that their presence, along with other Turing patterns, is tunable to initial conditions although no spatial structure formation has yet been witnessed in the $H_2O_2 - KSCN - Cu(II) - NaOH$ or phenol $- BrO_3^-$ oscillators.[97]

3.2.1 Archimedean Spirals

By using a closed stirred tank reactor (CSTR), Belmonte *et al.* were the first to experimentally determine a parameter space within which one could find spiral formation in the iron-catalysed BZ reaction.[99] Such spirals are virtually indistinguishable in shape from Archimedean, or arithmetic, spirals as described by Equation 3.2.[100] Archimedean spirals were first described by the Ancient Greek mathematician in 252 BC and their presence in unstirred Belousov-Zhabotinsky reactions confirmed in 1972.[83]

$$r = a + b\theta^{1/c} \tag{3.2}$$

where r is the radius of the spiral, a controls the turn of the spiral and b defines the separation between the spiral arms. For a normal Archimedean spiral $c = 1$. Since

the separation in an arithmetic spiral is constant calculation of the spiral pitch, Λ, is possible according to the relation

$$\Lambda = 2\pi b \tag{3.3}$$

3.2.1.1 Motion of Spiral Waves

The tip of a spiral wave moves in three distinct ways termed *rigid rotation*, *meander* and *drift*. The simplest of these is rigid rotation where, over time, the tip of the spiral traces a circle around the core. When a spiral tip is in a meandering regime the tip will trace out an epicycle with either inward or outward facing "petals".[101] Such motion is an inherent feature of the chemistry of BZ systems and is not due to an inhomogeneity in the system.[102] Drift is akin to rigid rotation except that the circle being trace out drifts with time due to a perturbation in $\frac{\partial \Psi}{\partial t}$. For a comprehensive review of drift and meander of spiral waves see the thesis by Foulkes.[93]

3.2.2 Spiral Wave Initiation in the BZ Reaction

Formation of spirals in a reaction-diffusion system cannot occur spontaneously without the presence of an inhomogeneity in the system.[103] Typically, the collision of two propagating wavefronts travelling perpendicular to one another results in broken waves that curl into a familiar spiral structure over time.[84,93] Spiral waves can also be formed by manipulating the system via the presence of an obstacle, sharp corner or by mechanically breaking a circular wavefront.[104]

3.2.3 Variations in Pitch with Time

The evolution of spiral waves in the unstirred BZ reaction has been an active research area since their discovery in the 1970s however has largely considered the initiation and motion of such spirals as discussed above.

Methodologies for studying spirals have typically isolated a single spiral through the use of lasers to control the core of a spiral or by initiation of a wave by introducing silver to the system; this relies on having a sub-excitable reaction medium capable of being initiated externally.[93,105,106] Relatively few studies have sought to map the behaviour of spirals over a broad concentration or time range under batch conditions. Nagy-Ungvarai *et al.* utilised the cerium catalysed system to study wave velocity, tip position and spiral pitch in batch conditions for up to 4 hours (or for as long as spiral waves were visible). Their investigations observed a linear increase in spiral pitch with time. A decrease in initial spiral pitch, Λ_0, followed an increase in the initial sulfuric acid concentration.

In all experiments the initial concentrations of sodium bromate and malonic acid were kept constant at 0.30 M and 0.366 M respectively. While these measurements matched simulations produced by the Oregonator model they again do not compare with the ferroin system.[102,108] These discrepancies have not yet been overcome in any study of the ferroin catalysed reaction. One of the earliest studies on spiral pitch evolution was completed in 1987 by Müller *et al.* who reported the following equation

$$\Lambda(t) = 0.994 \times 10^{-4}\, t + 1.188\,\mathrm{mm} \tag{3.4}$$

for the evolution of a simple spiral in the ferroin catalysed system over a 300 s period. Here Λ is the spiral pitch at time, t. Later work with sulfuric acid concentrations in the range 0.15 M - 0.70 M confirmed the Archimedian nature of chemical spiral waves at high acidity but highlighted that there are pronounced deviations from this geometry with decreasing acidity.[108] Through use of a CSTR,Belmonte *et al.*, undertook an experimental survey of a range of conditions.[98] This parameter space showed experimentally the tendency for low malonic acid concentrations to form meandering spirals as well as the shrinking of the spiral pitch with increased acid concentration. Increasing the concentration of malonic acid has a further effect on simple spirals by decreasing the pitch of the spiral at fixed sulfuric acid and sodium bromate concentrations.[110] However, being in a CSTR meant that the results did not show any aging process to the solution and so no variation in spiral pitch was observed with time.

This thesis offers a comprehensive map of spiral pitch evolution for the BZ reaction in unstirred batch conditions with a ferroin catalyst at $[H_2SO_4]$ = 0.50 M and 0.80 M as well as across a range of sodium bromate and malonic acid concentrations. The experimental method is given in Section 3.5.1. Experiments were also undertaken at $[H_2SO_4]$ = 0.25 M, however, as described by[108] spiral behaviour at such low acidity was not directly comparable to that of the higher acid concentrations.

3.2.4 Fitting Data

A method of monitoring multiple spirals in a single reaction was generated in Matlab and is presented in Appendix A.2. The method fitted an Archimedean spiral to points on the spiral wavefront, an example of which can be seen in Figure 3.2 that demonstrates the approximation of an Archimedean spiral was appropriate in monitoring the BZ reaction. The number of spirals varies with the initial concentrations of reagents as well as time. While a solution may initially contain one spiral it is possible that more will develop with time, or indeed these can be subsumed into other, more dominant, spirals.

As the whole system ages at a uniform rate it can be assumed that the majority of the spirals have the same parameters at any given point in time. A caveat to this

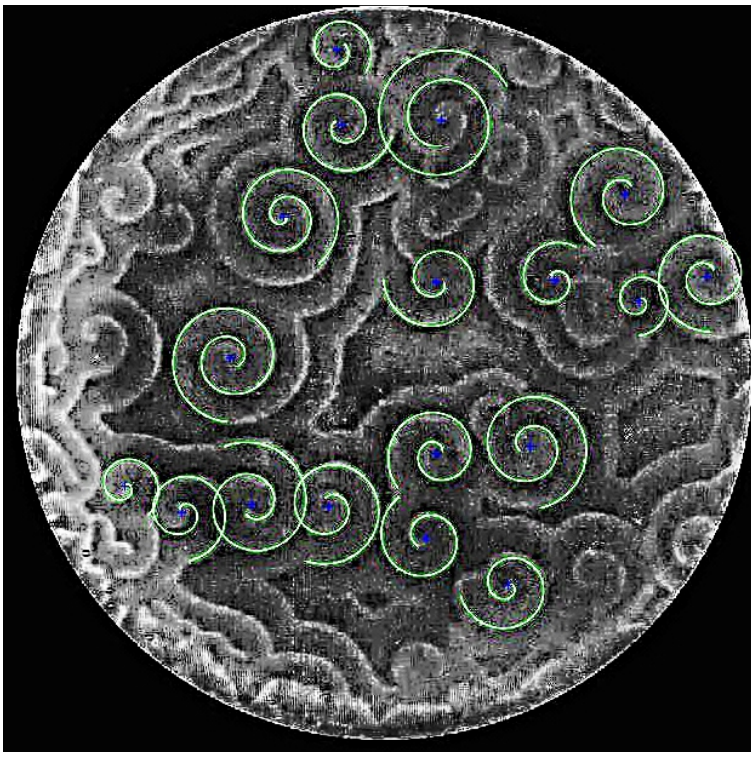

FIGURE 3.2: Example output from the spiral tracking algorithm highlighting the edges of spiral waves and their centres. The green line traces the edge of the spiral wave. The blue cross marks the calculated centre of each spiral. As can be seen here not all of the spirals are selected but sufficient to give a general overview of the system at that time.

is that local disturbances result in slight variations to the oscillation frequency, hence the presence of dominant spirals, or the presence of inhomogeneity-induced wave breaks giving new spirals. Yet, over short timescales, neither of these phenomena affect the results. Therefore, the average of the parameters output by the algorithm was used to model their time dependence. The initial stages of spiral wave evolution were modelled linearly as in Equation 3.5. At $t = 0$ the y-intercept of the line, Λ_0 indicates the minimum value of the spiral pitch and is dependent on the initial conditions. Here, α is the gradient of the line, $\frac{d\bar{\Lambda}}{dt}$.

$$\bar{\Lambda} = \alpha t + \Lambda_0 \tag{3.5}$$

As seen in Figure 3.3, on moving to longer timescales the evolution of spiral waves deviates from this simple linear relationship and transitions to either the reduced or oxidised state via an instability in the system, at this point the rate of change of $\bar{\Lambda}$ increases.[93,98,105]

Table D.1 lists the values for α and $\bar{\Lambda}_0$. Typically α is approximately 1×10^{-3}

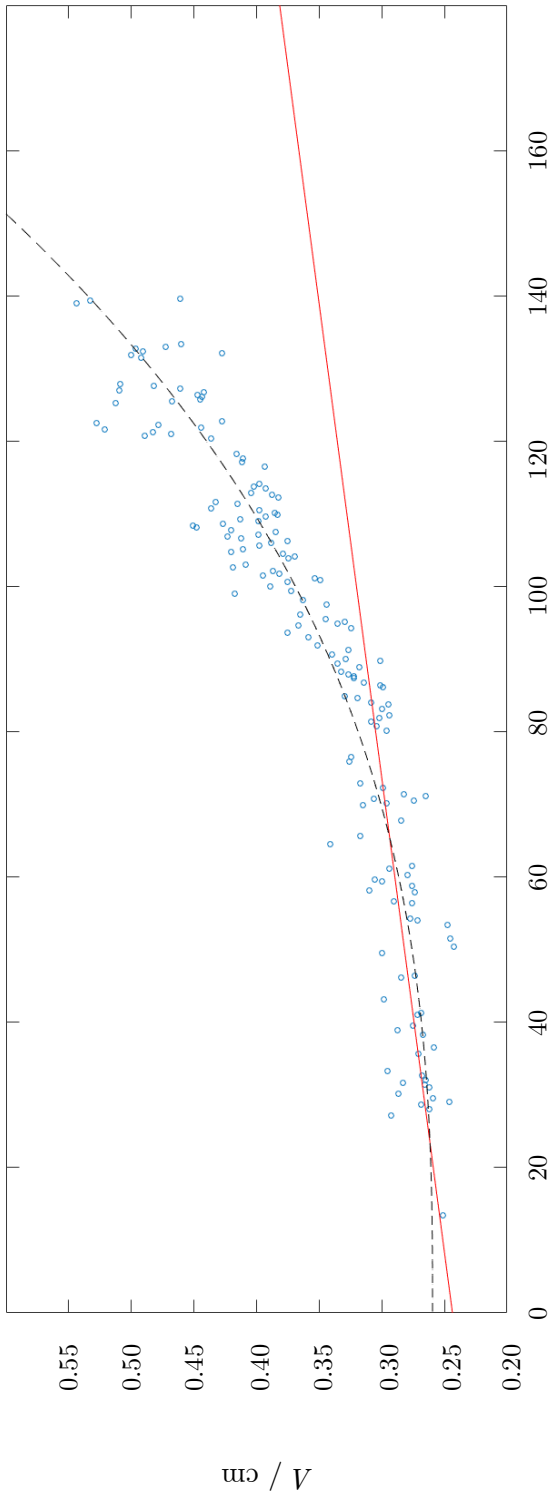

FIGURE 3.3: Spiral pitch deviates from linear growth with time as the system approaches an instability. $[H_2SO_4] = 0.80$ M, $[BrO_3^-] = 0.05$ M, [MA] = 0.05 M, [ferroin] = 2.0 mM.

min^{-1} while $\bar{\Lambda}_0$ is more dependent on initial conditions, as has been reported in literature.[98,109,110] This supports the findings from the stirred experiments in Section 2.4.1, where the rate at which the frequency of oscillations decayed was observed to be independent of the initial conditions.

From the data it is apparent that the initial pitch increases with higher sulfuric acid concentrations for comparable values of χ. Figure 3.4 shows the region at which the initial pitch of a spiral is at its highest is dependent on high [MA] and low [BrO_3^-].

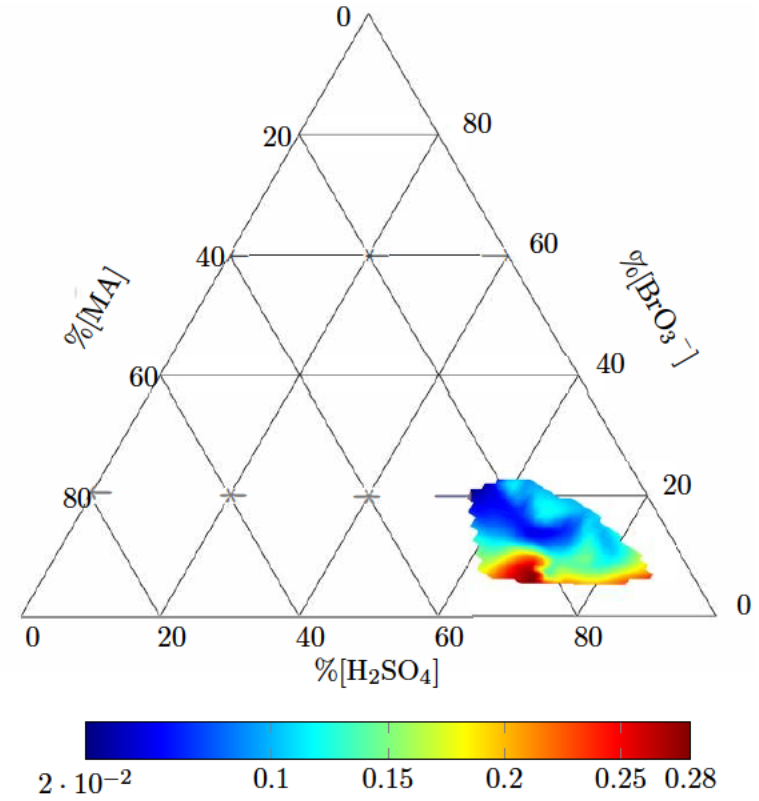

FIGURE 3.4: Ternary diagram plotting the initial spiral pitch, Λ_0 / cm, for a range of conditions using [H_2SO_4] = 0.50 - 0.80 M. As the concentration of sulfuric acid and sodium bromate increases the initial pitch decreases. Full results are detailed in Table D.1.

3.3 Mapping Chaotic Patterns by Initial Conditions

As the reaction proceeds the system passes through an instability to reach a steady state. This is evidenced by the increase in spiral wave diameter, seen previously in Figure 3.3, but can also be seen in the development of more chaotic patterns. Calculation of statistical parameters in image analysis from a region or the whole image enables quantification of visual differences.[111] Six distinct parameters that can be used for this purpose are:

1. Mean - the average intensity of a greyscale image

2. Standard deviation - the average contrast of the image
3. Third moment - the skewness of a histogram
4. Smoothness - measures the relative smoothness of the intensity of a region
5. Uniformity - measures uniformity of an image and is maximal when all intensity values are equal
6. Entropy - the randomness of the intensity values in an image

The difference in intensity between the red and blue colours of the Fe(II/III) redox couple observed with ferroin is pronounced on conversion to a greyscale image (Figure 3.5). As such the mean intensity and contrast will vary across the course of a reaction as the concentration of ferroin/ferriin changes. This methodology has utility as a tool for identifying the final steady state. However, the lack of spatial information encoded by this method makes quantification of patterns or the identification of transitions in behaviour by this method impossible.

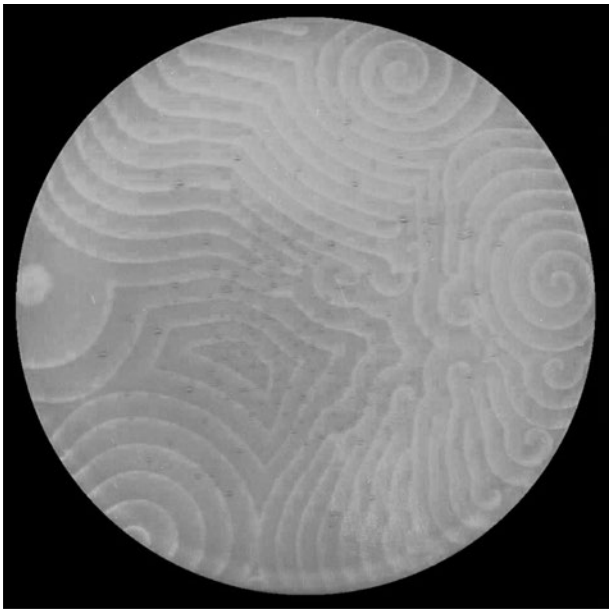

FIGURE 3.5: Greyscale image of the unstirred Belousov-Zhabotinsky reaction as used to calculate image entropy and uniformity.

Uniformity, smoothness and entropy are all measures that provide a degree of spatial information from an image. Where there are chaotic patterns an increase in entropy and a decrease in both smoothness and uniformity should be expected. The presence of periodic waves would be likely to increase uniformity but still have a relatively high entropy value, assuming these patterns are not accompanied by bubble formation.

A limitation of using just entropy is that although two images can be visibly different (low spatial correlation) they can have the same entropy value as seen in Figure 3.6.

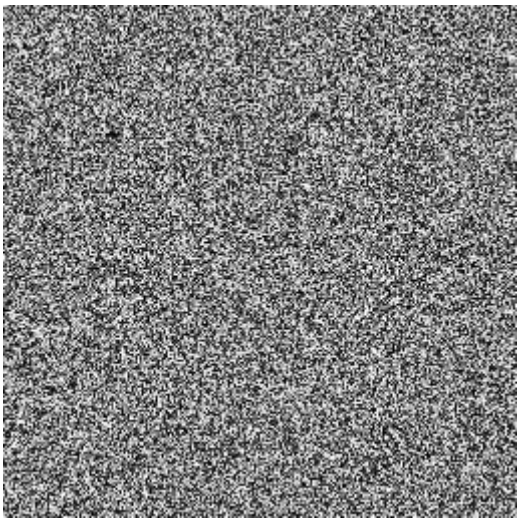

(a)

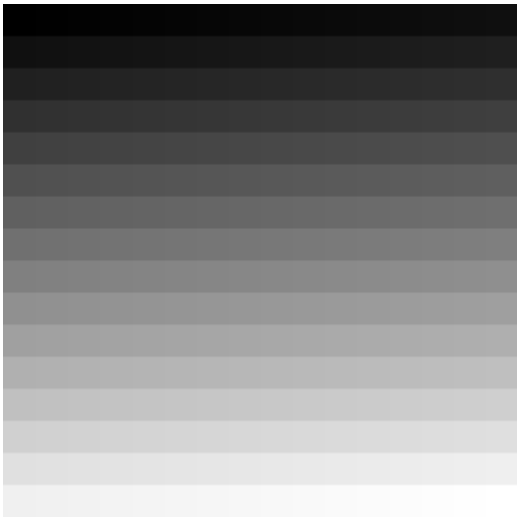

(b)

FIGURE 3.6: Two images with very low spatial correlation but equal image entropy.

Dividing the image entropy by the uniformity of the image (Equation 3.6) to give a new parameter, Γ, it was possible to visualise the transition of the reaction systems to chaos and ultimately their final steady state.

$$\Gamma = \frac{-\sum_{m=0}^{M-1}(p_m \log_2 p_m)}{\sum_{m=0}^{M-1} p_m} \tag{3.6}$$

where M is the number of grey levels and p_m is the probability associated with each grey level, m. Plotting this as a function of time yields distinct curves that relate to the state of the reaction (Figure 3.7).

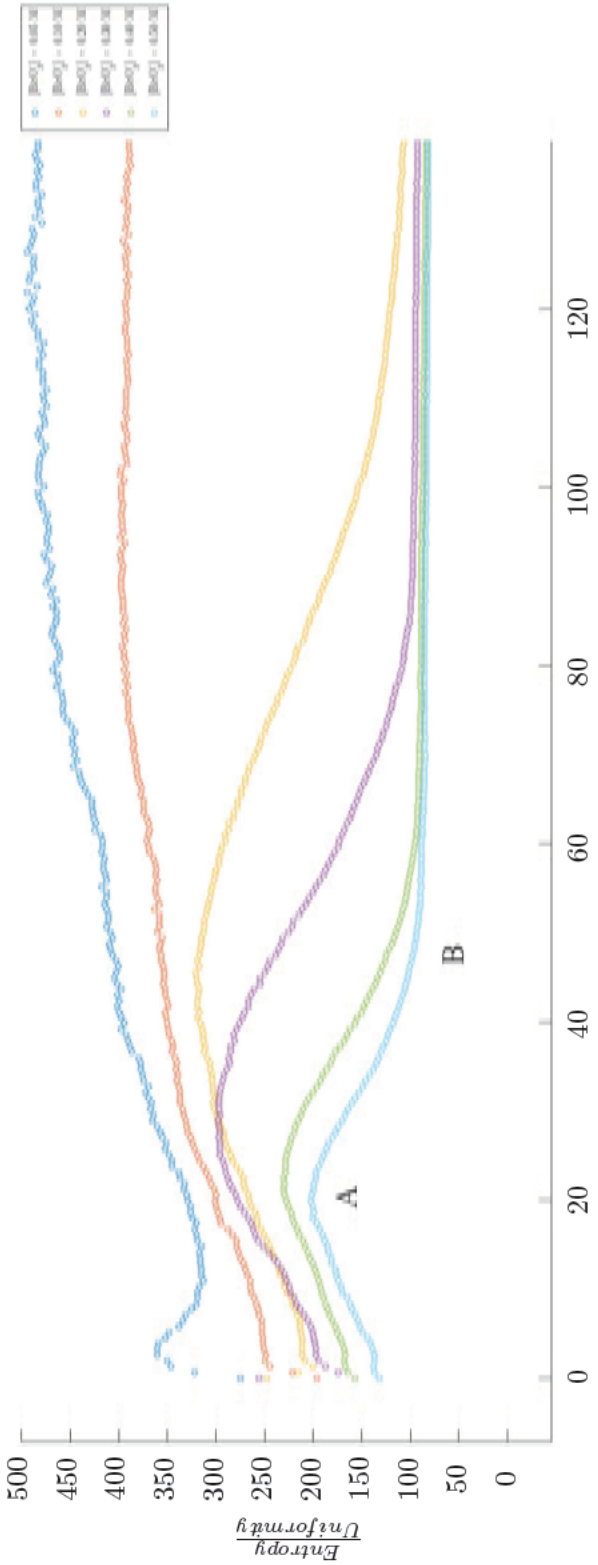

FIGURE 3.7: Entropy-Uniformity ratio as a function of time for reactions.

As the curve reaches a maxima, as depicted at position A in Figure 3.7, the system transitions to more chaotic patterns and as the gradient returns to zero (position B) the system approaches the oxidative steady state. If the curve reaches the maximum A but does not subsequently decrease then the system remains in the reduced steady state. Figure 3.7 also shows that this transition occurs earlier as the initial concentration of sodium bromate increases, this method is a more reliable approach to monitoring the age of a reaction than by following the retraction of spiral wavefronts since it tracks the dynamics of the whole system through each instability.

Moreover, it is possible to see the effect of malonic acid, sodium bromate and sulfuric acid on the aging of the system. Where increasing the concentration of sodium bromate shortened the time to chaos the effect is counteracted by increasing the concentration of malonic acid (Figure 3.8). A shortening in the time to transition is also observed with increasing sulfuric acid concentration.

3.4 Effect of Surfactants

Visual patterns are one aspect of the evolution of the BZ reaction with time, carbon dioxide and monoxide are also produced as the reaction proceeds.[56,112]. The formation of bubbles can cause distortions in image entropy measurements in Section 3.3. Although the use of the entropy-uniformity ratio largely negated this effect alternative methods were explored to limit the effect further. Surfactants reduce the surface tension of a solution in which they are dissolved.[113] Hence they were of use in preventing bubble formation in a classic BZ reaction. There are variants of the Belousov-Zhabotinsky reaction that are supposedly bubble-free but require the use of alternative organic substrates such as cyclohexadione (CHD).

Three surfactants were used in experiments: dioctyl sulfosuccinate sodium salt (Na-AOT), which is an anionic surfactant; a cationic surfactant in the form of cetyl trimethylammonium bromide (CTAB) and Triton X-100 (TX-100), which is neutral. All surfactants were added at a concentration below their critical micelle concentration (CMC), details of the experiments are included in Section 3.5.3.

When no surfactants were present bubbles of carbon dioxide appeared after approximately 2 minutes and observation of the highest rate of bubble formation occurred after 10 minutes. There is a near linear increase in the cumulative number of bubbles with time without surfactants.

2.4 mM Na-AOT in solution slowed the initial rate of formation from 16 bubbles per minute to 6 bubbles per minute. At [Na-AOT] = 4.8 mM the number of bubbles actually far exceeds the control experiment with no surfactant. A similar effect was seen with

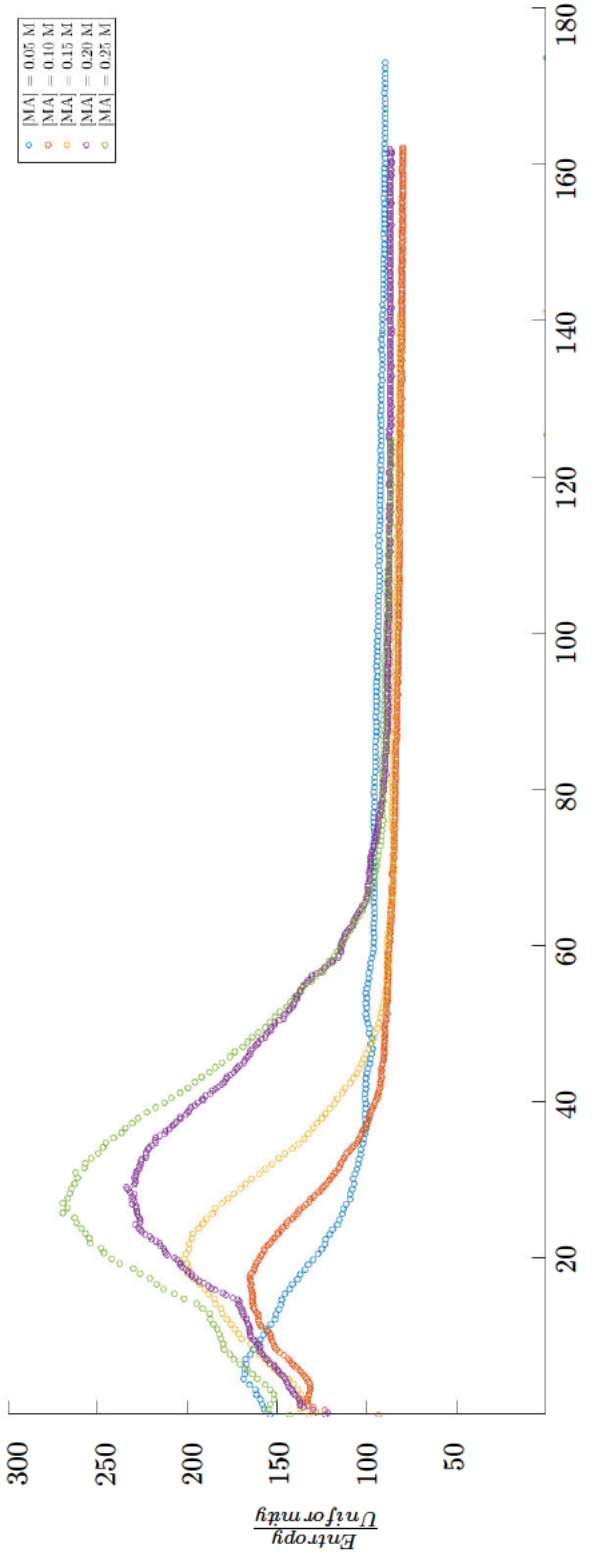

FIGURE 3.8: Entropy-uniformity ratios as a function of malonic acid concentration.

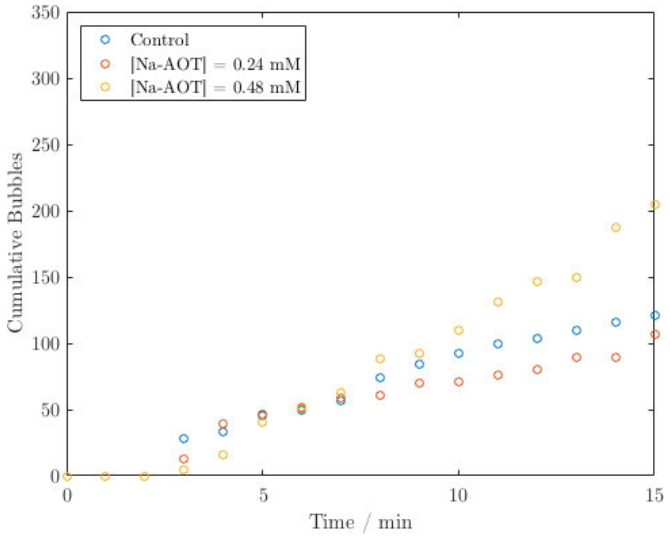

FIGURE 3.9: Cumulative bubble formation in the presence of AOT. AOT appears to slow the initial rate of formation of bubbles but at high concentrations can stabilise bubbles leading to a higher number of bubbles being observed.

CTAB, which again slows the rate of formation initially but eventually the cumulative total of bubbles exceeds that seen in the control.

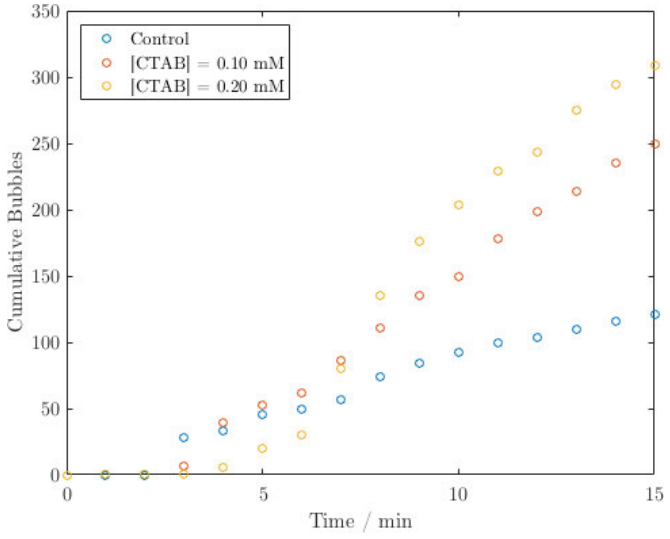

FIGURE 3.10: Cumulative bubble formation in the presence of CTAB. CTAB suppresses the initial formation of bubbles but lead to a rapid increase in the number of bubbles observed.

TX-100 sees an initial decrease in the cumulative number of bubbles produced as well as the rate of formation, however continues to rise beyond the values seen in the control solutions.

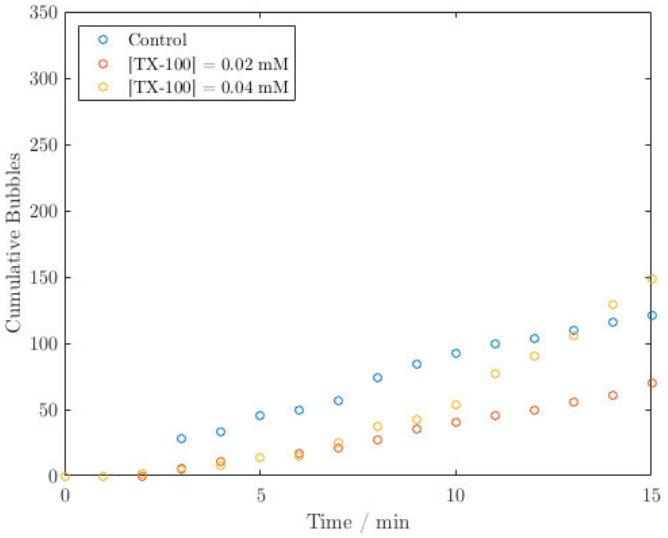

FIGURE 3.11: Cumulative bubble formation in the presence of TX-100. At low concentrations, TX-100 is effective in preventing bubble formation in the unstirred BZ reaction.

Surfactants inhibit the initial formation of bubbles by reducing the surface tension yet as the reaction still progresses in the presence of surfactants there was still the same quantity of gaseous products formed. At higher surfactant concentrations bubbles were stabilised leading to the higher cumulative totals. Surfactants at a level above the CMC affect the dynamics of the reaction in characteristic ways depending on their charge, or lack thereof.[82,114,115] Above the CMC there is the potential to form micelles around non-polar intermediates thereby changing the kinetics of some processes.[116–119] Altering the surface tension, ionic strength and viscosity of the solution may also effect a change in dynamics.[120,121]

Increasing the ionic strength (Equation 3.7) of the solution in which a surfactant is dissolved lowers the CMC. The ionic strength of a solution is defined as:

$$I = \frac{1}{2}\sum_{i=1}^{n} c_i z_i^2 \tag{3.7}$$

where z_i is the charge on each species and c_i is its concentration in solution. Ionic strength plays a role in lowering the CMC for all surfactant types including neutral and zwitterionic species.[122–125] The modified Corrin-Harkins relation (Equation 3.8) describes the change in CMC with increasing salt concentration, C_s.[126]

$$\ln \mathrm{cmc} = \alpha_s - \beta_s \ln C_s + \mathrm{cmc} - k_s\left(C_s + \mathrm{cmc}\right) \tag{3.8}$$

Where α_s is the logarithm of the equilibrium constant for the separation of the surfactant in solution between the monomeric and micellar state (Equation 3.9), β_s is the ratio of stoichiometry between counter-ion and surfactant and k_s is the salting out coefficient. This final term is typically ignored for low salt concentrations and in complex mixtures such as BZ media the value of k_s cannot be accurately estimated.

$$\alpha = lnK_{eq} = -\frac{\Delta G^\circ}{2.303RT} \tag{3.9}$$

Increasing ionic strength results in a decrease in the CMC, this relation holds true for all types of surfactant.

[NaCl] / mM	**CMC / mM**
0	6.41
100	6.21
200	5.94
500	5.64
1000	4.34
1500	4.10

TABLE 3.1: Critical micelle concentration of SDS as a function of increasing salt concentration, adapted from Chattopadhyay and Harikumar

The CMC of SDS is 8.1 mM in pure water but drops to about 2.2 mM in BZ media containing [$KBrO_3$] = 0.12 M, [KBr] = 1×10^{-4} M, [MA] = 0.01 M, [H_2SO_4] = 0.30 M, and [ferroin] = 3.4×10^{-4} M, corresponding to I = 1.051 M.[82] This is marginally lower than that used in the experiments detailed in Section 3.5.3 which had I = 1.816 M, however, the surfactant concentration used in those experiments was sufficiently low that micelles would not form or interfere with the reaction.

3.5 Experimental

3.5.1 Spiral Studies

Stock solutions were prepared from the following chemicals: malonic acid, sodium bromate, iron(ii) sulfate heptahydrate, 1,10-phenanthroline (all from Sigma-Aldrich, UK) and sulfuric acid (Riedel-de Haën). Dissolution of iron(ii) sulfate heptahydrate and 1,10-phenanthroline in 100 mL deionised water (Barnstead Diamond RO) yielded a 25 mM stock ferroin solution.

Solutions were transferred to petri dishes (⊘ 8 cm) to give a final solution volume of 9 mL and therefore a depth shallower than 2 mm preventing convective effects from altering the results.

Experiments were performed in batches where six solutions were monitored concurrently. Petri dishes were placed on a scanner (Canon CanoScan LiDE 100 / 210) and recorded for 180 minutes at intervals of no more than 40 seconds using an AutoHotKey script.

3.5.2 Image Entropy Analysis

Analysis of images utilsed the internal *entropy* command in Matlab 2015b. All images were masked prior to analysis to focus only on the reaction mixture, the script for doing so is given in Appendix A.3. All experiments were as conducted in Section 3.5.1 and images captured using the scanner method set out therein.

3.5.3 Surfactants

3.5.3.1 Control Experiments

Control solutions contained malonic acid (1.00 M, 1050 μL), sulfuric acid (2.50 M, 501 μL), ferroin (25.0 mM, 780 μL), all Sigma-Aldrich) and made up to volume in a Petri dish with deionised water (4155 μL). Addition of sodium bromate (1.50 M, 1404 μL) initiated the reactions. Swirling the Petri dishes immediately after initiation resulted in a uniform distribution of reagents. Image acquisition occurred every minute for 30 minutes and the number of bubbles analysed by eye.

3.5.3.2 Addition of Surfactants

Experimental solutions comprised malonic acid (1.00 M, 1050 μL), sulfuric acid (2.50 M, 501 μL), ferroin (25.0 mM, 780 μL) along with a surfactant (according to Table 3.2) and made up to volume in a Petri dish with deionised water. Again sodium bromate (1.5 M, 1404 μL) initiated the reactions and image acquisition occurred every minute for 30 minutes and the number of bubbles analysed by eye.

Surfactant	**[Surfactant] / mM**	**Volume of Surfactant / μL**	**Volume of Deionised Water / μL**	**[Surfactant] in Solution / mM**
Sodium AOT	2.00	600	665	0.024
		1200	65	0.048
CTAB	1.00	500	765	0.100
		1000	265	0.200
Triton X-100	0.20	500	765	0.020
		1000	265	0.040

TABLE 3.2: Experimental setup for testing the efficacy of a range of surfactants in suppressing bubble formation in the BZ reaction.

3.6 Conclusions

This chapter sought to continue the atlas of the BZ reaction by detailing the nature of the reaction in an unstirred system, largely focussing on the evolution of spiral waves with time. The initial pitch of spiral waves decreased as a function of increasing sodium bromate concentrations. Increasing the sulfuric acid concentration from 0.50 M to 0.80 M also yielded a decrease in the initial spiral pitch. When 0.25 M sulfuric acid was used in the experiment the spiral pitch varied considerably and was not directly comparable to that at the higher concentrations.

The evolution of spiral pitch is linear in the early stages of the reaction, however the system deviates from this as the solution passes through an instability towards its final steady state. The comparison of image entropy to image uniformity provided a metric by which the solution could be aged and consequently quantifying the point at which the system transitions to chaos. This method is the first reported image-based method by which such transitions and the final state of the system can be defined. As in Chapter 2 this transition to chaos is more prevalent as higher concentrations of acid and bromate are used.

Finally, this chapter reported the effects of a simple modification to the reaction medium whereby surfactants were added as a means to reduce bubble formation. In fact there were some cases in which a greater number of bubbles were produced by the system suggesting a stabilisation of the bubbles being formed. Although there is some indication in the literature that surfactants can affect the kinetics of the BZ reaction, the ionic strength of the solution in the experiments reported in this chapter meant

that the surfactants were added at a concentration below the CMC level and there was no evidence that the surfactants interfered with the reaction kinetics since the rate of formation of gaseous products, *e.g.* CO_2, was seemingly unaffected by their presence. As a result, it can be stated that the reaction network of the iron-catalysed BZ reaction is robust enough to endure the presence of low-level co-solutes.

Chapter 4

Use of Gelling Agents to Reduce Diffusion

Chapter 2 and Chapter 3 dealt with the typically studied stirred and unstirred BZ systems including the effect of modification to the reaction medium through the addition of surfactants. This chapter concludes the atlas of the reaction by investigating the use of a gel in place of a homogeneous solution as well as how this expands our understanding of complex reaction networks in crowded media.

Parts of this work was undertaken in collaboration with James Pugh and Ruben Green as part of their Final Year Undergraduate Projects.

4.1 Applications of Macromolecular Crowding

There are two main areas where a greater understanding of the effects of a crowded system on chemical reaction networks is useful, namely in the fields of biologically-inspired robotics and biochemical systems research. These create a greater awareness of our world on a macro- and microscopic level respectively.

4.1.1 Biologically-Inspired Robotics

Most of the robots ever developed comprise mechanical and electronic parts.[127] By contrast, animals with soft structures have existed throughout evolutionary history; some are completely boneless consisting solely of muscle, fluids and hydroskeletal features. These types of animal move by manipulating their environment or by expansion and contraction of muscle. Even for animals with rigid endoskeletons soft tissues and fluids take up a larger part of body mass than skeleton.[128,129]

It is possible to replace electrical components with isolated chemical systems and mechanical components with soft materials.[130,131] The aim of such steps is to produce a new link between traditional bio-mimetic robotic techniques and the natural world through utilisation of soft robotics. Soft robotics afford opportunities that conventional robotics cannot.[129] As they are typically formed from elastomeric materials they tend to have deformable structures that are capable of dealing with dynamic environments or grasping unknown objects.[130]

In recent years a number of groups have been working towards the generation of motion in soft robots by a variety of methods such as liquid pressure, electric field gradients, light-sensitive materials, hydrophobicity/hydrophilicity there is also interest in the use of reactive gels in robots capable of providing a suitable driving force for a sustained period of time.[132–135] Of note is the increased use of BZ gels as a potential source for such a driving force; by confining the reactions to a gel system it has been established that a chemomechanical swelling of approximately 5% is possible without flow and under a continuous flow a 163% volume change can occur.[136–138] Since this expansion and contraction is related to the oxidation and reduction of the transition metal catalyst it is theoretically possible to control the behaviour of the gel. By manipulating the shape of the gel and modifying the catalyst novel uses and increased biomimicry are being reported.[139–141] However, gel composition and the local environment of the catalyst both alter the behaviour of the oscillator by modifying the rate of diffusion of reactive species consequently a greater understanding of these systems is necessary.

4.1.2 Biochemical Systems

Cells have a high proportion of macromolecular species, between 20 and 30% of a cell's mass and volume is occupied by macromolecules such as proteins, DNA, ribosomes and membranes.[67,142] Crowding of this nature *in vivo* is known to alter the rate and equilibrium constants of biochemical species by an order of magnitude with possible implications on metabolic processes and function.[142–146]

A majority of biological catalysts are enzymatic species which diffuse through cells and so provide a perfect example of how complex reaction networks respond in crowded environments. By hindering diffusion of reaqents in the BZ system through the presence of gel matrices a system that is analogous to the biological construct is set up.

4.2 Gels

Reactive gels in the literature are organic based and fall into two main categories concerning the method by which the catalyst is incorporated: covalently-bound and electrostatically-bound. When it comes to the iron-catalysed system covalently-bound

reactive gels are a relatively new development. The use of a covalently-bound gel has the benefit of having a permanently held catalyst whose oscillations directly drive the expansion and contraction of the gel, providing a higher force than electrostatically-bound systems. However, these are costly and time-consuming to produce. An example of such a system has been demonstrated by Hara *et al.* using poly(*N*-isopropylacrylamide) (pNIPAAM) covalently bonded to a modified $Fe(bpy)_3$ catalyst moiety.

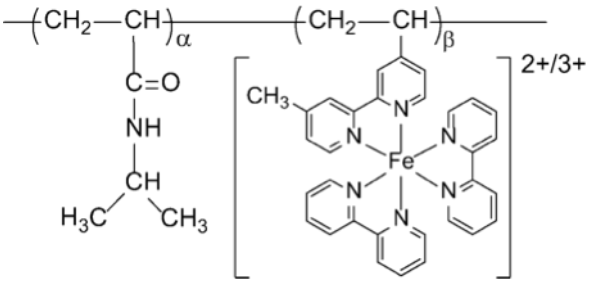

FIGURE 4.1: Example of covalently-bound catalyst as used byHara *et al.*.

Gel systems are a common feature of research into the BZ reaction and were used here to slow the rate of diffusion of the electrostatically-bound catalyst. Many groups have reported the use of covalently-bound catalysts to cause swelling and deswelling of a gel.[136,148–151]

Electrostatically-bound catalysts are less effective yet can be produced more easily and on a larger scale. Nonetheless some methods of incorporation require the gel to be made over a period of ~ 15 days. This thesis explores methods by which reactive gels can be produced quickly, cheaply and still able to create effective oscillations by utilisation of an iron-catalysed BZ reaction and therefore readily available to study reaction dynamics in biologically relevant systems.

The first concern in generating such a system was to develop a method in which all of the components of the gel could be distributed uniformly and without initiating any further reactions. Experiments have looked into the effect of different gel compositions (as a weight-by-volume (w/v) concentration) and depth of the gel, as well as using an array of different initial reagent concentrations. In all cases, the concentration of sulfuric acid was optimised to ensure a strong gel consistency while the concentration of ferroin was kept constant.

Testing various high molecular weight organic gelling agents gave a better understanding of how gel thickness and composition can alter the reaction dynamics. Gelatin, ι-carrageenan, Xanthan gum, sodium alginate, poly-N-isopropylacrylamide (all Sigma-Aldrich, UK) and Laponite-RD (Rockwood Additives Ltd, UK)[152] were all considererd and tested for stability under the highly acidic and oxidising conditions present in the BZ reaction. Of these gelatin-based gels showed the most promise.

4.3 Gelatin

Gelatin is a protein composed of Gly-X-Y triplets where X and Y are often proline or hydroxyproline residues, which result in a triple helical structure and its ability to undergo gelation.[153] Alanine, arginine, aspartic acid and glutamic acid are also all present in the peptide sequence at levels greater than 5 g / 100 g of dry ash-free protein.[154]

The relatively high proportion of amino acids with carboxylic acid termini means that there is a large amount of readily oxidisable material that can act as the organic substrate within the BZ reaction when another suitable substrate is absent. On addition of bromate to a malonic acid-free gel a monotonic oxidation of the gel occurred with no visually distinguishable oscillations. The presence of malonic acid in a gelatin gel resulted in the typical patterns observed in unstirred BZ systems. Therefore any potential competitive side-reactions with gelatin must happen at a lower rate than for malonic acid and subsequently such reactions were not a major concern in studying the reaction dynamics.

4.3.1 Velocity of Wave Propagation in a Gelatin Medium

Wave propagation velocity in the BZ reaction in any medium is dependent on the initial concentrations of bromate and sulfuric acid.[3] The velocities observed for wave propagation in homogeneous systems are well established and are consistent across the literature, the example in Equation 4.1 here is as reported by Wood and Ross,[155]

$$\nu = -3.2 + 28.3\chi \tag{4.1}$$

where ν is the initial wave velocity in mm.min^{-1} and

$$\chi = \sqrt{[H_2SO_4][BrO_3^-]} \quad / \quad \text{M} \tag{4.2}$$

enables comparison between systems.

The same is true where the catalyst is localised on polystyrene beads and taking into account the additional distance travelled by the reactants around the beads results in Equation 4.3. With gradients of 28.3 mm.min^{-1}.M^{-1} and 23.7 mm.min^{-1}.M^{-1} respectively for the homogeneous and localised catalyst systems the velocities of the systems are comparable.[85]

$$\nu = -2.45 + 23.7\chi \tag{4.3}$$

Utilising gelatin as the reaction medium slowed the rate of initial wave propagation compared to a homogeneous solution yet there was still a linear increase in velocity as the sodium bromate concentration increased. Figure 4.2 compares the data obtained for a 10% gelatin w/v ([G]) medium to that observed in the homogeneous and localised catalyst systems. Since there were no geometric considerations to apply here that could account for the lower rate of propagation a relationship between the concentration of gelatin and the rate of wave propagation was inferred.

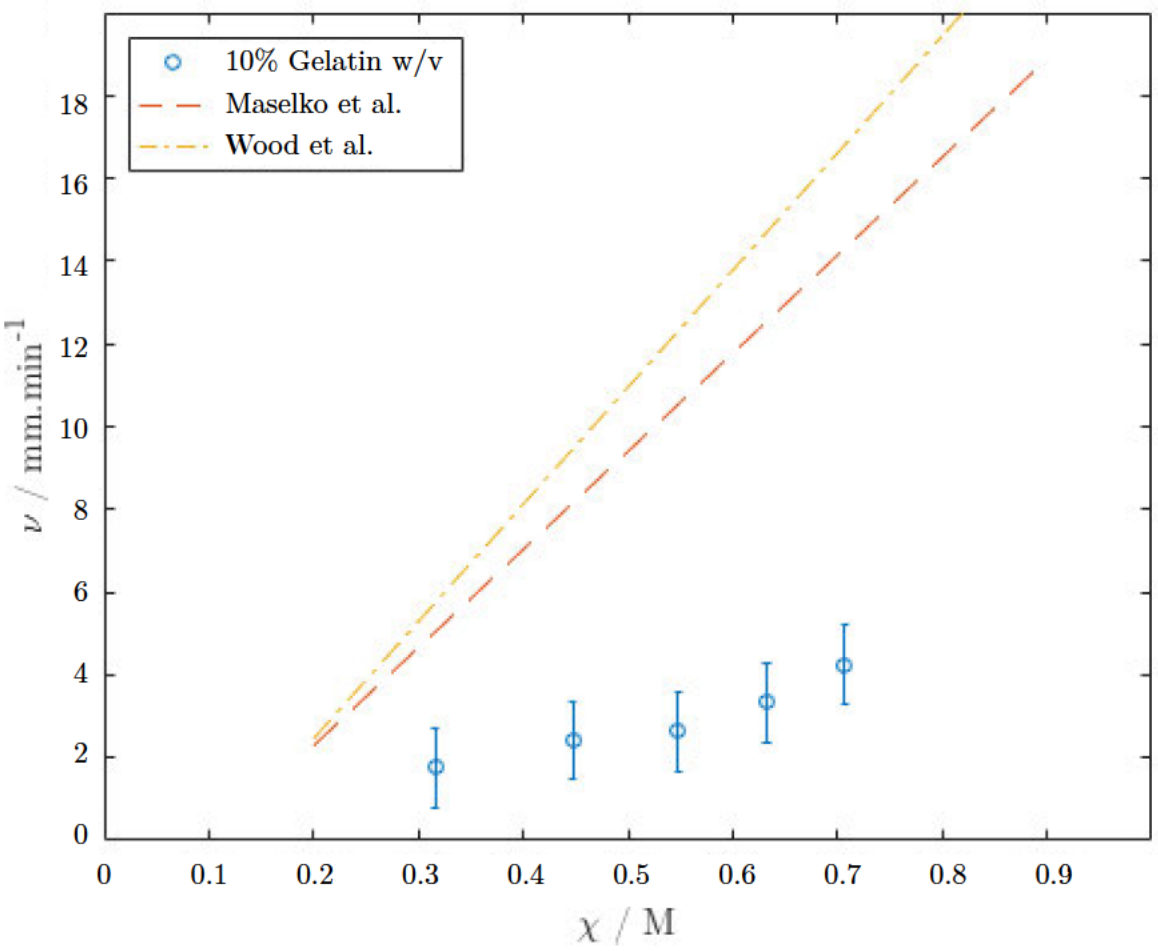

FIGURE 4.2: Comparison of data for homogeneous solutions as reported by Maselko *et al.* (–·) and Wood and Ross(–) with that observed for a 10% gelatin medium.

4.3.1.1 Dependence of Wave Velocity on Gelatin Concentration

Gelatin is a long-chain, high molecular weight protein obtained from partially denatured collagen.[156,157] On gelation a network of closely interwoven threads form, leading to pores within the gel structure, which can act as a sieve and obstruct large molecules.[158,159] Increasing the concentration of gelatin in a system results in a decreasing mesh size, ξ, of the gel and plays an important role in limiting diffusion.[160]

Pezron *et al.* reports the values in Table 4.1 as the dependence of mesh size on gelatin concentration, as determined by small-angle neutron scattering in a 0.1 M sodium chloride solution.

[G]	**Mesh Size, ξ / Å**
1% w/v	70 ± 10
2% w/v	51 ± 5
5% w/v	35 ± 3

TABLE 4.1: Mesh size dependence on gelatin concentration, adapted from Pezron *et al.*.

When using gelatin in pure water other literature values state that ξ can be as small as 50 Å in a 1% [G] solution.[158,162] Although a 1% [G] gel has a mesh size far greater than the hydrodynamic radius of any species in the reaction mixture it is still possible for diffusion to become limited as [G] increases.

Figure 4.3 suggests a power law relation between [G] and initial wave velocity (Equation 4.4). This provided the basis for the subsequent analysis in Section 4.3.1.2

$$\nu = 5.9439\,[G]^{-0.4468} \tag{4.4}$$

4.3.1.2 Effect of Increasing Bromate Concentration at Different Gelatin Concentrations

At or below 1% [G] it can be assumed that the system is effectively dilute since the pore size is larger and therefore no longer hindering molecular diffusion.[161] From this, and data at 10% [G], a series of theoretical curves were produced from Equation 4.5 which predicts the initial wave velocity in gelatin, ν_g, given the velocity in water, ν_w and inital concentration of acid and bromate, χ, as shown in Equation 4.2.

$$\nu_g = \nu_w(\chi^{-0.6}) \tag{4.5}$$

Using the values obtained by Wood and Ross and Maselko *et al.* detailed in Section 4.3.1 together with Equation 4.5 suggests that for a 10% [G] medium waves will propagate according to Equation 4.6.

$$\nu_g = -0.710 + 6.53\chi \tag{4.6}$$

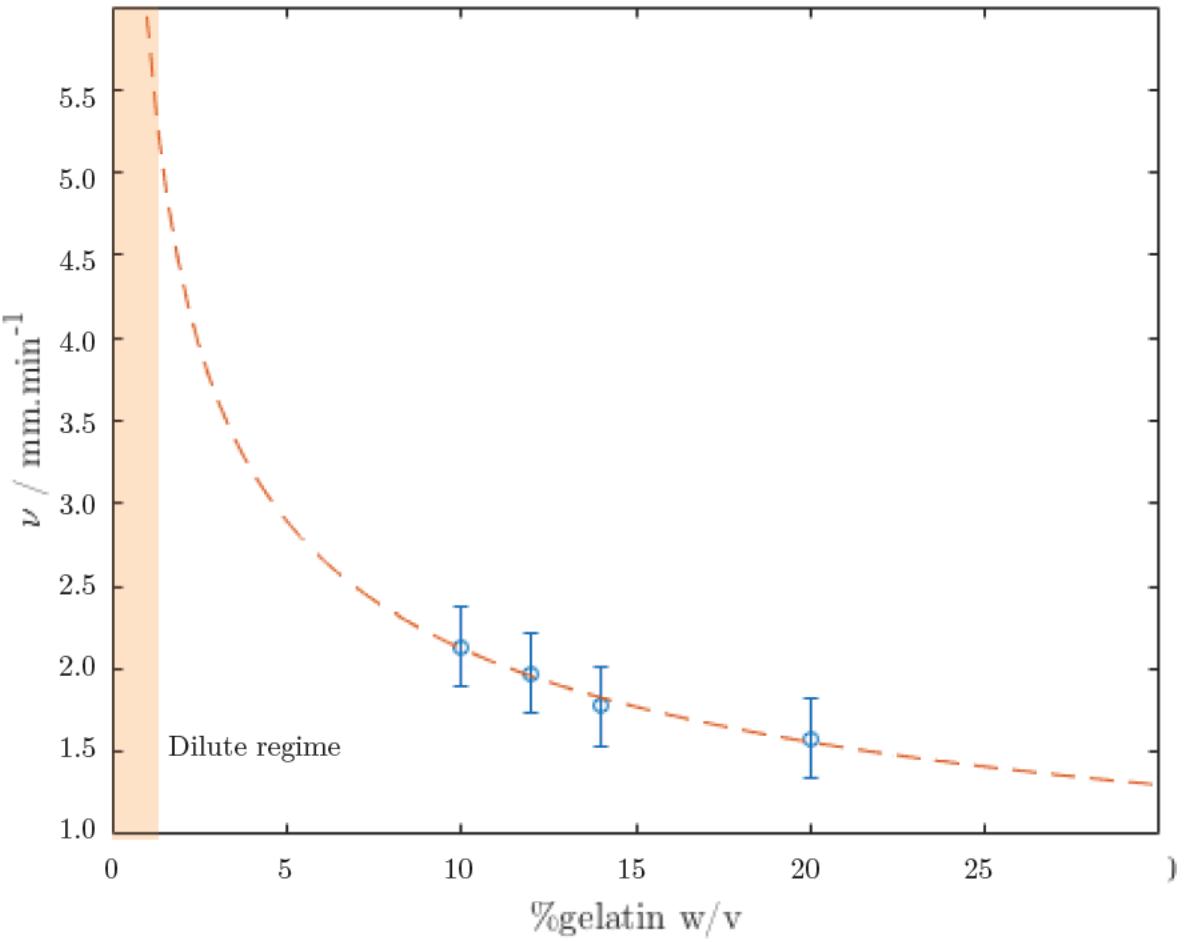

FIGURE 4.3: Relationship between wave velocity and gelatin concentration. Increasing the concentration of gelatin reduces mesh size and effectively limits chemical diffusion.

In producing the theoretical curves (Figure 4.4) for increasing gelatin concentration, ν_w was taken to be the average of experimental values seen for homogeneous (Maselko *et al.*) and localised catalyst (Wood and Ross) systems, since the $\leq$ 1% [G] system should fall in this dilute region. The data obtained for experiments at 10% [G] fit the theoretical relationship as seen in Figure 4.4.

Thus the retardation of waves is primarily due to a decreasing gel mesh size. There may also be some interplay between the amino acid residues in gelatin with the ionic species in the reaction; gelatin is known to bind metal ions, being the basis of its use in the photographic industry, yet this was deemed to play only a small role in limiting diffusion.[156,157,163]

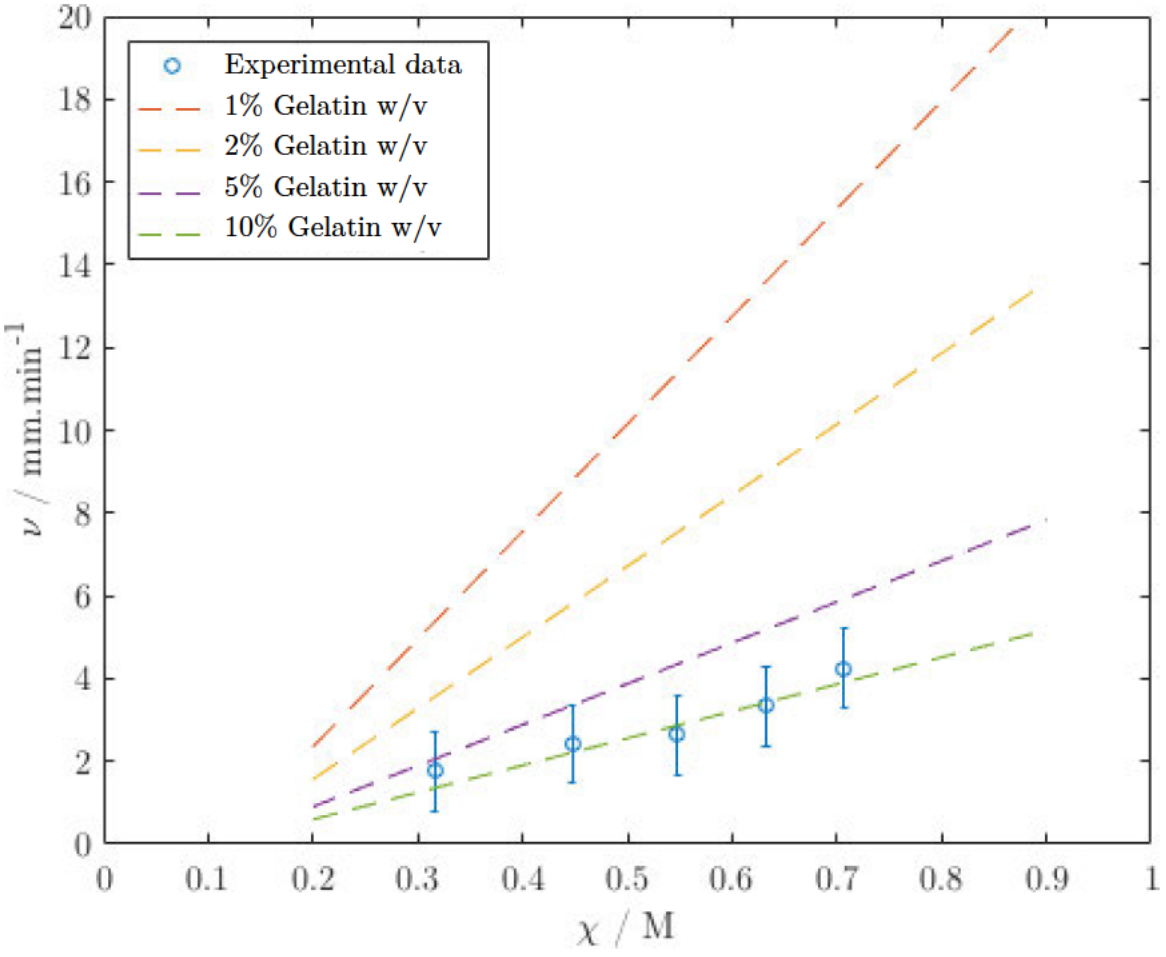

FIGURE 4.4: Theoretical curves for gelatin concentrations 1% to 10%. When using a 10% w/v gel the wave velocity matches that predicted by mesh size.

4.4 Gelatin Spiral Studies

On increasing the bromate concentration (0.2 M to 0.4 M) at a constant gelatin concentration (10% w/v)the initial spiral pitch remained relatively constant (around 0.03 cm/min^{-1}), in line with what was observed in the previous chapter. The results were suggestive that gelatin plays little role in the aging of the solution.

Experiments where the gelatin concentration was increased from 0% to 20% confirmed this hypothesis. The initial spiral pitch, Λ_0, is unchanging during the linear phase with increasing gelatin concentration as evidenced by Figure 4.5.

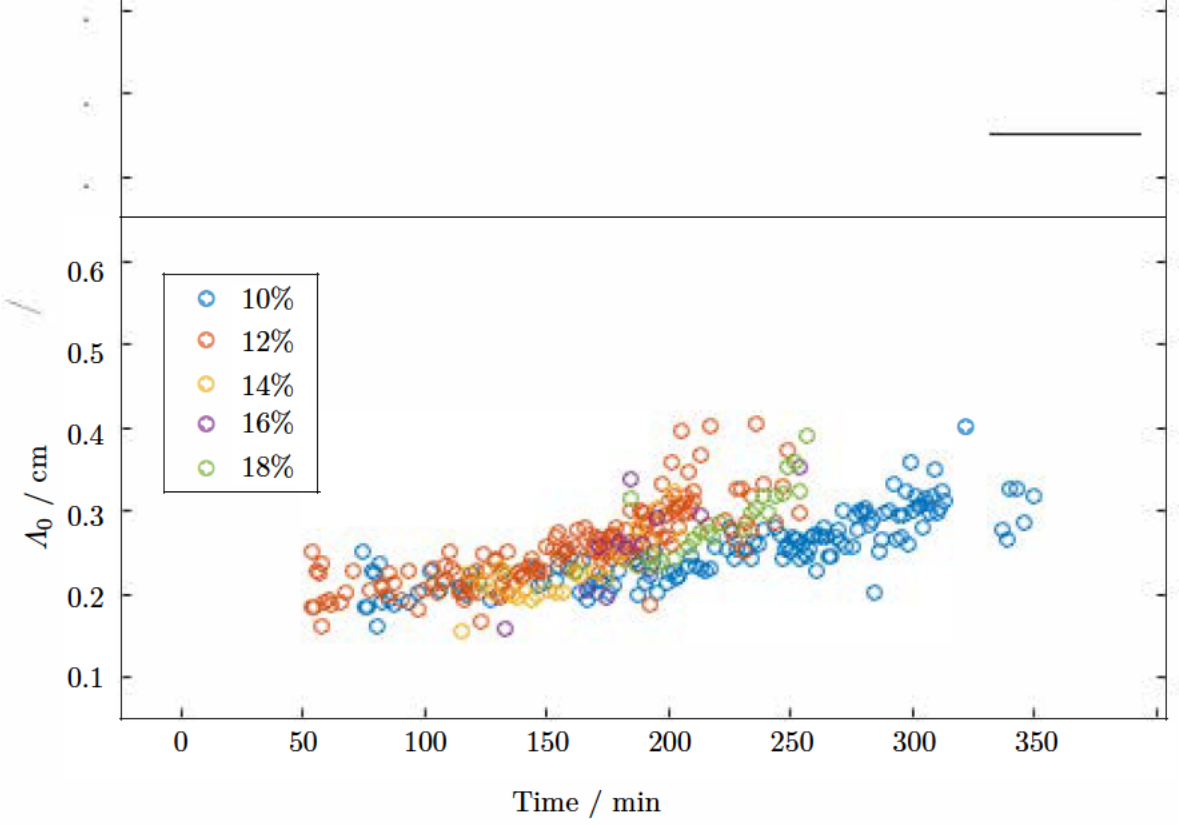

FIGURE 4.5: Evolution of spiral waves in a gelatin-based medium of varying gelatin composition (10 - 20 % w/v), $[H_2SO_4] = 0.50$ M, $[BrO_3^-] = 0.40$ M, [MA] = 0.10 M and [ferroin] = 2.0 mM. Little difference is observed in the linear phase of spiral growth.

4.5 Alternative Reaction Media

Laponite-RD had poor reproducibility and bubble formation affected observation of oscillations. Both pNIPAAM and ι-carrageenan were rejected due to the complexity of producing the gels. Therefore xanthan gum (Section 4.5.1) and gelatin (Section 4.3) proved to be the most appropriate gelling agents for studying oscillations in a crowded medium.

4.5.1 Xanthan Gum

Xanthan gum Figure 4.6 is typically used as a food stabiliser due to its ability to form hydrogels across a broad pH range (pH $\leq$ 8).[164,165] It was this stability at low pH that suggested its potential use in the creation of an effective gel medium, seeing as the BZ reaction takes place in highly acidic conditions (pH $\leq$ 4).

Xanthan gum-based gels were produced according to the procedure in Section 4.6.3. On addition of sodium bromate to xanthan gum gels containing all BZ reagents, the reactions progressed rapidly with few observable waves; the high concentration of sulfuric acid (1.0 M) required may have been a contributory factor. Although there were clear oscillations in such experiments the gels degraded rapidly via oxidation of the xanthan gum as evidenced by formation of CO_2 bubbles (Figure 4.7). Furthermore, the process by which the gels were produced (Section 4.6.3) could have led to decomposition and subsequent reaction of the monomer units.

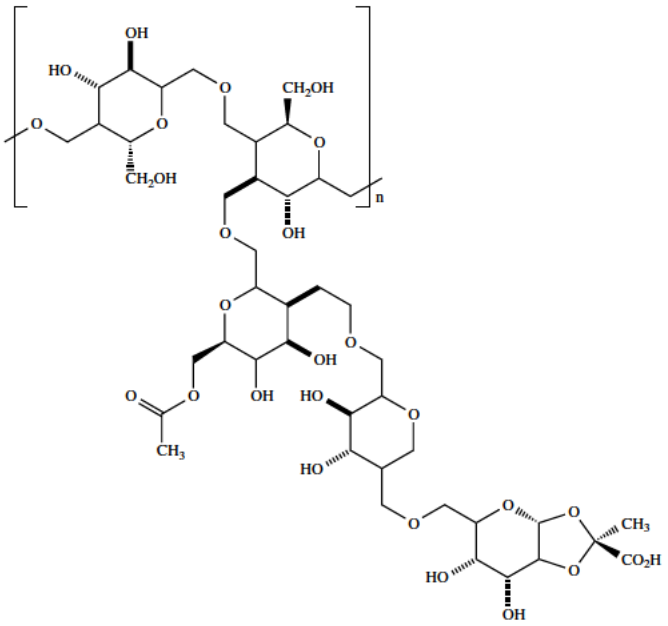

FIGURE 4.6: Xanthan gum ($C_{35}H_{49}O_{29}$) repeat unit, n

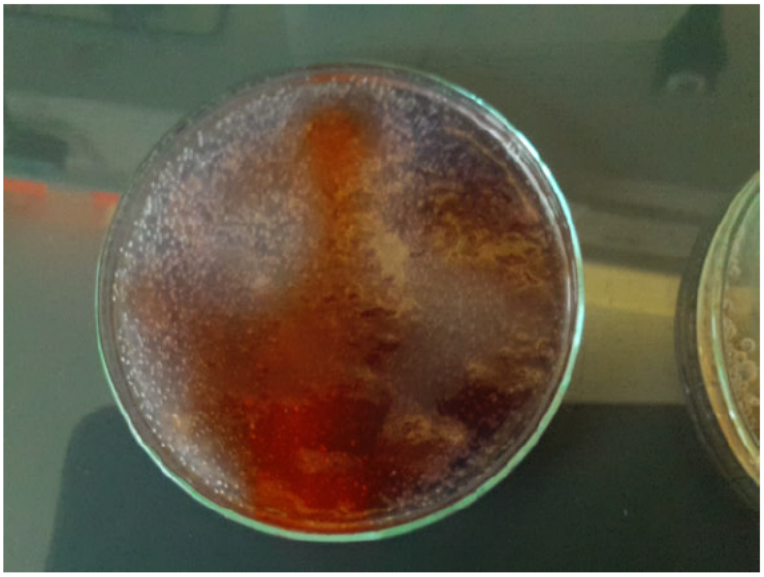

FIGURE 4.7: Formation of CO_2 degraded gel structure and thus caused a significant issue when trying to design a suitable gel.

4.5.2 Paper

Gels are not the only method for studying the Belousov-Zhabotinsky reaction. Cellulose filter paper offers a microscopically thin surface allowing for diffusion solely in two dimensions. Preliminary investigations on paper demonstrated the reaction can proceed and oscillate, which matches with the observations in experiments performed with bulk cellulose as well as examples from the literature that utilised cellulose membranes. However, there was the potential for oxidation of the C6-hydroxyl group to a carboxylic acid

by acidified sodium bromate. Consequently, this side reaction could have lead to further reactions in place of the organic acid substrate.

Protecting groups were considered to overcome this potential issue. Soaking a filter paper in acidified bromate for 3 hours resulted in a yellowing of the paper and after 48 hours the paper had degraded, without bromate there were no signs of degradation and likely resulted in cellulose sulfate (Figure 4.8) rather than the oxidised cellulose.

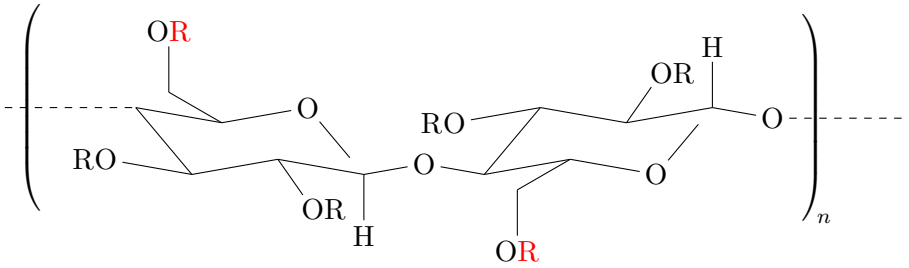

FIGURE 4.8: Structure of the modified cellulose polymer after reaction with sulfuric acid. Here R = SO_3H or H depending on the extent of the reaction. The C6-hydroxyl is highlighted in red as the most likely position of reaction.

When using the paper treated with sulfuric acid was used as the medium for the reaction there was an increased colour contrast and no effect on the reaction; this is an effective method for protecting the cellulose.

4.6 Experimental

4.6.1 Gelatin Experimental

Gelatin was weighed out and dissolved in the minimum amount of hot (65 °C) distilled water (Barnstead RO, 42.0 mL). Malonic acid, sulfuric acid were added to the solution and vortexed to ensure homogeneous mixing. Lastly, ferroin was added to the solution and the solution made up to the desired volume with water. Gels were poured into a petri dish (⌀ 80 mm) and cooled overnight in a fridge resulting in a homogeneous gel. A second set of gels were produced without any malonic acid to determine whether there was an interaction between gelatin and sodium bromate.

4.6.2 Preparation of Gels

Gels were made up in glass Petri dishes (⌀ 80 mm) before the addition of sodium bromate to initiate the reaction. A scanner (Canon LiDE series), controlled by an AutoHotkey script, captured images of six Petri dishes every 20 s or 40 s simultaneously for approximately 3 hours. This methodology ensured a constant illumination of the samples and enabled direct comparison between them.

4.6.3 Xanthan Experimental

Initial experiments showed that in order to prevent clumps of gel forming the xanthan gum needed to be dissolved slowly in acid and water at high temperatures ($\geq 60\,^{\circ}\mathrm{C}$) while stirring. Xanthan gum at a quantity of less than 1% w/v leads to a highly viscous fluid rather than a gel, while a 5% w/v gel yielded a gel that is too thick and impermeable to the addition of sodium bromate solution, as such gels of a thinner consistency were produced. This ensured that an even oxidation of the gel occured. Figure 4.9 gives an example of oxidation in an initial experiment using a 2% w/v gel, subsequent experiments used a 1% w/v gel formed by the process below.

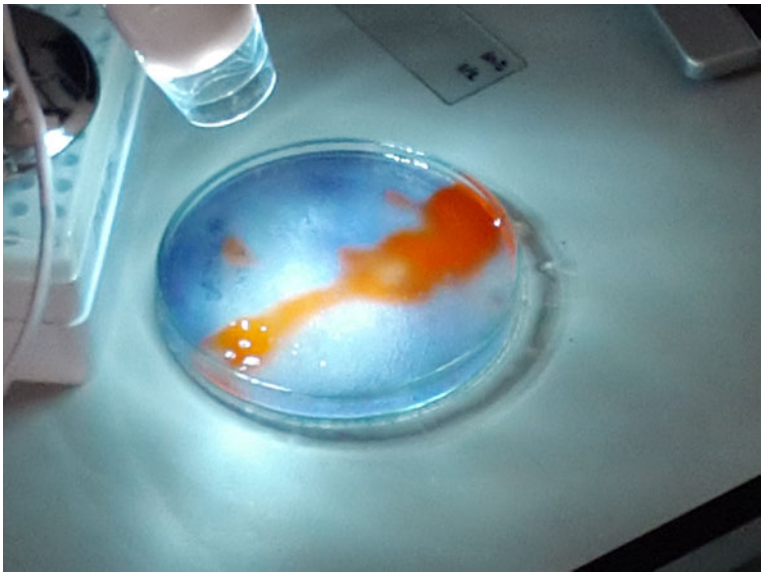

FIGURE 4.9: Uniform oxidation of a 2% w/v xanthan gel containing 1.0 M H_2SO_4, 0.1 M malonic acid and 2.0 mM ferroin. The reaction had been initiated with 0.2 M sodium bromate solution.

An RBF fitted with a condenser was placed in an oil bath at 75 °C. Distilled water (Barnstead RO, 42.0 mL), H_2SO_4 (5.0 M, 12.0 mL) and malonic acid (1.0 M, 6.0 mL) were added and xanthan gum (3.0 g) was added over 72 hours. Once the powder had completely dissolved, the gel was transferred to three petri dishes (⊘ 80 mm) resulting in gels (10 mL) containing 0.1 M MA, 2 mM ferroin and 1.0 M H_2SO_4.

4.7 Conclusions

This chapter finalised the atlas by modifying the reaction medium to use a gel, most commonly gelatin, in place of an aqueous solution. This has demonstrated that gels containing an electrostatically-bound catalyst are simple to produce as well as effective modifiers of Belousov-Zhabotinsky systems. The calculated mesh size of the gelatin gel suggested that the initial wave velocities should slow as a function of gel concentration yet still increase with added sodium bromate. There was strong agreement between the

model and the experimental results with the 1% [G] closely matching the data for a homogeneous system, as was implied from the theory set out by Pezron *et al.*. This method of incorporating the catalyst is far more effective at reducing the initial rate of wave propagation in comparison to a system in which the catalyst is immobilised on beads.

Experiments exploring the effect of gelatin concentration on the pitch of BZ spirals determined that there is no change in the initial spiral pitch and that the gradient during the linear phase is similar across gelatin concentrations. This showed that the spiral behaviour was dependent solely on the reagent concentrations and that the gelatin played no role in the actual reaction. The only difference observed was in the time taken for oscillations to begin, with a slight delay observed for higher gelatin concentrations. This effect shows that non-competitive molecular crowding has the potential to inhibit the onset of reactions but once started the reactions should progress according to their normal reaction pathways.

Modelling Belousov-Zhabotinsky Reactions and the Relationship with Biochemical Systems

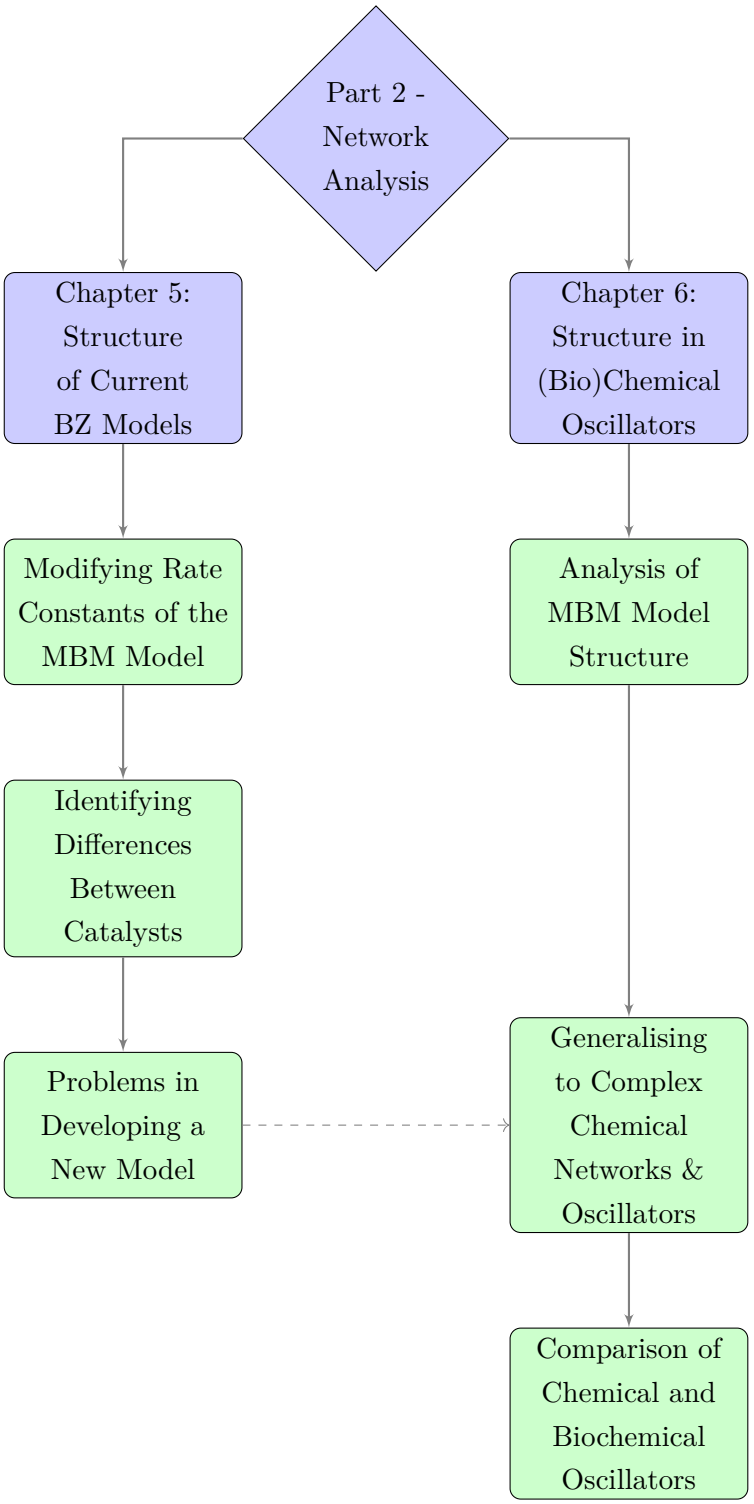
Part 2 - Network Analysis
Chapter 5: Structure of Current BZ Models
Chapter 6: Structure in (Bio)Chemical Oscillators
Modifying Rate Constants of the MBM Model
Analysis of MBM Model Structure
Identifying Differences Between Catalysts
Problems in Developing a New Model
Generalising to Complex Chemical Networks & Oscillators
Comparison of Chemical and Biochemical Oscillators

Chapter 5

Comparison of Existing Models to the Iron-Catalysed System

Chapter 2 discussed models of the BZ reaction proposed in the literature, of these the most comprehensive mechanistic approach is provided by the Marburg-Budapest-Missoula model.[50] However the model was developed for the cerium(IV)-catalysed system and is known not to match the iron(II)-catalysed system.[50,56] The long initial induction period of the cerium(IV) BZ reaction prior to the oscillatory regime is a prime example of a feature which is present in the cerium system but not the iron-catalysed reaction. The higher oxidative strength of cerium(IV) compared to iron(III) results in differences in mechanism, as is true with any of the other catalysts that have been studied.[32,33] Nonetheless, the BZ reactions are characterised by an oxidation of an organic substrate resulting in the formation of stable organic products and gases. The extent to which the system forms CO_2 varies with each catalyst used, the same result is observed in other oscillating systems such as the BR reaction. If inorganic radicals such as $BrO_2^{\bullet}$ always formed first in every oscillator then the resulting CO_2 concentration ought to be comparable for different catalysts ions, it is possible that organic free radicals form by reaction with the coordination sphere of the metal ion as has been observed with malonic acid.[166,167] Consequently, only some of the single electron transfer reactions directly involving the organic species and catalyst ought to be affected. An oscillating system can be constructed logically and so it is possible to determine not only the reactions in observed mechanisms that cause differences but also find whether the difference is due to a change in rate constants or through the presence of a hitherto unknown reaction or intermediate.[168]

5.1 An Algorithmic Approach to Modifying the MBM Model

The Marburg-Budapest-Missoula model does not accurately depict the behaviour of the iron-catalysed reaction system yet overall it should exhibit similar features. If the reaction mechanism only differed in the rate at which elementary reactions proceeded within the MBM model then it should have been possible to modify the rate constants for the cerium-catalysed model to produce an accurate model for the iron-catalysed system.

If the MBM model were to be modified to fit with data obtained from the atlas set out in Part 1 of this thesis then 61 rate constants required simultaneous optimisation. Typical unidirectional (vector-based) or steepest descent (gradient-based) methods would be inefficient since these are usually constrained to 2 or 3 dimensional optimisation problems.

Swarm intelligence (SI) algorithms provide a more appropriate means of simultaneously optimising multiple variables and were first proposed in 1993.[169] These algorithms are inspired by natural flocking and hunting patterns, unlike evolutionary algorithms the previous search results are remembered between iterations and so quickly converge on the best results.[170]

Since the rate constants in the reaction model span several orders of magnitude a random search was also unlikely to converge on a satisfactory result. As such a swarm intelligence approach is more computationally efficient.[171,172] The grey wolf optimiser (GWO) was selected as the method for the analysis. The GWO mimics the leadership heirarchy and hunting mechanisms of grey wolves and allows for fast convergence through using multiple search agents.[170] Although it would appear that the only difference between the systems is the catalyst and thus only affecting the reactions that involve single electron transfer processes the stability of the products and the electrochemical potential of the alternative catalyst has repercussions across the entire chemical network - as such a complete approach to the system had to be explored.

5.1.1 Definining a Fitness Metric

A fitness metric defines the extent to which an optimisation algorithm produces a solution to a problem; therefore how well an optimisation algorithm runs is dependent on the suitability of the metric to the situation and consequently how quickly the algorithm converges on the best possible result.[173] Given this work was comparing a simulated to experimental dataset a correlation function was deemed the most suitable metric.

Pearson's correlation coefficient has great utility when comparing linearly related datasets. However, when looking at oscillating time series data this method of correlation can fail and provide spurious correlation results since it relies on the arithmetic mean of the series. The analysis carried out in this thesis implemented an alternative correlation coefficient postulated by Erdem *et al.*, $\hat{\rho}_o$, in which the problems of Pearson's correlation coefficient are avoided, the metric is given in Equation 5.1.[174]

$$\hat{\rho}_o = \frac{A_{xy}}{\sqrt{A_x^2 \cdot A_y^2}} \tag{5.1}$$

where $A_x^2 = \frac{1}{T-1} \cdot \sum_{t=2}^{T}(X_t - X_{t-1})^2$, $A_y^2 = \frac{1}{T-1} \cdot \sum_{t=2}^{T}(Y_t - Y_{t-1})^2$ and $A_{xy} = \frac{1}{T-1} \cdot \sum_{t=2}^{T}(X_t - X_{t-1})(Y_t - Y_{t-1})$, with T being the length of the time series in seconds and A_{xy}, A_x^2 and A_y^2 are the correlation functions of dataset X_t and Y_t.

5.1.2 Validating the Optimisation Method

As an initial test of the robustness of the GWO, the conditions used by Hegedűs *et al.* were input into the cerium-catalysed MBM model with the rate constants set to random values in the range $k \pm 0.1k$, where k is the literature value for the rate constant.[50]

Not only should an optimisation algorithm be accurate it should also be fast in the convergence to a result. Table 5.1 shows the constraints applied to the rate constants, the number of iterations required to reach an acceptable level of correlation ($\rho = 0.95$) and rate of improvement observed. As the search space widens the convergence rate decreases linearly. The presence of local maxima in the fitness metric meant that a search agent would remain fixed until new stable point was found in the search space. With a widening search space the distance to that next maximum increases resulting in the observed drop in improvement.

By seeding the generation of random values for the rate constants at the beginning of the simulation there is an element of repeatability to the simulations. However the algorithm is non-deterministic hence the broad range of results observed while validating the optimisation method. The use of a fixed k run prior to the other experiments demonstrates that the algorithm provides no errors in its initialisation.

Results of an further optimisations are shown in Figure 5.1 and suggested a high degree of accuracy, $\hat{\rho}_o > 0.95$, when the intial conditions were varied.

k_{lower}	k_{upper}	Average Iterations	Average Improvement
k	k	1	-
$0.90k$	$1.10k$	237 ± 2.94	$(1.25 \pm 0.15) \times 10^{-3}$
$0.75k$	$1.25k$	190 ± 67.3	$(1.87 \pm 1.17) \times 10^{-3}$
$0.50k$	$1.50k$	247 ± 3.77	$(1.04 \pm 0.22) \times 10^{-3}$
0	$2.00k$	250 ± 0.00	$(0.12 \pm 0.12) \times 10^{-3}$

TABLE 5.1: Results from repeat runs of the GWO. Average iterations required to reach $\rho = 0.95$ are reported along with the average improvement on each iteration as well as the standard deviation for each. The rate of improvement drops linearly as the range of possible k values widens.

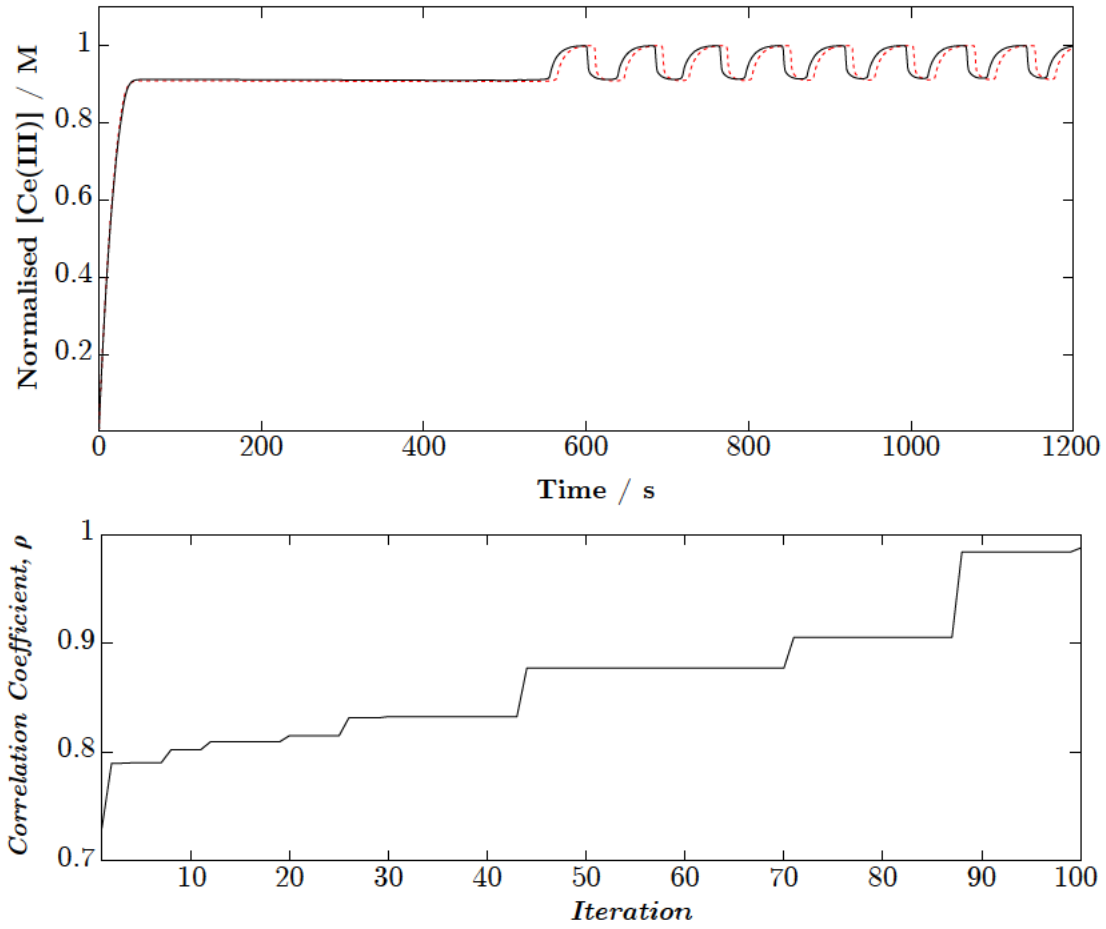

FIGURE 5.1: Comparison of the experimental data to simulations using the Marburg-Budapest-Missoula model and GWO method when constrained to $k \pm 0.1k$: (top) correlation curve at each iteration step and (bottom) overlay of simulated data using rate constants obtained from the grey wolf optimiser (red) on experimental data (black). Data was normalised prior to correlation; $[H_2SO_4] = 0.5\,M$, $[NaBrO_3] = 0.4\,M$, $[Ce(IV)] = 0.004\,M$, $[MA] = 0.2\,M$.

Figure 5.2 shows the results of the optimisation algorithm for $k \pm k$. As expected, the degree of fitness was lower than observed above with a lower range of possible rate constants but still managed to converge on a result that yielded oscillatory behaviour.

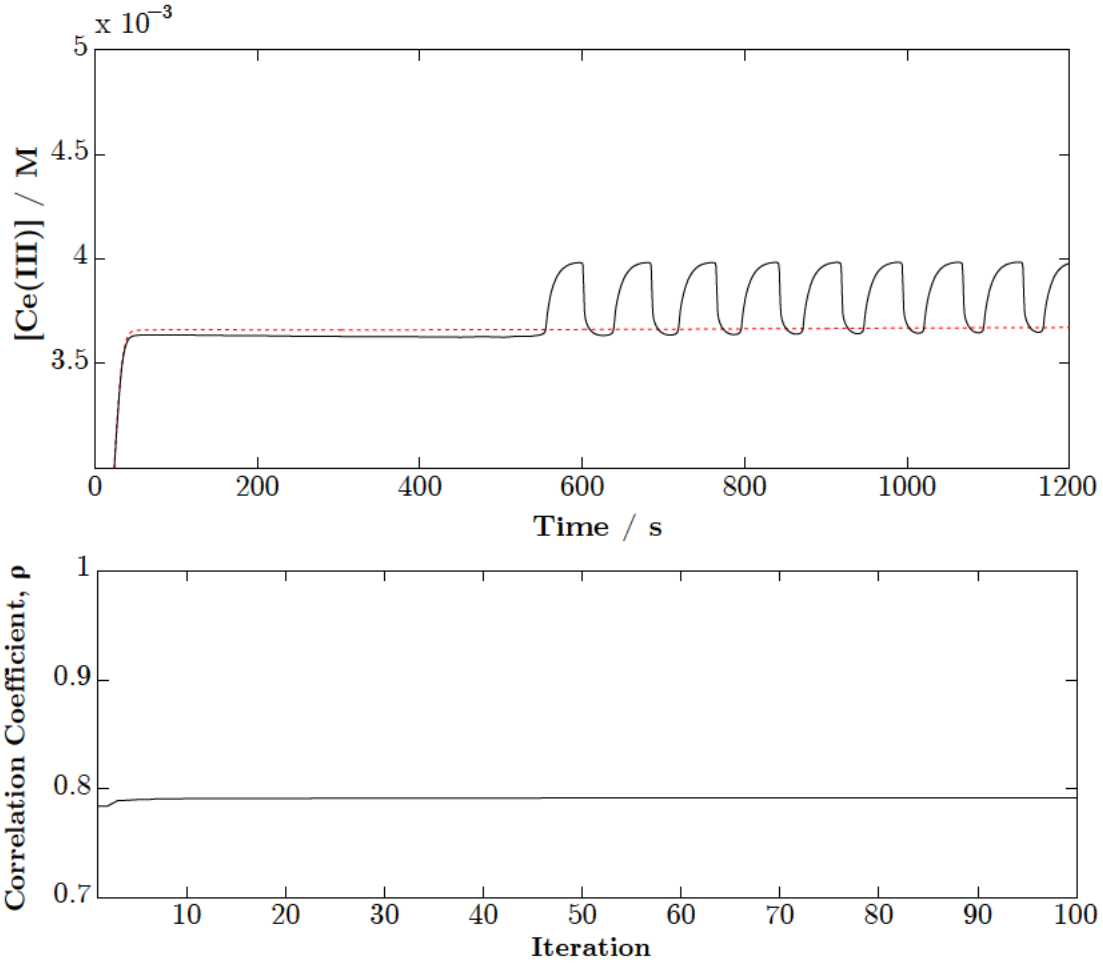

FIGURE 5.2: Comparison of the experimental data to simulations using the Marburg-Budapest-Missoula model and GWO method when constrained to $k \pm k$: (top) correlation curve at each iteration step and (bottom) overlay of simulated data using rate constants obtained from the grey wolf optimiser (red) on experimental data (black).

It can be inferred from these results that there is no singular set of rate constants responsible for the behaviour observed, while many of the rate constants in the model are experimentally determined not all of them are. As such there is scope for a computer based method to find a new set of rate constants that fits the iron-catalysed BZ system.

5.1.3 Open-Ended Simulation

With all 61 variables able to be selected in the range $k = 0 - 1 \times 10^{13}$ the simulation failed to converge on the expected data since the result of the solver would fall outside of

the software's in-built tolerances, furthermore the level of computation required is prohibitive. Consequently, a strategy to minimise the number of variables being optimised simultaneously was devised.

5.2 Identifying Causes for Differences Between Models

An obvious difference between the iron-catalysed Belousov-Zhabotinsky reaction and that catalysed by cerium is the shortening of the induction period (IP) when using an iron catalyst. A cerium-catalysed reaction can have induction period of up to 10 minutes whereas the induction period is less than 1 minute for the iron-catalysed reaction. Having established that a completely free choice on rate constants in the Marburg-Budapest-Missoula model was computationally inefficient even for the cerium-catalysed system it would therefore be impossible to replicate the dynamics of the iron-catalysed reaction effectively by this method. As such reactions were systematically eliminated from the model so as to observe discrepancies with the full MBM model.

The differences could be categorised into three sections:

1. No oscillations
2. Delayed onset of oscillations
3. Early onset of oscillations

These three categories represent an overview of the major differences observed between the original simulation results and the modified model. No oscillations was defined as there being no change in concentration or there being a singular change in concentration of the catalyst species and no further redox process.

Early peaks are the feature most similar to that observed in the iron-catalysed system. Peaks did not have to persist indefinitely in simulations to be classified within the early peak category as the aim was to identify reactions that would remove the induction period.

There are distinct types of reactions that yield each behaviour, in Table 5.2, Table 5.3 and Table 5.4 the directions of the reaction arrows denote the direction in which an equilibrium reaction is pushed by this rate constant.

5.2.1 No Oscillations

Many of the reactions listed in Table 5.2 are those that are integral to the minimal bromate oscillator and are at the core of most models. This demonstrates the obvious

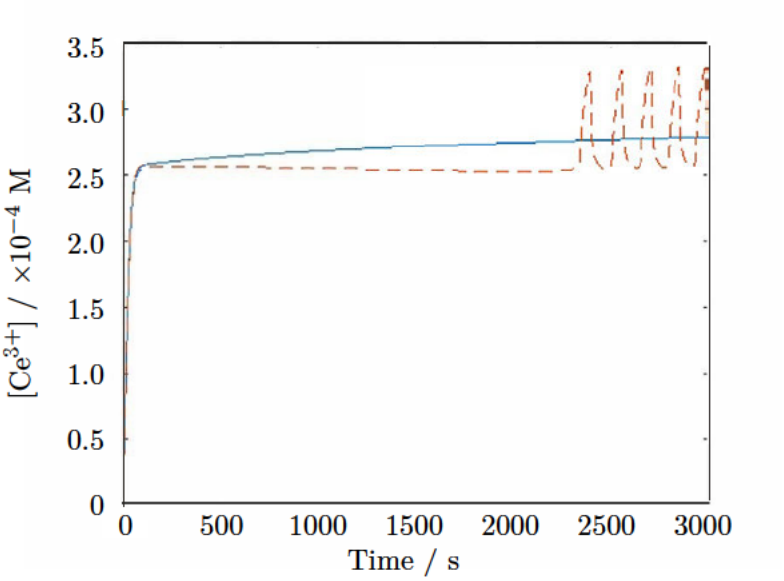

FIGURE 5.3: Removal of k_3 results in no oscillations being present, in this case the concentration changes once but then does not proceed to oscillate. The dashed line represents the result of the unaltered system.

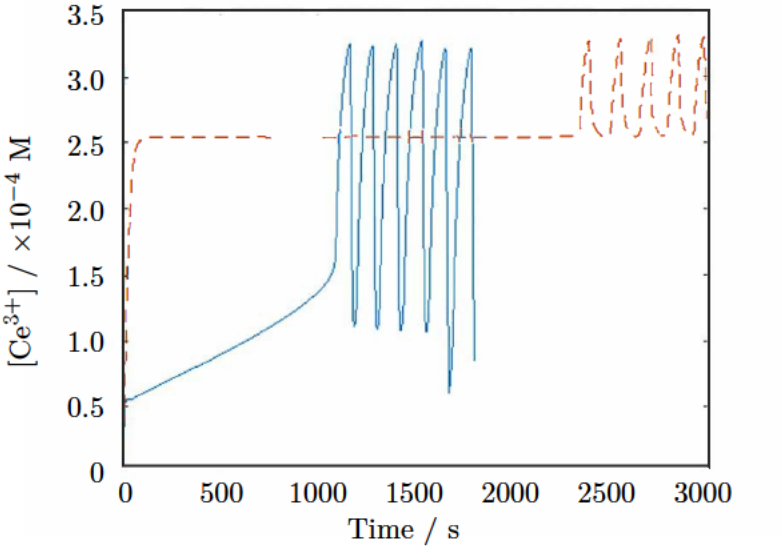

FIGURE 5.4: Removal of k_{15} results in oscillations starting earlier, depending on the initial concentrations this effect can be more pronounced, evidently in this case the system reaches a point at which the solver fails. The dashed line represents the result of the unaltered system.

that disruptions to the early reaction processes, *e.g.* the consumption of sodium bromate, enolisation of malonic acid or the production of the autocatalyst, prevents oscillatory behaviour.

Rate Constant(s), k	**Reaction**	**Reaction Number**
3	$Br^- + HBrO_2 + H^+ \longrightarrow 2\,HOBr$	2
7 & 8	$HBrO_2 + H^+ \rightleftharpoons H_2BrO_2{}^+$	4
9	$HBrO_2 + H_2BrO_2{}^+ \longrightarrow HOBr + BrO_3{}^- + 2\,H^+$	5
10	$HBrO_2 + BrO_3{}^- + H^+ \longrightarrow Br_2O_4 + H_2O$	6
12	$Br_2O_4 \longleftarrow 2\,BrO_2{}^\bullet$	7
14	$Ce(III) + BrO_2{}^\bullet + H^+ \longrightarrow Ce(IV) + HBrO_2$	8
29	$MOA + Ce(IV) + H_2O \longrightarrow OA + Ce(III) + COOH^\bullet + H^+$	20
30	$OA + Ce(IV) \longrightarrow COOH^\bullet + Ce(III) + H^+ + CO_2\uparrow$	21
33	$COOH^\bullet + BrMA \longrightarrow MA^\bullet + Br^- + H^+ + CO_2\uparrow$	24
39	$MA \longrightarrow MA\ (enol)$	29
41	$MA\ (enol) + Br_2 \longrightarrow BrMA + Br^- + H^+$	30
43	$MA^\bullet + BrO_2{}^\bullet \longrightarrow MABrO_2$	32
44	$MABrO_2 \longrightarrow MOA + HOBr$	33

TABLE 5.2: List of reactions and rate constants, which when removed result in no oscillations being observed

Those reactions that relate to later processes, or those within the "organic subsystem" of the MBM model, can also inhibit oscillatory behaviour. Many of the species in these reactions are thought to be inhibitors of the reaction if their concentration increases, *e.g.* bromide or mesoxalic acid, yet counter-intuitively the removal of reactions that consume these can still prevent oscillations, thus it can be inferred that rather than having purely inhibitory effect they are part of more complex feedback loops.

5.2.2 Delayed Start

Delayed oscillations were a rare feature when removing reactions. Many of the products of the reactions listed in Table 5.3 need to reach a threshold concentration for oscillations to begin, by preventing there formation the induction period was lengthened.

For example, bromomalonic acid, when used as the primary substrate, will trigger oscillations with no observable induction period.[50] However, if malonic acid is the primary substrate, BrMA will accumulate over time prior to the onset of oscillations. Removal of the direct conversion step (R11, Table 5.3) from BrMA to $BrO_2^\bullet$ prevents the formation of $BrMABrO_2$ and therefore forces the system to bypass the decomposition of this intermediate into mesoxalic acid (MOA) and bromotartronic acid (BrMA) resulting in delayed oscillations.

Rate Constant(s), k	**Reaction**	**Reaction Number**
18	$BrMA + Ce(IV) \longrightarrow BrMA^\bullet + Ce(III) + H^+$	11
25	$BrMA^\bullet + BrO_2^\bullet \longrightarrow BrMABrO_2$	16
28	$BrTA \longrightarrow Br^- + MOA + H^+$	19
58	$TA^\bullet + BrO_2^\bullet \longrightarrow TABrO_2$	45
59	$TABrO_2 \longrightarrow MOA + HBrO_2$	46
61	$MA^\bullet + BrO_3^- + H^+ \longrightarrow BrO_2^\bullet + TA$	48

TABLE 5.3: List of reactions and rate constants, which when removed result in delayed oscillations being observed *i.e.* after 600 s

There is evidence indicating that malonyl, tartronyl and bromomalonyl radicals all play a key part in the induction period of the cerium-catalysed reaction, therefore inhibiting the formation or consumption of any of these significantly impacts on the observed behaviour.[50]

5.2.3 Early Peaks

Hydrolysis of malonyl bromite ($MABrO_2$) is a necessary reaction for the induction period to occur.[50] Removal of this reaction, with rate constant k_{45}, is important in shortening the induction period as many small oscillations were observed before dying off quickly. Simulations removing k_{15}, the oxidation of $HBrO_2$ by cerium(IV) ions, led to a situation that most closely resembled the appearance of oscillations in the iron-catalysed reaction. It can thus be inferred that a major mechanistic difference between the two catalysts is within the generation of the autocatalyst. Indeed the majority of the reactions in Table 5.4 involve the bromite radical and bromous acid.

Rate Constant(s), k	**Reaction**	**Reaction Number**
11	$HBrO_2 + BrO_3^- + H^+ \longleftarrow Br_2O_4 + H_2O$	6
13	$Br_2O_4 \longleftarrow 2\,BrO_2^\bullet$	7
15	$Ce(III) + BrO_2^\bullet + H^+ \longleftarrow Ce(IV) + HBrO_2$	8
32	$COOH^\bullet + Ce(IV) \longrightarrow Ce(III) + H^+ + CO_2\uparrow$	23
35	$COOH^\bullet + BrO_2^\bullet \longrightarrow HBrO_2 + CO_2\uparrow$	26
45	$MABrO_2 \longrightarrow TA + HBrO_2$	34

TABLE 5.4: List of reactions and rate constants, which when removed result in oscillations being observed before 200 s

Since it is possible to remove the induction period in simulations a number of conclusions regarding the current model can be drawn. Firstly, the MBO is core to both reaction networks and so must be retained in any future model. There are a number of reactions which are also necessary to the reaction and their removal leads to a longer induction period. At the same time, not all of the reactions in the MBM model are necessary for the system to oscillate as evidenced by their removal resulting in oscillations that appear with a far shorter induction period. Therefore by keeping the core reactions from the MBO and their rate constants fixed it creates a framework to build upon and reduce the scale of the optimisation problem. Secondly, that the iron(II)-catalysed system must feature further reactions and intermediates in order to show its own distinct dynamics.

5.3 Application of the GWO to the Iron(II)-Catalysed System

The conclusions above provided a set of rules on which the GWO could be run, with the aim of applying constraints to the simulations and consequently improving efficiency.

An initial simulation with the GWO sought to benchmark how effectively the MBM model could fit experimental data. Initial conditions were set according to Table 5.5 as had been used in the stirred experiments from Chapter 2. This data was used as the test data against which the simulations would be matched. Both the simulated and experimental datasets were normalised prior to correlation thereby allowing comparison. Results of the optimisation experiments are detailed in Appendix F.

Species	**Concentration / M**
Sulfuric Acid (H_2SO_4)	0.25
Sodium bromate ($NaBrO_3$)	0.20
Malonic acid	0.05
Ferroin	0.002

TABLE 5.5: Initial conditions used for the experiment and simulation comparison

As expected, after 100 iterations in the range $k \pm \frac{k}{2}$ there was little correlation, $\hat{\rho}_o < 0.30$, between the observed data and the simulated data (Figure 5.5).

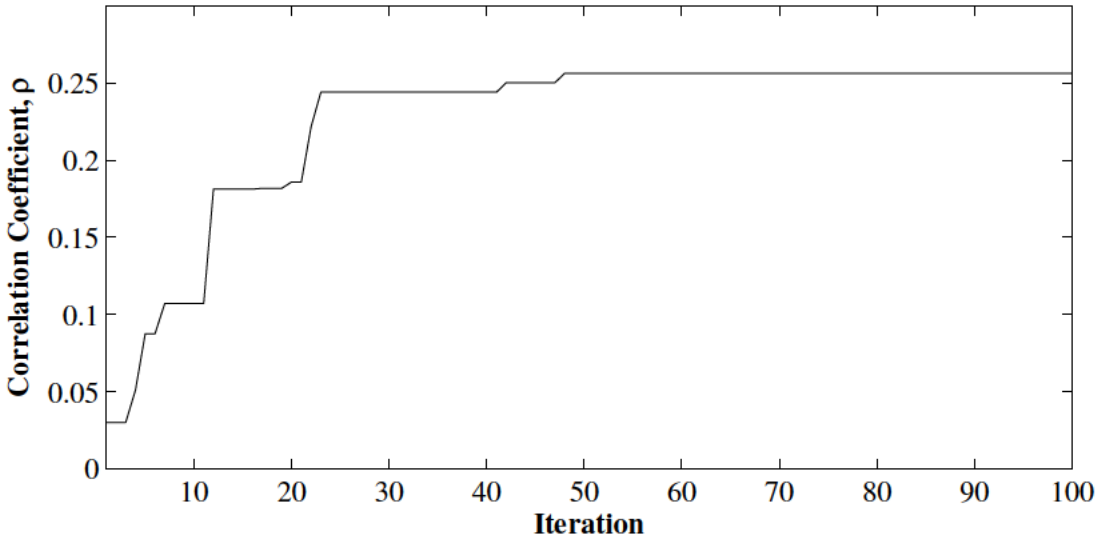

FIGURE 5.5: Correlation at each iteration step for UV-vis data obtained from the iron(II)-catalysed experiments compared with simulated data using the MBM model

A modified set of reactions was then used to find whether any rate constants could force the reactions of the MBM model to fit the iron(II)-catalysed experimental data. As a first port of call only the reactions that directly involved the catalyst were modified, then by altering the rate constants in the organic subsystem that had created early oscillations, however neither approach yielded a drastic improvement in the correlation between the simulated and experimental data, implying that the model does not account for a particular pathway that is present in the iron-catalysed reaction.

5.4 Experimental

5.4.1 Solving ODEs in MATLAB

The MBM model was written as a system of ordinary differential equations (ODEs) in the MATLAB software environment and solved using the *ode23s* solver. This solver is recommended for systems where the problem is stiff and crude error tolerances are present[175]. A stiff ODE is defined as an ODE where normal numerical methods, e.g. the trapezoidal method, are numerically unstable without a very small integration step; for a dynamic system the typical measure of numerical stability is the Lyapunov stability. Coexistence of time constants spanning several orders of magnitude results in stiffness this is found in vast chemical networks and thus also models of the BZ reaction[176].

5.4.2 Validating the GWO for correlating experimental and simulated data

A total of 30 search agents were used to determine how wide the search space could be. In all cases a maximum of 250 iterations of the GWO were allowed with the goal of obtaining a correlation above 95%. Erdem's correlation coefficient represented the fitness of the simulation to the expected data, if ρ_o reached 0.95 prior to the maximum number of iterations the simulation was ended and deemed to have converged sufficiently.

5.5 Conclusions

The MBM model is largely irrelevant to the iron(II)-catalysed system. Hegedűs *et al.* stated that there are significant differences in the recorded data from the iron- and cerium-catalysed systems.[50] Further reactions have been postulated to explain the reaction behaviour but none have satisfactorily encompassed the full dynamics of the iron(II) system.[18,56,79,177]

Although the simulations never matched the experimental data from the atlas, the ability of the network to maintain oscillations despite the removal of reactions has benefit moving forwards. In a network where nodes x and y are connected by a 4 step path through node z it is now possible to add a hypothetical node xy' that leads to a 2 step path connecting these species Figure 5.6 without affecting the overall network, this principle enables the possibility for predicting new reactions.[178].

The grey wolf optimiser algorithm was validated as a means of deriving rate constants. This was achieved by using the modified Pearson's correlation coefficient as a measure of fitness. Using the rate constants presented in the literature with a tolerance

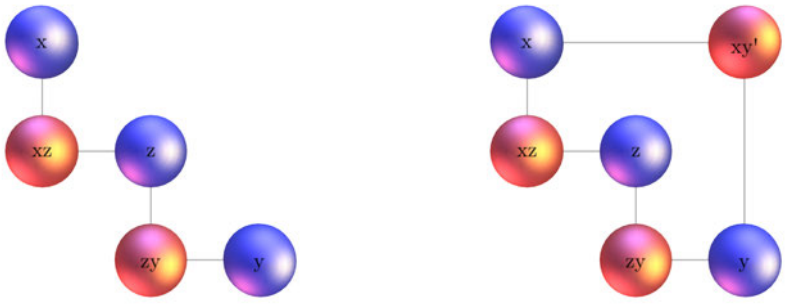

(a) (b)

FIGURE 5.6: (a) Representation of the 4 step network and (b) 2 step network containing the theoretical reaction node xy'.

of up to 10% either side the algorithm was able to achieve correlation of $\hat{\rho_o} > 0.95$, at increasing tolerances the convergence speed dropped linearly, yet gave confidence in the GWO as a method of optimising the rate constants when using a realistic starting position.

The methods presented here in Section 5.1 are "top-down" approaches that break the network down to a pseudo-skeleton framework. Consequently their utility for understanding the mechanisms of the iron(II)-catalysed BZ reaction is limited, an alternative to this would be to explore the stability of network partitions and thus define communities within the overall network, the quality of which would deliver a deeper understanding of that region of the network - ultimately providing a global perspective as opposed to a local one.[179] While this approach was not taken, the methods explored, along with those presented in the first part of the following chapter form the basis of a "bottom-up" data-driven modelling approach. By creating a pseudo-skeleton network using the network analysis methods in this chapter in conjunction with data obtained in Part 1, as well as the optimisation algorithms presented here it should be possible, with sufficient computational resource to iteratively create a model that captures the behaviour of iron(II)-catalysed system.

Chapter 6

Analysis of Oscillatory Chemical and Biochemical Networks

The previous chapter demonstrated that the ability to recreate the iron-catalysed reaction network by altering rate constants was not feasible. An attempt at deconstructing the MBM model offered some clues as to the features of the iron catalysed network. However, this method of deconstructing the network is limited as a top-down approach. The alternative would be to use a network-based methodology to build up a reaction network.

Therefore it was sensible to take the same approaches that are applied to biological pathways and apply them to a complex chemical system. Network theory has had great success in unravelling the complexity of metabolic networks and has previously demonstrated a theoretical limit to the size of metabolic networks as well as some sense of their connectivity with energy molecules (*e.g.* ATP) and catalytic species being the most highly connected.[180]

Numerous (bio)chemical databases exist that demonstrate the vast expanse of the chemical world, notably the KEGG and Beilstein (Reaxys) databases.[181] By developing a method that explored the network characteristics of an isolated complex chemical system there becomes potential for further exploration of these databases to find new chemical oscillators. Building a library of chemical oscillators is one small step in understanding the process of autocatalysis in living systems and therefore the mechanisms that were likely available to protocells.

6.1 Overview of the the Marburg-Budapest-Missoula Network

The Belousov-Zhabotinsky reaction networks are complex with a range of multi-molecular reactions. The number of nodes in a chemical network does not necessarily determine the level of complexity of that network. Rather complexity is defined in terms of the number of reactions, the number of reactive species, and the range of multi-molecular reactions. Within the MBM model there are 48 elementary reactions (of which 13 are quantifiable reversible processes) and 35 reactive species. This yields a network containing 83 nodes and 246 edges. Comparatively this is large for a chemical network but is dwarfed by the complexity of a metabolic network, which typically contains hundreds of interconnected reactions.[180]

In such a network there is a range of reaction molecularities; molecularity is typically defined as the number of reactants that are present in the rate-determining step of a reaction. This range of molecularities has use in large networks, specifically biological networks as low order molecularity often yields larger molecules quickly or increases the number of reactive species, thereby making the whole system more economical. Unimolecular reactions typically yield their products through (ionic / radical) dissociation, isomerisation or tautomerisation. Where dissociation reactions occur there are often a number of products, therefore there is benefit in their appearance within a complex network of reactions. Bimolecular reactions are most common in any reaction network as a result of the high probability of a successful collision between two molecules; disproportionation, isomerism and tautomerism are all examples of unimolecular reactions and can occur but often require high energies or a prior activation step as set out in the Lindemann-Hinshelwood mechanism and related theories.[182–184]

The likelihood of elementary termolecular or quadmolecular reactions is very low unless the concentration of all colliding species is suitably high (Equation 6.1) to facilitate a fast rate of reaction.

$$rate = k[A][B][C] \tag{6.1}$$

Assuming that each reaction in the MBM model is elementary, Figure 6.1 depicts the molecularities of reactions in the network. Only reactions that utilise bromate and sulfuric acid are capable of seemingly quadmolecular reactions.

Bimolecular reactions are the most common within the reaction network explaining why such a vast range of molecules are created within the system. The reactions that appear as with a molecularity of three or more are unlikely to be truly elementary

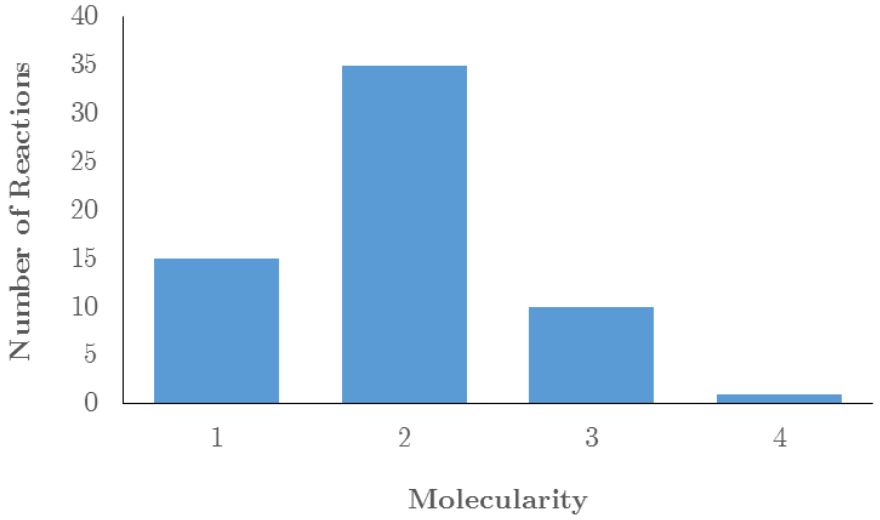

FIGURE 6.1: The distribution of the molecularity, shown in blue, in comparison to the distribution of products, shown in red, for the Marburg-Budapest-Missoula model.

processes and more likely to be of the form

$$\mathrm{A} + \mathrm{B} \xrightarrow{\mathrm{C}} \mathrm{P} \tag{6.2}$$

where C is a third-body and forces the reaction to proceed through two bimolecular steps where A and B form an activated complex before further reaction with C.

$$\begin{aligned} \mathrm{A} + \mathrm{B} &\longrightarrow \mathrm{AB}^* \\ \mathrm{AB}^* + \mathrm{C} &\longrightarrow \mathrm{P} + \mathrm{C} \end{aligned} \tag{6.3}$$

Although it is unlikely that all 12 of the ter-/quadmolecular reactions are elementary the assumption that they are simplifies models of the reaction network. The incidence of unimolecular steps in the network is also indicative of the importance of radical reactions and dissociative processes.

6.1.1 Chemical Reaction Network Representations

When it is possible to partition a network into two subsets (S_1 and S_2) where for every node in S_1 there is an edge connecting it to a node in S_2 then the graph is said to be bipartite.[185] In the case of a chemical reaction network these two subsets are the reactions and the chemical species. A bipartite representation of the MBM reaction network was produced in Cytoscape[186] and is shown in Figure 6.2.

Bipartite representations have been used in the evaluation of networks as well as in a predictive role in both drug synthesis and metabolic pathway analysis.[187,188] Bipartite

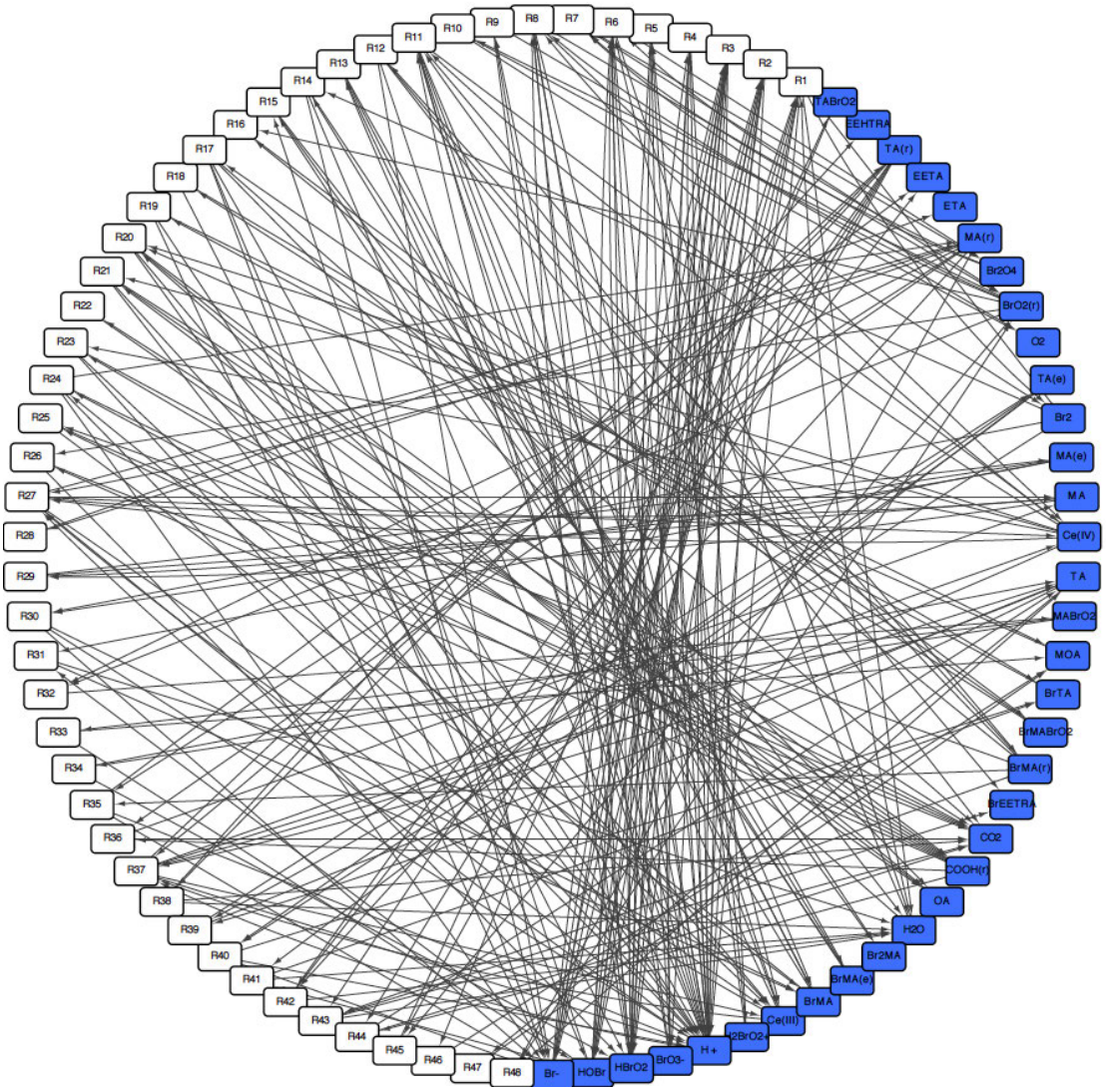

FIGURE 6.2: Bipartite representation of the cerium(IV)-catalysed system as detailed in the Marburg-Budapest-Missoula model. Reactions are shown in white boxes while reactive species are in blue boxes

networks not only allow for an understanding of connectivity within the current network but have the potential to predicting further reactions and species that may be present in the iron(II)-catalysed Belousov-Zhabotinsky reaction.

6.1.1.1 Unipartite Representations of the Network

As an alternative to the bipartite representation where two subsets had been shown with reaction nodes connecting multiple species nodes or vice versa. By eliminating these connecting nodes to give a system of pseudo-paths the unipartite representations were constructed. These pseudo-paths are not genuine since they lose the reactivity information but provide an idea of what molecular transformations can occur, the unipartite graph of chemical species is shown in Figure 6.3. Although a unipartite graph

of reactions can be created it affords no information on the scale or reactivity of the network.

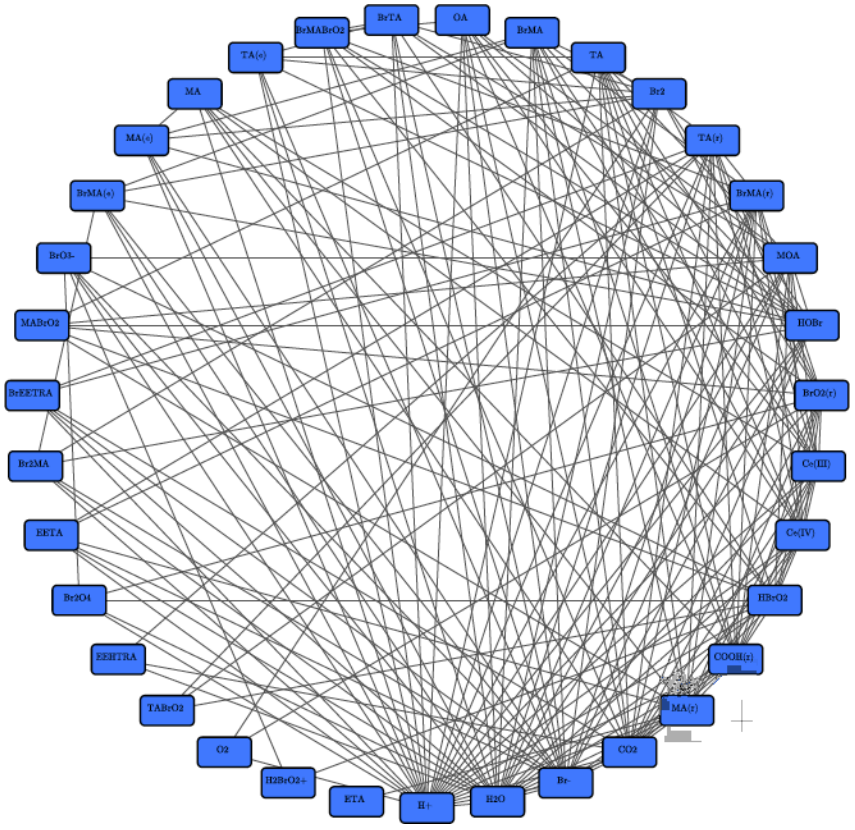

FIGURE 6.3: Unipartite representations of the full MBM network, whereby the reactions subset and species subset have been been separated.

By studying the individual chemical subset as well as the full bipartite network it was possible to separate the effects the nodes had on one another without any intervention from the second subset. This was of use in understanding the construction of the network and is discussed later in Section 6.6.1.

6.1.2 Network Regions: Sources, Sinks and the Bulk

A reaction network can be broken down into different regions defined by the nodes that they contain. Source nodes are defined as being the input to the network with nothing preceding their position as shown in Figure 6.4. In this work the sources will in fact be defined as the starting reagents due to their concentration being large relative to the intermediate species in the bulk of the network.

When undertaking simulations of a network terminal products, *i.e.* those with no output, will often have their concentration fixed to zero and are termed sink nodes.

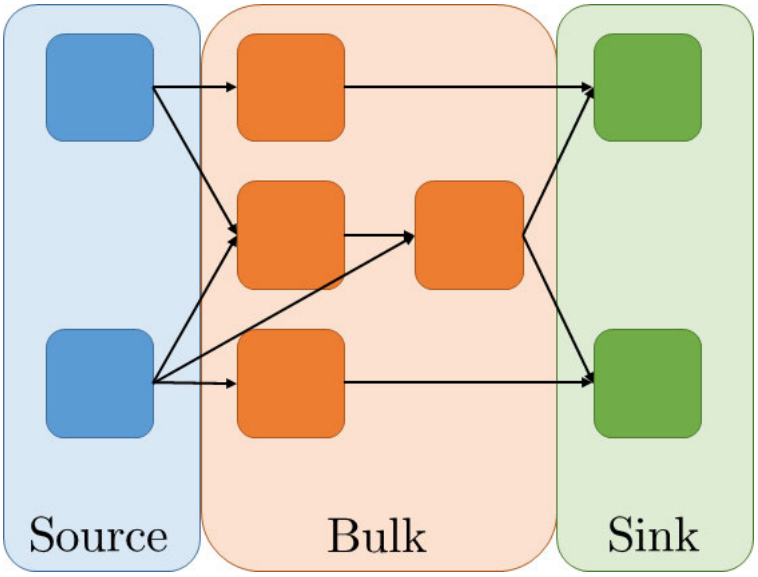

FIGURE 6.4: Diagram showing the arrangement of sources and sinks in a network. Unlabelled nodes are the bulk nodes.

In reality they are being continuously formed however this adjustment simplifies the kinetics and thus computational expense of any simulation. Moreover, in the Belousov-Zhabotinsky reaction this is a simplification has further validity since many products are either gases (e.g. CO_2 and O_2) or are produced in relatively small quantities (e.g. BrEETRA). The bulk contains the majority of nodes; sources will lead into the bulk and sinks will remove from it. In general an increase in network size and complexity should lead to there being more happening within the bulk.[180]

There are far fewer sources and sinks than overall species in any network, for metabolic network an average of 8.97% ($\sigma = 1.67\%$) of all metabolites are source nodes and 8.45% ($\sigma = 1.71\%$) are sinks.[180] In comparison 14% of nodes in the MBM model can be defined as source nodes while 20% of species are sinks. The percentage of sources and sinks should decrease with increasing network complexity; the MBM model is not as complex as a metabolic pathway and so has a higher percentage of sources and sinks.

6.1.2.1 Hub Nodes

Within the bulk of the network there are a fraction of highly connected nodes that facilitate a number of reactions. The simplest method for defining hub nodes in a network is to rank the nodes by the degree of connectivity, n, the sum of edges in to and away from a node, denoted n_{in} and n_{out} respectively.

The species nodes were ranked by n in Table 6.1, a high degree of connectivity means a high hub character. Hub reactive species are found in most reactions in a network and

Species	***n***	**Species**	***n***
H_2SO_4	32	MA	5
$HBrO_2$	17	OA	4
Br^-	14	BrMA	4
HOBr	12	BrMA (enol)	4
CO_2	11	MA (enol)	4
H_2O	11	TA (enol)	4
Ce^{III}	11	Br_2O_4	4
Ce^{IV}	11	$BrMABrO_2$	3
$BrO_2^\bullet$	10	$MABrO_2$	3
$COOH^\bullet$	9	$H_2BrO_2^+$	3
$MA^\bullet$	9	$TABrO_2$	2
BrMA	8	O_2	2
TA	8	BrEETRA	2
BrO_3^-	8	Br_2MA	2
$BrMA^\bullet$	7	EETA	2
$TA^\bullet$	7	ETA	2
Br_2	6	EEHTRA	1
MOA	5		

TABLE 6.1: Ranking of species nodes by n

provide a driving force for the system, in a biological context these tend to be energy molecules such as ATP; here the sulfuric acid, bromous acid and bromide ion are the highest ranked species and fulfil the same role in the network with all of them being integral to the inorganic cycle of the BZ reaction.

In most real-world networks there tends to be a lot of low-connectivity nodes with only a small probability of highly connected nodes. A rudimentary approximation for this probability distribution is given by the Poisson distribution, those that follow this construction perfectly are termed Erdös-Renyi networks. Although the MBM model has a sharp drop off in the number of highly connected nodes it does not follow this distribution exactly and an alternative approach for comparing the model to random networks is detailed in the following section.

6.2 Chung-Lu Model for Network Generation

Random networks are a core tool for inferring the presence of features within networks that occur more frequently than by chance alone. Comparison to random networks is regularly used in social network anaylsis, physics and telecommunication networks as well as for biological networks. Quite often a real-world network will be compared to random networks in the form of Erdös-Renyi graphs. This leads to a situation however where there are no nodes within the random network with $n_i = 1$, where n_i is the degree of the node i. Consequently, the structure of these networks does not offer a true representation of self-contained real-world networks. An alternative approach which retains the degree distribution of the original real-world network is to utilise the Chung-Lu model.[189,190]

A graph (G) is defined by its vertices (V) and edges (E). It is possible to represent the network as a V-by-V adjacency matrix,A_ij:

$$A_{ij} = \begin{cases} 1 & \text{if } (v_i, v_j) \in E \\ 0 & \text{otherwise} \end{cases} \tag{6.4}$$

where v_i and v_j are vertices in the set V and connected as an edge (v_i, v_j) in the set E. From this it is possible to calculate the degree, n, of each node from the diagonal of the matrix

$$D_{ij} = \begin{cases} \sum_j A_{ij} & \text{if } i = j \\ 0 & \text{otherwise} \end{cases} \tag{6.5}$$

which yields the degree of the vertex, v_i, at position D_{ii}. The probability matrix, P_{ij}, gives the likelihood of there being an edge between two vertices given uniform sampling of the adjacency matrix(Equation 6.6).

$$P_{ij} = \frac{A_{ij}}{n_i} \tag{6.6}$$

The Chung-Lu model generates a random graph from a real-world network, G, using the above properties of the network. This approach creates an edge between vertices based on the probability

$$P(v_i, v_n) = \frac{n_i n_j}{2M} \tag{6.7}$$

where M is the number of edges in the original network G, evidently this leads to the expected degree distribution of the generated network being the same as the original, an alternative and commonly used method, is the Erdoös-Renyi (ER) method which relies on a random binomial distribution to populate a graph. Figure 6.5 highlights why the Chung-Lu (CL) method of network generation is more effective in replicating the degree distribution of chemical networks since it allows for nodes to be connected to only one other node ($k = 1$) whereas the ER method creates closed networks with unrealistically high degrees of connectivity.

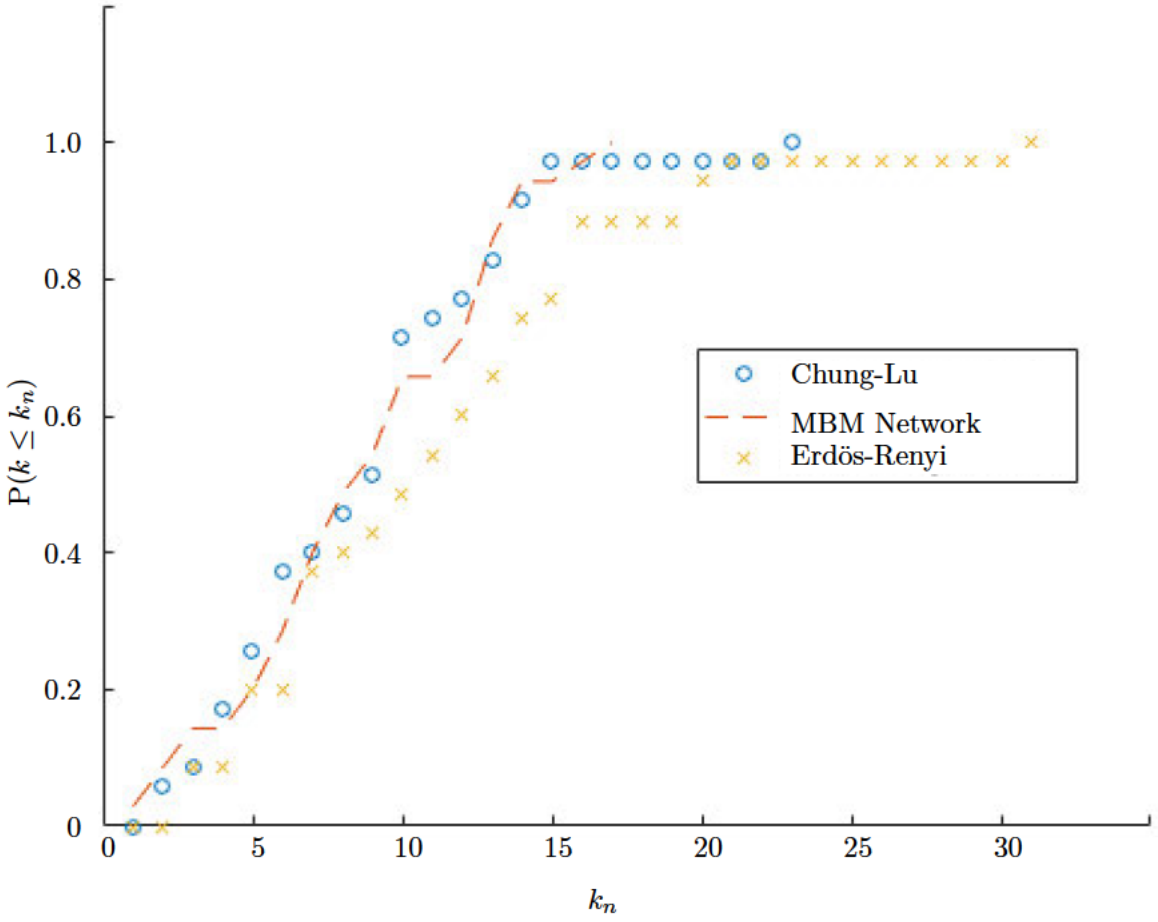

FIGURE 6.5: Comparing methods of network generation. The Chung-Lu method preserves a more accurate network degree distribution from its parent network than the Erdös-Renyi method that produces completely random networks.

6.3 Motifs and Network Size for Analysing the MBM Model

6.3.1 Diameter

In a network, species are connected by a number of unitary paths. In an undirected network it is possible to connect any two nodes by a series of these paths. This enables the identification of "shortest paths", which are the sum of the unitary steps between nodes, l_{ij}. One can quantify aspects of the network using this "shortest path" approach by looking at the network diameter (the longest of the "shortest paths") and the average "shortest path" length, L between all pairs of nodes, N_{nodes} (Equation 6.8).

$$L = \frac{\sum l_{ij}}{N_{nodes}} \tag{6.8}$$

The diameter of a network can infer a the degree of complexity, with a larger diameter suggesting a higher level of complexity, it should be noted that a large diameter does not imply a large number of nodes, also across a disconnected network the diameter is infinite.[185]

6.3.2 Motifs

A motif is a simple (directed) pattern of activation and inhibition among a small number of interacting molecular species or nodes. When such a network motif carries out a defined function it is said to be a "module".[191] Consequently, there is a lot of interest in searching for motifs in biochemical systems since they afford some idea of the effect of network topology on biological function. Analysis of motifs typically involves counting appearances within a larger network and determining whether such motifs are over- or under-represented compared to chance.

Number of Nodes	Corresponding Motifs
2	2
3	13
4	199
5	9,364
6	1,5430,843

Table 6.2: The number of motifs scales exponentially with the number of nodes

Table 6.2 gives an indication to the challenge that this poses as calculating the number of appearances of $n \geq 5$ motifs in biochemical networks becomes computationally

prohibitive meaning that larger motifs, and thus functional modules, may well be ignored. The values in Table 6.2 are for motifs without any self-interactions, if these were to be included then the number of motifs for 3 nodes would increase to 104 possible arrangements.[192] Self-interactions are commonly excluded from motif calculations and have been from this work since they only really matter when autoregulation or autocatalysis is concerned.[193,194] Overlooking autocatalysis when exploring the nature of the BZ reaction may appear counter-productive, yet, the purpose of this approach was to elucidate how information flows through the network in any direction and therefore stoichiometry can be largely disregarded. The flow of information in a chemical system is more important since this occurs irrespective of any self-interaction if sufficient molecules are present.

$$A + B \rightarrow 2B \tag{6.9}$$

It is possible to draw Equation 6.9 as a unipartite representation either including or excluding self-interactions as shown in the figure below. If it is assumed that the interactions are $A \rightarrow B$ and $B \rightarrow B$ then the latter of these is not changing the information within the system therefore only the former represents any change in the arrangement of atoms in the system.

(a)With self-interaction of species B (b)No self-interaction

FIGURE 6.6: Two equivalent unipartite representations of Equation 6.9. Figure 6.6(a) accounts for the stoichiometry and is useful for following the flow of matter in the system while Figure 6.6(b) ignores the stoichiometry and demonstrates how structural information is transferred in the system

6.4 Graphlets

Motifs in reaction networks arise from the transformation of chemical species into one another. Typically this can be seen as a flow of information from one species to another with the product retaining a great deal of chemical similarity to the reactants. While the similarity property principle is not detailed further here it does offer a deeper exploration of the structure of a network

Graphlets are an alternative means to identify features of a network.[195] These are undirected and therefore do not have as many possible arrangements, only 30 exist in total ranging in size from two to five nodes as depicted in Figure 6.7. By comparing to random networks, the z-score and subgraph ratio profile (SRP) are calculable in the same way as achieved for motifs.

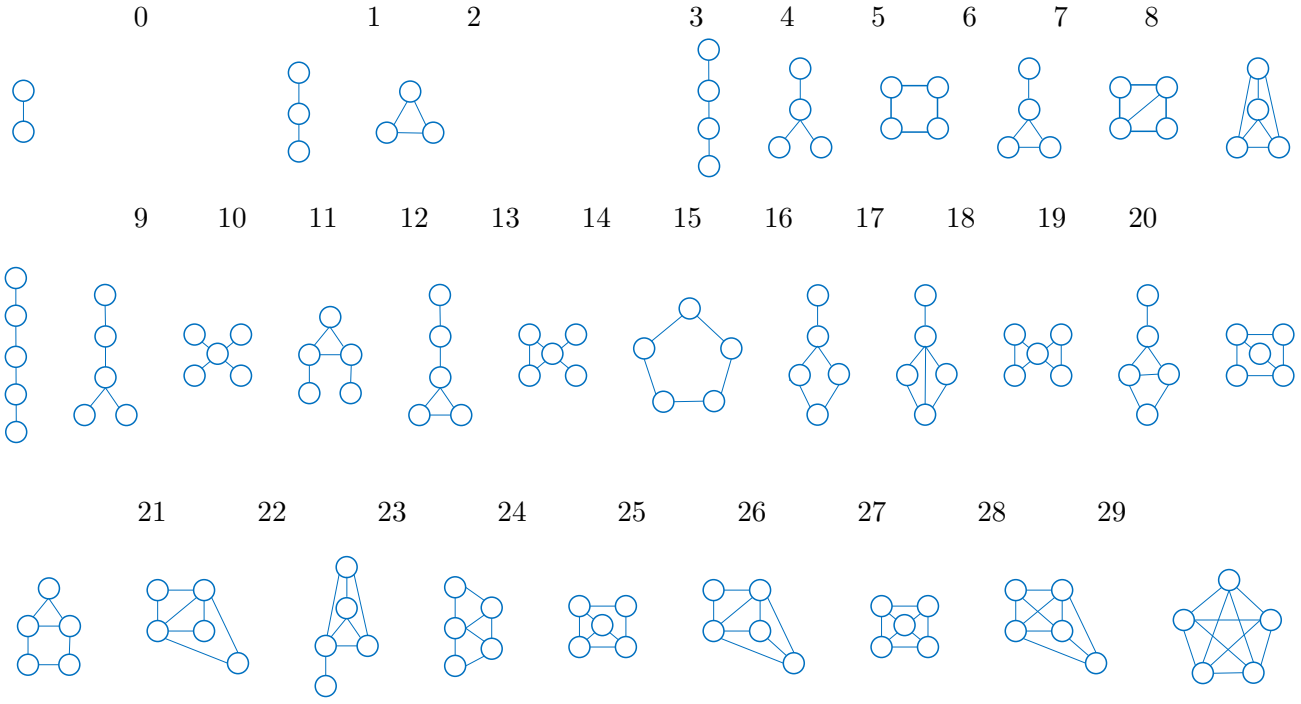

FIGURE 6.7: Depiction of all 30 graphlets grouped by number of nodes as set out by Yaveroglu *et al.*.

6.5 Z-Score

In order to quantify what is an "important" or over-represented feature within a network the z-score is calculated as per Equation 6.10. The z-score represents how many standard deviations (σ) the variable (N) is from the mean ($\bar{N}$).

$$z_i = \frac{(N_{real} - \bar{N}_{random})}{\sigma(N_{random})} \tag{6.10}$$

This metric assumes a normal distribution is obtained within the ensemble of random networks. The further the value of z_i deviates from the mean the more that graphlet is over- or under-represented in the network; as $z_i \to \infty$ the likelihood of over-representation increases.

Normalised z-scores for undirected motifs or graphlet show a high dependency on network size and so a secondary metric, the subgraph ratio profile has been established to account for the relative abundance of motifs compared to random networks as opposed to the use of z-scores.[196] The SRP is derived in Equation 6.11 and Equation 6.12

$$\delta_i = \frac{N_{real} - \bar{N}_{random}}{N_{real} + \bar{N}_{random} + \epsilon} \tag{6.11}$$

where ϵ is a factor that ensures $|\delta|$ is not an extreme value when a motif rarely appears in either the real or random networks. In this work ϵ was taken to be the square of the smallest value of $\bar{N}_{random}$.

$$SRP_i = \frac{\delta_i}{(\sum_{i=1} \delta_i)} \tag{6.12}$$

The SRP is the vector of δ_i normalised to 1, deviation from 0 suggests over- or under-representation depending on whether SRP is positive or negative, respectively.

6.5.1 Comparison to Randomly Generated Networks

The z-score was calculated and most graphlets were to be found within a single standard deviation of the mean. Through use of this metric graphlet 12 ($z = -2.359$) is the most under-represented graphlet compared to random networks.

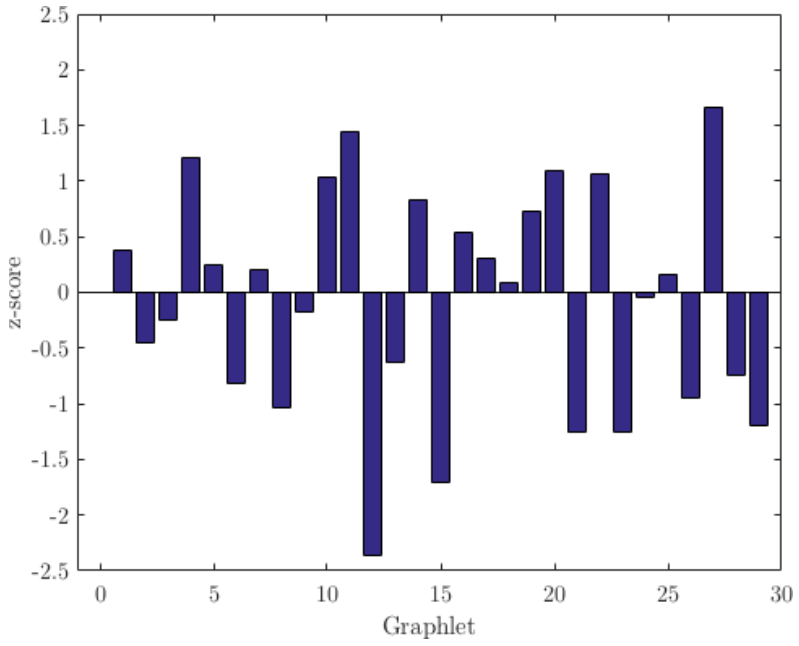

FIGURE 6.8: MBM z-score profile comparison with 100 randomly generated networks.

If however the SRP is considered then the graphlets that are more often under-represented are the larger graphlets with a high degree of connectivity between all nodes *e.g.* graphlet 29 does not appear at all in the MBM network. Perhaps surpisingly for an oscillating system not all of the circular motifs are favoured. While graphlets 2 and 5 are both found as often as expected the larger five-node graphlet 15 is under-represented in the network, suggesting a preference for smaller cycles between molecules, likely due to the increase in efficiency that these would bring about.

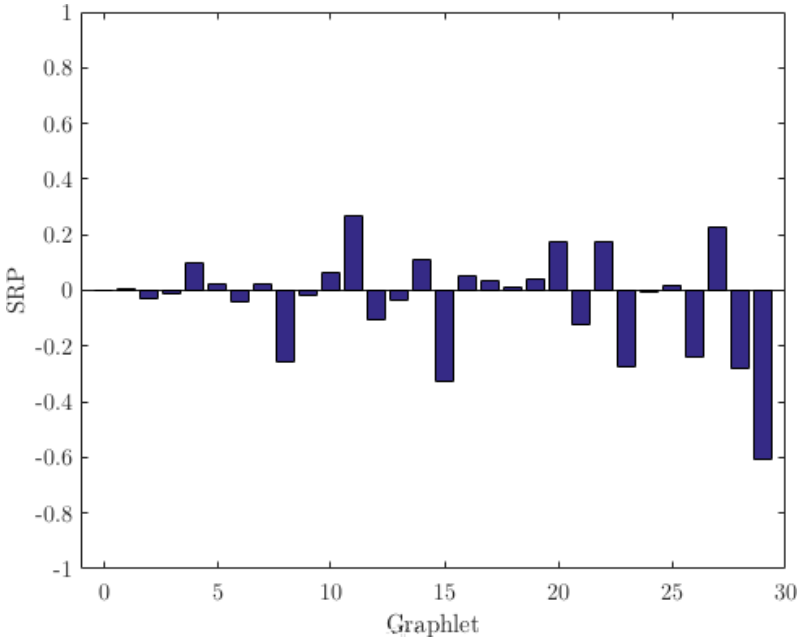

FIGURE 6.9: Subgraph ratio profile for each graphlet represented in the MBM network. Most small graphlets appear as often as would be expected however the most highly connected graphlets appear under-represented with graphlet 29 not being present at all.

6.6 Structure in the MBM Network

6.6.1 Removing Species Nodes

Networks have a reliance upon the hub nodes, with these being a key component of many reactions. In order to test this dependence the network was deconstructed by removing nodes and the average shortest path length recorded. This deconstruction led directly from Section 5.1 and was important in highlighting how the reactive species and the reactions themselves build the network. A total of 4 trial conditions were set up: random removal of species nodes, targetted removal of species nodes, random removal of reaction nodes and targetted removal of reaction nodes. Differentiating between the random and targetted approaches enables clarification of the effect of the hub nodes.

6.6.1.1 Species Nodes

The targeted removal of the most connected species nodes was conducted by sequentially removing nodes in the order detailed in Table 6.1. This led to a rapid increase in the average "shortest path" length (Figure 6.10) as the removal of such nodes forces the network to pass through less favoured nodes in order to reach a target node, thus illustrating the detachment between network size and "shortest path" lengths.

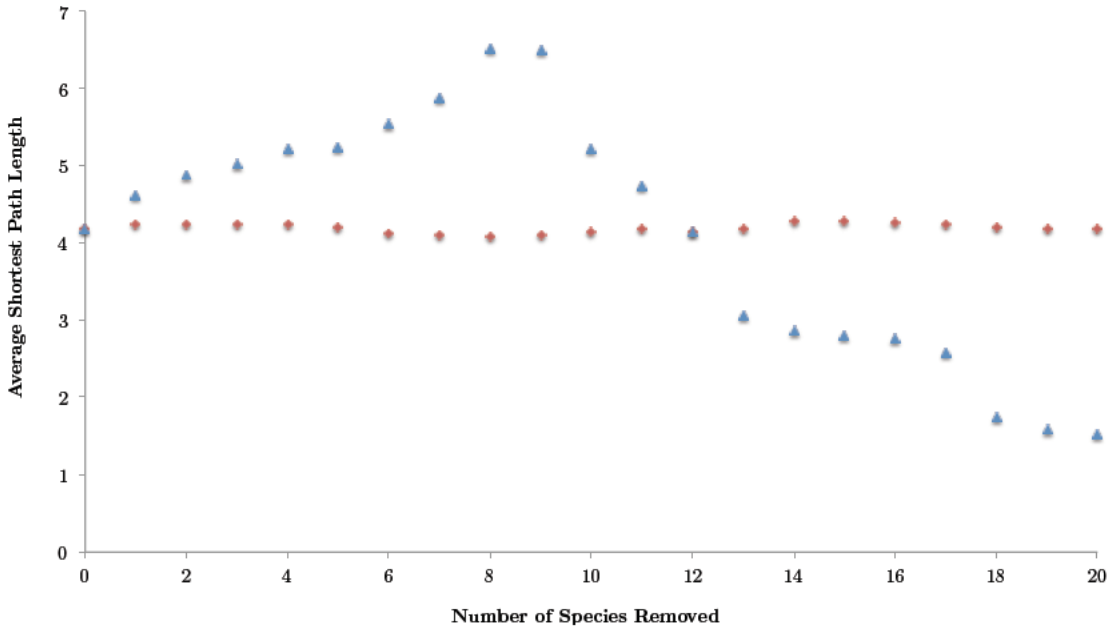

FIGURE 6.10: Comparison of the average shortest path length targetted (blue, △) and random (red, ◊) removal of species nodes. For the targetted node removal species were removed in the order shown in Table 6.1.

After the top 8 species hubs are removed the network started to fragment and the average "shortest path" across all fragments decreases once again. Most reactions tend to contain at least one hub node and so it is unsurprising that the network reaches this fragmentation point so quickly as reactions are effectively removed[180]. The random removal approach causes little change in the average "shortest path" length as a result of some hub nodes being retained. This shows conclusively that there is a reliance of the network on the most connected species but also that the addition or removal of singularly connected species nodes will have little effect on the structure of the network.

A similar conclusion can be reached by looking at how the average value of k changes as nodes are removed. The constant decrease in connectivity is expected from the continuous removal of the most connected nodes, however the random removal approach has regions of relative stability. This stability can be accounted for by the power law seen in the ranking of nodes where the majority of nodes have a low degree of connectivity. The steep drops in the average value of k are caused by the removal of the nodes with a higher hub character.

6.6.1.2 Reactions Nodes

In the full network all reaction nodes are in the bulk region of connectivity and have a far lower variability in their degree of connectivity when compared to the species nodes. There are a number of species in the network that are structurally similar illustrated in Figure 6.12.

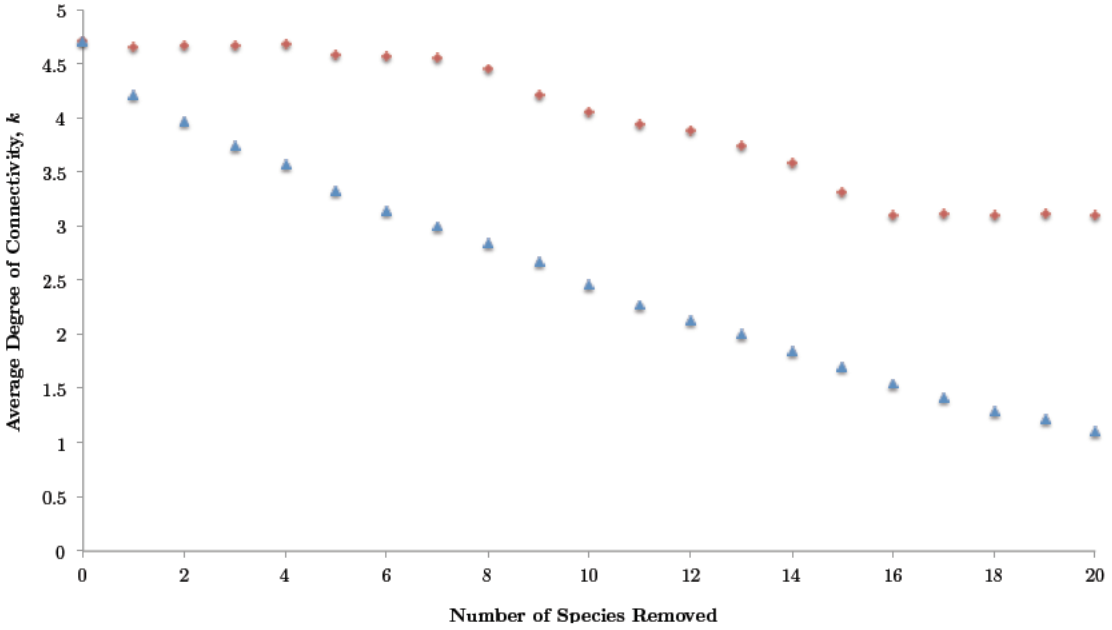

FIGURE 6.11: Comparison of degree of connectivity for targetted (blue, △) and random (red, ◊) removal of species. Node removal was conducted in the same manner as for Figure 6.10.

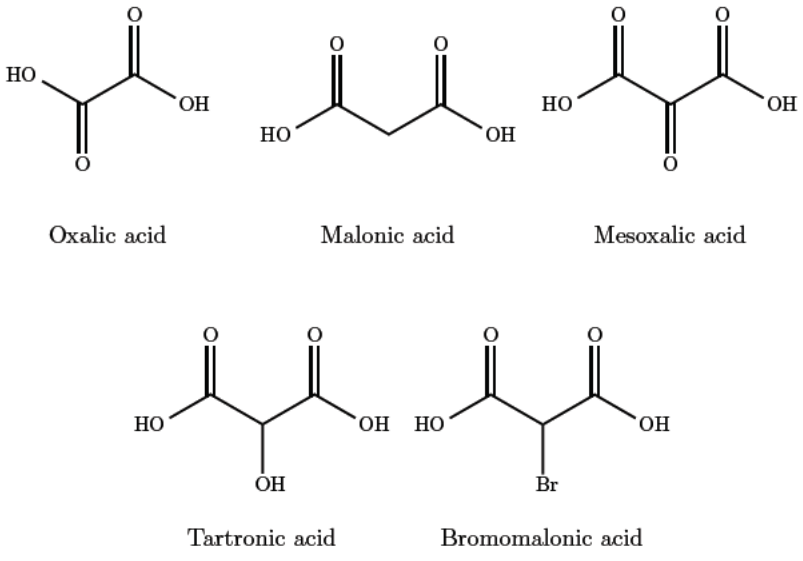

FIGURE 6.12: Organic acids found within the Marburg-Budapest-Missoula model. All have structural similarities and react via the same functional groups.

In turn this leads to similar reactivities and consequently low reaction variability. It can be seen from Figure 6.13 that the targetted removal of the most connected nodes is only marginally more effective at breaking down the network than random removal of nodes.

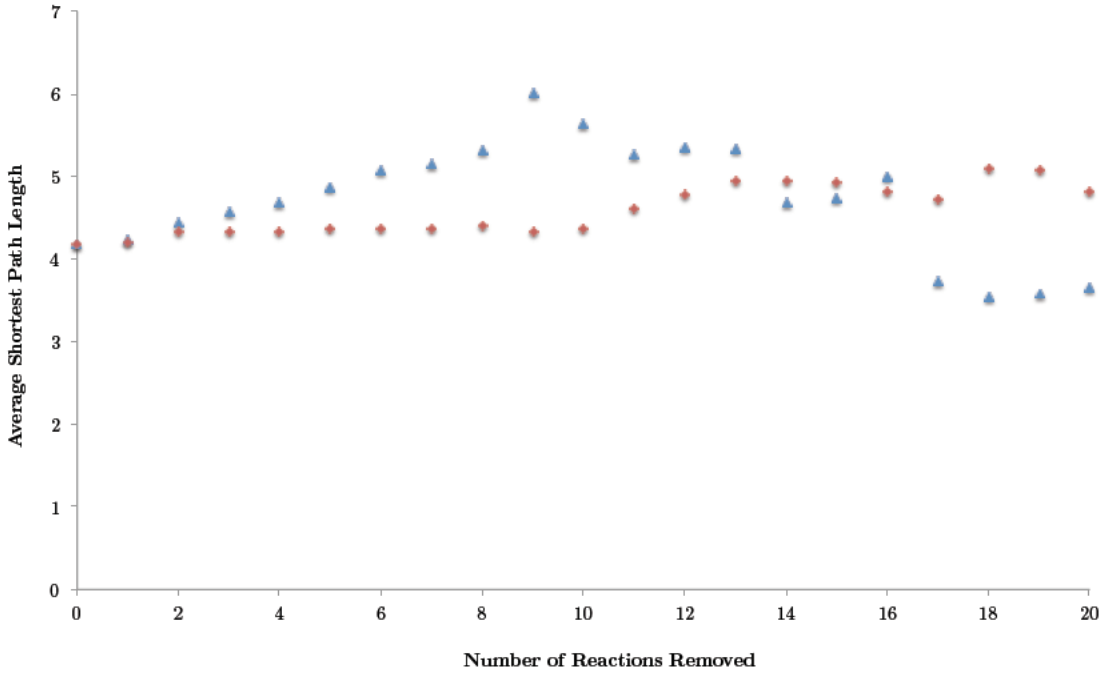

FIGURE 6.13: Comparison of average shortest path length for targetted (blue, △) and random (red, ◊) removal of reactions. For the targetted node removal reactions were removed in order of decreasing connectivity.

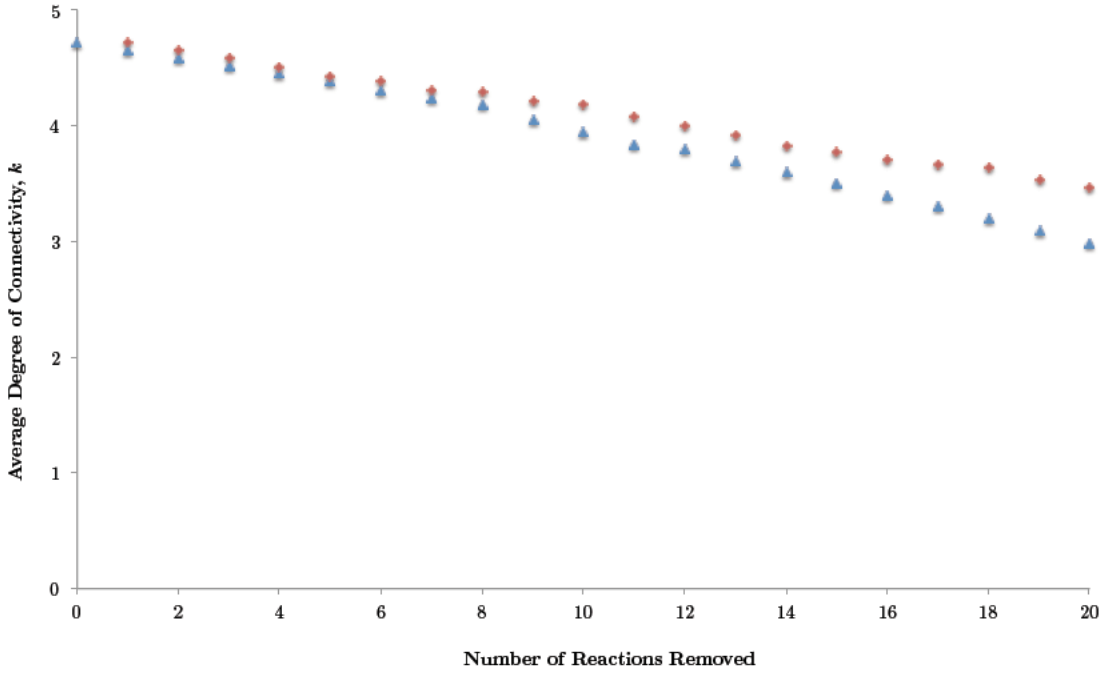

FIGURE 6.14: Comparison of degree of connectivity for targeted (blue, △) and random (red, ◊) removal of reactions. Node removal was conducted in the same manner as for Figure 6.13.

6.7 Comparison of the KEGG Database and MBM Network

Belousov-Zhabotinsky reactions are notoriously complex yet only contain a few dozen chemical species and reactions. Cellular metabolism consists of several large connected networks with typically an order of magnitude more chemical species and reactions. The KEGG database (available at `http://www.genome.jp/kegg/`) contains over 17,000 metabolites and small molecules that feature in more than 10,000 reactions. If an evolved biochemical system contains a similar structure to a smaller complex network then it is possible to extrapolate the results of the macromolecular crowding studies to a real world scenario.

In order to minimise errors in analysis the compounds in the KEGG database were encoded as SMILES from their PubChem ID strings and matched to those found in reactions. Any duplicated compounds, gene products, and drugs were removed from the analysis to yield a base level biochemical network where only simple chemical interactions and transformations were studied. All stoichiometric information was removed but stereochemistry was retained in the production of the SMILES strings.

Looking at the KEGG database as a large-scale chemical network overlooks the modularity that many seek from such systems yet in doing so it affords the ability to compare a highly evolved composite of reactions to simpler chemical systems such as that represented by the Marburg-Budapest-Missoula model. This comparison gives a snapshot of how well a known complex reaction network exhibits the features of evolved chemical systems.

6.7.1 Chemical Similarity

Chemical similarity, as defined by the Tanimoto index, is not explored in detail here but remains a valid point for the comparison of the networks because it gives an understanding of how matter flows through the system. A comparison of the distribution chemical similarities for every species in each network is given in Figure 6.15. The large number of low similarity components in both reflects the importance of small molecules and ions in modifying structure such as $BrO_2\cdot$ or H^+ in the MBM network. Such distributions give credence to the idea that small complex networks can be used to understand much larger metabolic pathways.

6.7.2 Graphlet Prevalence

Comparing the prevalence of each graphlet between the networks gives the clearest indication that small complex chemical networks can be extrapolated to explain the

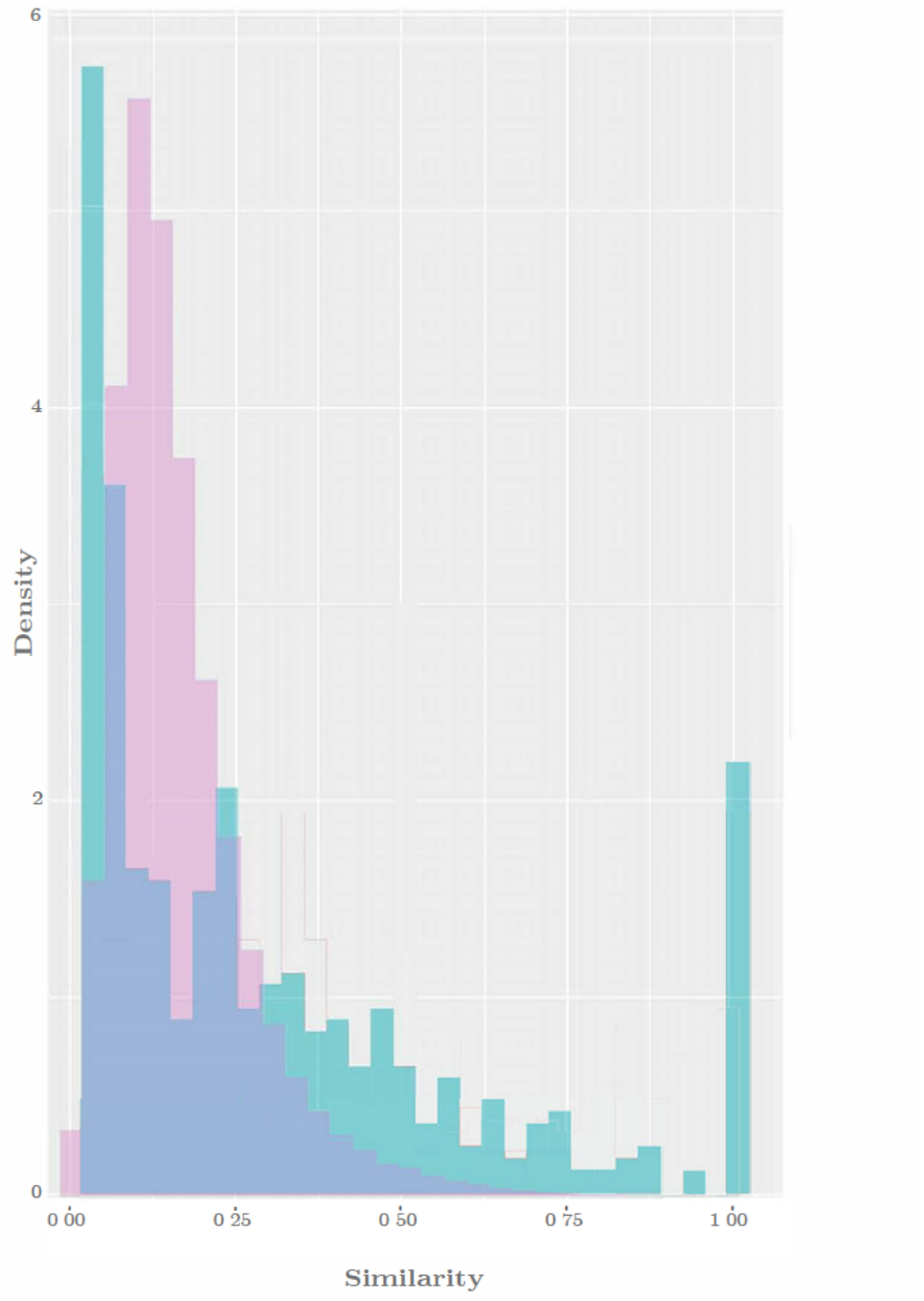

FIGURE 6.15: Comparison of chemical similarities in the MBM network (green) and the KEGG database (pink). In both cases there is a tendency for there to be a high proportion of low similarity species.

behaviour of biochemical networks. Figure 6.16 shows that there is a correlation between both networks in terms of the most common graphlets in each network, with a sufficiently large network all of the graphlets are feasible but obviously not in the same proportion. As there is agreement between the chemical and biochemical network we can assume that the conclusions drawn from building the atlas in part 1 of this thesis would hold up across a range of scales.

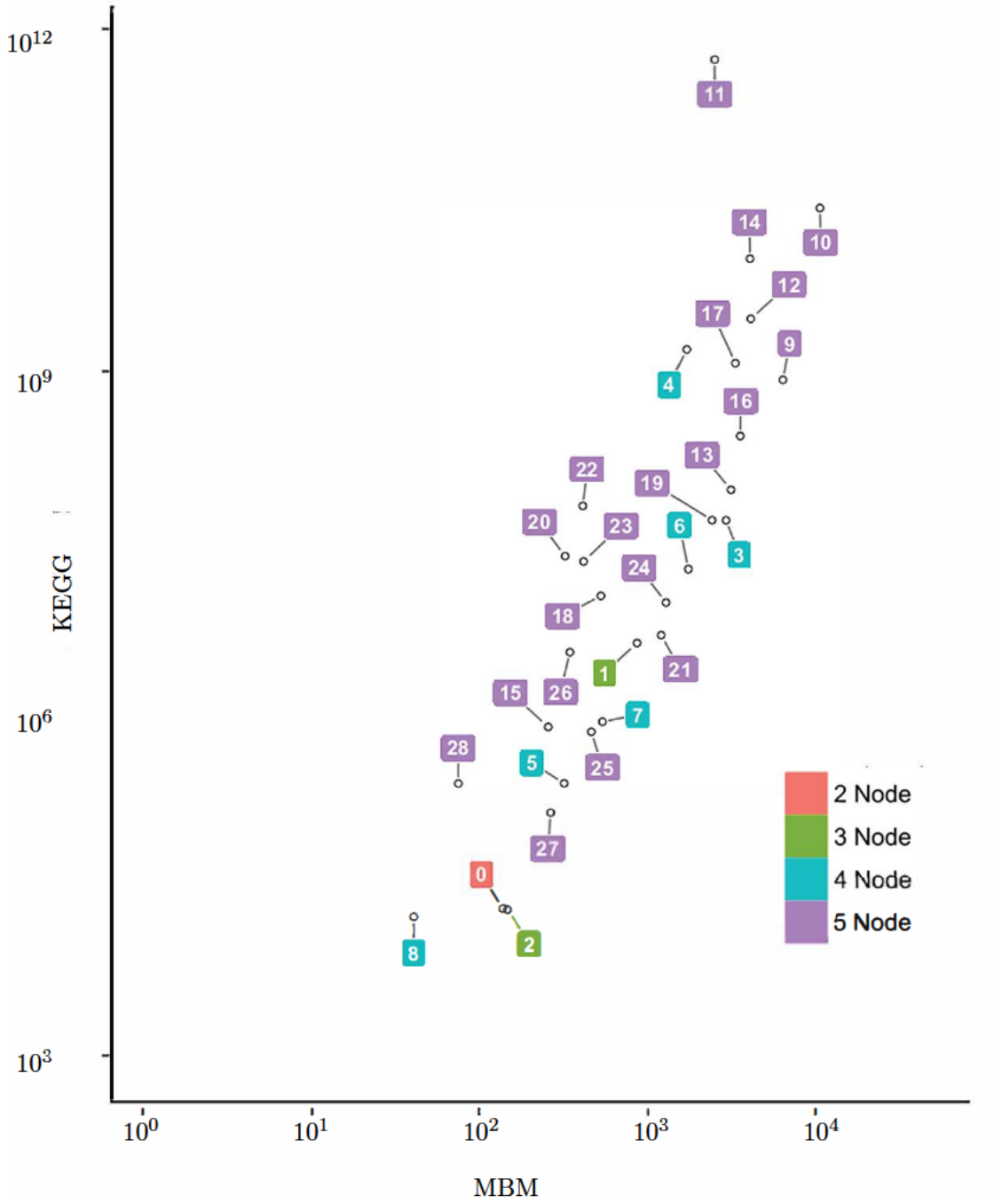

FIGURE 6.16: Prevalence of each graphlet in the KEGG database compared with the MBM network. Graphlets that are well represented in one network appear to also be so in the other suggesting that such features are inherent in complex networks.

6.8 Conclusions

The key species of the MBM model were identified via removal of the network hubs. Targetted removal of these hub species was far more effective in breaking down the species network projection compared to random removal, which left numerous degenerate paths across the network. Since the degree of connectivity, k, in the reaction network projection ranged from $k = 2$ to $k = 7$ the targetted removal was only marginally more effective than random removal and therefore was not a useful measure of the network dynamics (Figure 6.13). By further comparing the chemical network to the biochemical it becomes apparent that the two are closely related in terms of structure with the prevalence of highly connected graphlets more common in both cases despite the vast difference in size. As such the conclusions drawn from the MBM network are also applicable to large scale biochemical networks, this means that the utility of work on understanding crowded media in the previous chapters can offer new insights into how complex intracellular networks are affected by their molecular environment - specifically that the reactions are not necessarily altered but that they are hindered, further work in this area could show that the crowding of a system could maintain reaction mechanisms.

Chapter 7

Conclusions and Further Work

This thesis aimed to develop an atlas of the behaviour of the iron-catalysed Belousov-Zhabotinsky reaction with the intention of building a greater understanding of the ways in which complex reaction networks respond to their environment and setting out a framework by which further explorations of large-scale (bio)chemical reaction networks could be explored.

While the cerium-catalysed Belousov-Zhabotinsky reaction has been well studied and numerous models reported for the system there presently remains a lack of mechanistic detail when it comes to the iron-catalysed reaction. Experiments following the stirred reaction using the ferroin absorption maxima at 512 nm highlighted a wide range of dynamic phenomena from periodic oscillations through to transient chaos. The fundamental frequencies of the oscillations for each set of experiments were mapped and provides further depth to the literature. As was expected from these experiments an increase in oscillation frequency was observed with an accompanying increase in the concentration of either sulfuric acid or sodium bromate. By increasing the concentration of sulfuric acid to over 1.00 M the transition to unstable behaviour was seen and fast oscillations ceased. Nonetheless, an underlying slow oscillation was observed of approximately 0.004 s^{-1} demonstrating a complexity of behaviour which goes beyond what is currently known of the system.

All experiments were conducted in batch conditions and so demonstrated aging of the solution. This enabled the modelling of the stirred oscillations as a chirp sequence since there is a tendency for the frequency of the oscillations to slow as the reaction progresses. In so doing it became apparent that the rate at which the oscillations slowed was largely independent of the initial conditions, a result that was further supported by the linear evolution of the spiral pitch in an unstirred system. This has implications for further research in this area since it suggests that although the initial conditions can alter the appearance of oscillations and the length of time the system oscillates for there

are key features of the network within the bulk of intermediate nodes that control the rate at which oscillations slow.

The discovery of oscillation "rebirth", or "zombie" behaviour, in the iron-catalysed reaction has remained largely uninvestigated by the scientific community.[24] *Onuma* et al. *managed to identify the rebirth of oscillations after anywhere between 2 and 12 hours after the supposed death of the oscillator. The behaviour is purported to be found in the region between the reduced and oxidised final states. Such behaviour indicates that there is some underlying mechanism that is as yet unknown but could potentially be related to the slow oscillations that were observed in this work. Simulations on similar chemical systems have suggested that this behaviour should be identifiable in a range of chemical and biochemical oscillators.*

To complete the work on the unstirred reaction, a novel image based approach was produced that has the capability to elucidate transitions within an unstirred reaction medium. This method enabled the identification of chaotic transitions that would otherwise have been detected by eye offering a greater level of quantification than had previously been accessible to researchers. Results from the unstirred system showed good agreement with the stirred reactions with the chaotic transition occurring more readily as the concentration of sulfuric acid increased.

This method would work on all systems of this kind and could potentially highlight further differences between each catalyst used in the BZ reaction, whether it be Fe(II/III), Ce(III/IV) or Ru(II/III). Spiral waves and aging are just one element of interest in unstirred systems with there also being much scrutiny of the effect of the depth of solution on the behaviour of the reaction. By setting out an experimental framework and an atlas of data points for the unstirred system this thesis provides the foundation for further work on the transitions observed in unstirred media.

The final stage in developing the atlas was to allow for modification of the reaction medium. This provided the first tie in to the overarching aim of the work: to understand how a complex reaction network would respond in a crowded environment. This is more biologically relevant since cells contain a large number of chemical networks that work cooperatively to sustain metabolism but do so in an environment that features a vast quantity of macromolecules. The initial velocity of wavefronts was retarded by using gelatin to create a mesh-like medium, hindering diffusion of the catalyst and offering a further degree of electrostatic attraction. There was strong agreement between the mesh size model and experimental results with the 1% [G] closely matching the data for a homogeneous system, as was implied from the theory set out by Pezron *et al.*. This method of incorporating the catalyst was far more effective at reducing the initial rate of wave propagation in comparison to a system in which the catalyst is immobilised on beads and made these results more transferrable to a biological context. Experiments demonstrated that after spirals formed their behaviour was dependent solely on initial reagent

concentrations and that the gelatin played no role in the actual reaction. As gelatin concentration increased oscillations began later; this effect means that non-competitive molecular crowding has the potential to inhibit the onset of reactions but once started the reactions should progress according to their normal reaction pathways.

Electrostatic interactions can hinder diffusion in a biological system. However, macromolecular crowding also results in areas between molecules being dehydrated, therefore limiting diffusion by alternative means. Utilising microfluidic structures to control the flow and interaction of reactive species or incorporating the reaction mixture into liquid crystal phases and monitoring the change in surface structure offers better representations of physiological environments and thus provide a deeper understanding of how intracellular oscillating reactions proceed. Work undertaken in Electronic and Computer Science (ECS) at Southampton has shown that the same patterns are observed in microemulsion droplets as are observed in a larger reaction vessel, again demonstrating that the results of the thesis are applicable to smaller scale systems.

Having developed the atlas of the reaction this thesis then moved to explore how the reaction network is structured. While obtaining a new functioning model of the iron-catalysed reaction has not been possible a number of key conclusions could still be drawn from a more thorough analysis of the Marburg-Budapest-Missoula model. Using this as the basis for exploring the network of reactions present it was possible to identify key reactions which cause differences in the behaviour of the reaction that enable the cerium-based model to more closely replicate the behaviour of the iron-catalysed system. Although modification of these reaction rate constants did not result in a close correlation between experimental and simulated data they laid the foundations for further work in developing a model. The method for extracting chemical information from online resources and converting to networks is applicable to any chemical database and can be scaled to any network size, therefore enabling the analysis of individual reaction modules or larger complex systems of reactions.

Indeed our understanding of all complex reaction networks would be enhanced if further work were to be undertaken along these lines. Results on the comparison of the MBM network to the large scale Kyoto Encyclopedia of Genes and Genomes database demonstrated a level of agreement that makes this work a platform for further exploration of features that define chemical networks.

Chemical similarity is just one measure that can be explored. This was used sparingly in this thesis but offers a vast opportunity to delve deeper into the world of chemical networks. In combining the graphlet approach to chemical similarity metrics the flow of matter through a chemical network is more clearly elucidated, unfortunately at present such an approach would require significant computational resource.

Taken as a whole this thesis yields a depth of information on a range of phenomena within the iron-catalysed Belousov-Zhabotinsky reaction that were previously unexplored. By taking a novel approach to exploring our best models of the reaction it was possible to find a method that could be applied across the chemical sciences for improving our understanding of complex mechanisms. Although this did not provide a new mechanism for the iron-catalysed reaction it provided a stepping stone towards it through identification of the impact that individual reactions have not only to the observed behaviour but also to the structure of the network. By investigating the effect of macromolecular crowding on a complex network it is possible to extrapolate these results to a wider range of complex reaction networks, adding a significant contribution to the field.

"We grow in direct proportion to the amount of chaos we can sustain and dissipate"

Ilya Prigogine

Bibliography

[1] E. Villar Álvarez, J. Carballido-Landeira, J. Guiu-Souto, P. Taboada and A. P. Muñuzuri, *The Journal of Chemical Physics*, 2011, **134**, 094512.

[2] I. R. Epstein, *An introduction to nonlinear chemical dynamics: oscillations, waves, patterns, and chaos*, Oxford University Press, New York, 1998.

[3] R. J. Field and M. Burger, *Oscillations and traveling waves in chemical systems*, Wiley, New York, 1985.

[4] R. J. Field, E. Koros and R. M. Noyes, *J. Am. Chem. Soc.*, 1972, **94**, 8649–8664.

[5] M. Aller Pellitero, C. Álvarez Lamsfus and J. Borge, *J. Chem. Educ.*, 2013, **90**, 82–89.

[6] K. S. Kiprijanov, *ANNALEN DER PHYSIK*, 2016, **528**, 233–237.

[7] W. O. Friesen and G. D. Block, *American Journal of Physiology - Regulatory, Integrative and Comparative Physiology*, 1984, **246**, R847–R853.

[8] A. M. Zhabotinsky, *Chaos*, 1991, **1**, 379–386.

[9] M. Fecher, *Journal für Chemie und Physik*, 1828, **53**, 129–151.

[10] W. Ostwald, *Abhandlungen der Königlich Sächsischen Gesellschaft der Wissenschaften zu Leipzig*, 1899.

[11] G. Bredig and J. Weinmayer, *Zeitschrift für Physikalische Chemie*, 1903, **42**, 601–611.

[12] K. F. Bonhoeffer, *J Gen Physiol*, 1948, **32**, 69–91.

[13] A. J. Lotka, *J. Phys. Chem.*, 1909, **14**, 271–274.

[14] A. M. Turing, *Philosophical Transactions of the Royal Society of London B: Biological Sciences*, 1952, **237**, 37–72.

[15] I. Prigogine, *Introduction to Thermodynamics of Irreversible Processes*, John Wiley & Sons, Inc., New York, 2nd edn., 1961.

[16] A. M. Zhabotinskii, *Biofizika*, 1964, **9**, 306–311.

[17] N. B. Ganaie and G. M. Peerzada, *J. Braz. Chem. Soc.*, 2009, **20**, 1262–1267.

[18] A. F. Taylor, *Prog. React. Kinet. Mech.*, 2002, **27**, 247–325.

[19] V. A. Vavilin, P. V. Gulak, A. M. Zhabotinskii and A. N. Zaikin, *Russ Chem Bull*, 1969, **18**, 2467–2467.

[20] Q. Bi, *Sci. China Technol. Sci.*, 2010, **53**, 748–760.

[21] J. L. Hudson, M. Hart and D. Marinko, *The Journal of Chemical Physics*, 1979, **71**, 1601–1606.

[22] G. Biosa, M. Masia, N. Marchettini and M. Rustici, *Chemical Physics*, 2005, **308**, 7–12.

[23] F. Rossi, M. A. Budroni, N. Marchettini, L. Cutietta, M. Rustici and M. L. T. Liveri, *Chem. Phys. Lett.*, 2009, **480**, 322–326.

[24] H. Onuma, A. Okubo, M. Yokokawa, M. Endo, A. Kurihashi and H. Sawahata, *J. Phys. Chem. A*, 2011, **115**, 14137–14142.

[25] W. Jahnke and A. Winfree, *J. Chem. Educ.*, 1991, **68**, 320–324.

[26] A. M. Zhabotinskii, *Biofizika*, 1964, **9**, 306–311.

[27] E. Körös, *Nature*, 1974, **251**, 703–704.

[28] E. W. Hansen and P. Ruoff, *J. Phys. Chem.*, 1989, **93**, 264–269.

[29] J. Babu and K. Srinivasalu, *Proc. Ind. Natn. Sci. Acad.*, 1976, **42**, 361–363.

[30] L. Hu, G. Hu and H.-H. Xu, *J Anal Chem*, 2006, **61**, 1021–1025.

[31] E. Körös and M. Orbán, *Nature*, 1978, **273**, 371–372.

[32] E. Kőrös, M. Burger, V. Friedrich, L. Ladányi, Z. Nagy and M. Orbán, *Faraday Symp. Chem. Soc.*, 1974, **9**, 28–37.

[33] N. Ganapathisubramanian and R. M. Noyes, *The Journal of Physical Chemistry*, 1982, **86**, 5158–5162.

[34] *CRC handbook of chemistry and physics: a ready-reference book of chemical and physical data*, ed. W. M. Haynes and D. R. Lide, CRC Press, Boca Raton, Fla., 96th edn., 2015.

[35] K. B. Yatsimirskii, L. P. Tikhonova and A. S. Kovalenko, *Theor Exp Chem*, 1978, **13**, 533–536.

[36] F. Widdel, S. Schnell, S. Heising, A. Ehrenreich, B. Assmus and B. Schink, *Nature*, 1993, **362**, 834–836.

[37] A. F. Taylor, V. Gáspár, B. R. Johnson and S. K. Scott, *Physical Chemistry Chemical Physics*, 1999, **1**, 4595–4599.

[38] O. Benini, R. Cervellati and P. Fetto, *Int. J. Chem. Kinet.*, 1998, **30**, 291–300.

[39] G. Jones, P. H. King, H. Morgan, M. R. R. de Planque and K.-P. Zauner, *Artificial Life*, 2015, **21**, 195–204.

[40] C. T. Hamik, N. Manz and O. Steinbock, *J. Phys. Chem. A*, 2001, **105**, 6144–6153.

[41] M. M. Britton, *J. Phys. Chem. A*, 2003, **107**, 5033–5041.

[42] I. Szalai, K. Kurin-Csorgei, I. R. Epstein and M. Orban, *J. Phys. Chem. A*, 2003, **107**, 10074–10081.

[43] K. KurinCsorgei, A. M. Zhabotinsky, M. Orban and I. R. Epstein, *J. Phys. Chem.*, 1996, **100**, 5393–5397.

[44] Z. Noszticzius and J. Bodiss, *J. Am. Chem. Soc.*, 1979, **101**, 3177–3182.

[45] F. Krüger, Z. Nagy-Ungvárai and S. C. Müller, *Physica D: Nonlinear Phenomena*, 1995, **84**, 95–102.

[46] R. P. Rastogi, S. N. Singh and P. Chand, *Chem. Phys. Lett.*, 2004, **385**, 403–408.

[47] H. X. Li, R. H. Jin, W. L. Dai and J. F. Deng, *Chem. Phys. Lett.*, 1997, **274**, 41–46.

[48] P. Sevcik and L. Adamcikova, *J. Phys. Chem.*, 1985, **89**, 5178–5179.

[49] J. Gorecki, J. Szymanski and J. N. Gorecka, *The Journal of Physical Chemistry A*, 2011, **115**, 8855–8859.

[50] L. Hegedűs, M. Wittmann, Z. Noszticzius, S. Yan, A. Sirimungkala, H.-D. Försterling and R. J. Field, *Faraday Discussions*, 2002, **120**, 21–38.

[51] R. M. Noyes, R. J. Field and R. C. Thompson, *J. Am. Chem. Soc.*, 1971, **93**, 7315–7316.

[52] K. Bar-Eli, *The Journal of Physical Chemistry*, 1985, **89**, 2855–2860.

[53] T. Turanyi, L. Gyorgyi and R. J. Field, *J. Phys. Chem.*, 1993, **97**, 1931–1941.

[54] H. D. Foersterling and Z. Noszticzius, *J. Phys. Chem.*, 1989, **93**, 2740–2748.

[55] H.-D. Försterling, S. Murányi and Z. Noszticzius, *React Kinet Catal Lett*, 1990, **42**, 217–226.

[56] L. Hegedüs, H.-D. Försterling, L. Onel, M. Wittmann and Z. Noszticzius, *J. Phys. Chem. A*, 2006, **110**, 12839–12844.

[57] M.-L. Smoes, *The Journal of Chemical Physics*, 1979, **71**, 4669–4679.

[58] J. Ungvarai, Z. NagyUngvarai, J. Enderlein and S. C. Muller, *J. Chem. Soc.-Faraday Trans.*, 1997, **93**, 69–71.

[59] A. Sirimungkala, H. D. Forsterling, V. Dlask and R. J. Field, *J. Phys. Chem. A*, 1999, **103**, 1038–1043.

[60] K. Pelle, M. Wittmann, K. Lovrics, Z. Noszticzius, M. L. T. Liveri and R. Lombardo, *J. Phys. Chem. A*, 2004, **108**, 5377–5385.

[61] J. J. Tyson, *The Belousov-Zhabotinskii reaction*, Springer-Verlag, Berlin ; New York, 1976.

[62] N. Shanks, *Foundations of Chemistry*, 2001, **3**, 33–53.

[63] J. D. Johnson, J. G. Mehus, K. Tews, B. I. Milavetz and D. O. Lambeth, *J. Biol. Chem.*, 1998, **273**, 27580–27586.

[64] H. Gest, *Biochem Soc Symp*, 1986, **54**, 3–16.

[65] B. Novák and J. J. Tyson, *Nat Rev Mol Cell Biol*, 2008, **9**, 981–991.

[66] A. T. Winfree, in *Frontiers in Mathematical Biology*, ed. S. A. Levin, Springer Berlin Heidelberg, 1994, pp. 139–158.

[67] R. J. Ellis, *Trends in Biochemical Sciences*, 2001, **26**, 597–604.

[68] E. Meléndez-Hevia, T. G. Waddell and M. Cascante, *J Mol Evol*, 1996, **43**, 293–303.

[69] O. Ebenhöh and R. Heinrich, *Bull. Math. Biol.*, 2001, **63**, 21–55.

[70] S. K. Scott, *Chemical chaos*, Clarendon Press ; Oxford University Press, Oxford : New York, 1991.

[71] H. L. Swinney, *Physica D: Nonlinear Phenomena*, 1983, **7**, 3–15.

[72] J. Maselko and H. L. Swinney, *Physics Letters A*, 1987, **119**, 403–406.

[73] C. Gasquet, *Fourier analysis and applications: filtering, numerical computation, wavelets*, Springer, New York, 1999.

[74] J. W. Cooley and J. W. Tukey, *Mathematics of Computation*, 1965, **19**, 297–301.

[75] S. J. Formosinho, *J. Chem. Ed.*, 1982, **59**, 281–284.

[76] R. Lambiotte, J.-C. Delvenne and M. Barahona, *arXiv:1502.04381 [physics.soc-ph]*, 2015.

[77] K. A. Bacik, M. T. Schaub, M. Beguerisse-Diaz, Y. N. Billeh and M. Barahona, *arXiv:1511.00673 [q-bio.NC]*, 2016.

[78] S. Hoops, S. Sahle, R. Gauges, C. Lee, J. Pahle, N. Simus, M. Singhal, L. Xu, P. Mendes and U. Kummer, *Bioinformatics*, 2006, **22**, 3067–3074.

[79] M. Mrákavová, M. Melicherčík, A. Olexová and u. Treindl, *Collection of Czechoslovak Chemical Communications*, 2003, **68**, 23–34.

[80] Y. Chou, H. Lin, S. Sun and J. Jwo, *J. Phys. Chem.*, 1993, **97**, 8450–8457.

[81] G. Nord and O. Wernberg, *J. Chem. Soc., Dalton Trans.*, 1975, 845–849.

[82] A. Paul, *J. Phys. Chem. B*, 2005, **109**, 9639–9644.

[83] A. T. Winfree, *Science*, 1972, **175**, 634–636.

[84] R. J. Field and R. M. Noyes, *Nature*, 1972, **237**, 390–392.

[85] J. Maselko, J. Reckley and K. Showalter, *J. Phys. Chem.*, 1989, **93**, 2774–2780.

[86] N. Tompkins, N. Li, C. Girabawe, M. Heymann, G. B. Ermentrout, I. R. Epstein and S. Fraden, *PNAS*, 2014, **111**, 4397–4402.

[87] J. M. Greenberg and S. P. Hastings, *SIAM Journal on Applied Mathematics*, 1978, **34**, 515–523.

[88] J. Ross, S. C. Muller and C. Vidal, *Science*, 1988, **240**, 460–465.

[89] D. S. Cohen, J. C. Neu and R. R. Rosales, *SIAM Journal on Applied Mathematics*, 1978, **35**, 536–547.

[90] N. Wiener and A. Rosenblueth, *Arch Inst Cardiol Mex*, 1946, **16**, 205–265.

[91] J. M. Davidenko, A. V. Pertsov, R. Salomonsz, W. Baxter and J. Jalife, *Nature*, 1992, **355**, 349–351.

[92] P. Foerster, S. Muller and B. Hess, *Development*, 1990, **109**, 11.

[93] A. Foulkes, *Ph.D. thesis*, University of Liverpool, United Kingdom, 2009.

[94] J. Lechleiter, S. Girard, E. Peralta and D. Clapham, *Science*, 1991, **252**, 123–126.

[95] I. R. Epstein, *Science*, 1991, **252**, 67–67.

[96] A. N. Zaikin and A. M. Zhabotinsky, *Nature*, 1970, **225**, 535–537.

[97] M. Orbán, K. Kurin-Csörgei, A. M. Zhabotinsky and I. R. Epstein, *Journal of the American Chemical Society*, 1998, **120**, 1146–1150.

[98] A. L. Belmonte, Q. Ouyang and J.-M. Flesselles, *Journal de Physique II*, 1997, **7**, 1425–1468.

[99] A. Belmonte and J.-M. Flesselles, *Phys. Rev. Lett.*, 1996, **77**, 1174–1177.

[100] S. C. Muller, T. Plesser and B. Hess, *Science*, 1985, **230**, 661–663.

[101] D. Barkley, *Physical Review Letters*, 1994, **72**, 164–167.

[102] G. S. Skinner and H. L. Swinney, *Physica D: Nonlinear Phenomena*, 1991, **48**, 1–16.

[103] J. Maselko and K. Showalter, *Physica D: Nonlinear Phenomena*, 1991, **49**, 21–32.

[104] K. Agladze, J. P. Keener, S. C. Muller and A. Panfilov, *Science*, 1994, **264**, 1746–1748.

[105] Q. Ouyang and J.-M. Flesselles, *Nature*, 1996, **379**, 143–146.

[106] P. Foerster, S. C. Müller and B. Hess, *PNAS*, 1989, **86**, 6831–6834.

[107] Z. Nagy-Ungvarai, J. Ungvarai and S. C. Müller, *Chaos: An Interdisciplinary Journal of Nonlinear Science*, 1993, **3**, 15.

[108] T. Plesser, S. C. Mueller and B. Hess, *The Journal of Physical Chemistry*, 1990, **94**, 7501–7507.

[109] S. C. Müller, T. Plesser and B. Hess, *Physica D: Nonlinear Phenomena*, 1987, **24**, 87–96.

[110] Y. Li, S. Bai and Q. Ouyang, *The Journal of Chemical Physics*, 2000, **113**, 11280–11283.

[111] R. C. Gonzalez, R. E. Woods and S. L. Eddins, *Digital Image processing using MATLAB*, Pearson/Prentice Hall, Upper Saddle River, NJ, 2004.

[112] L. Onel, M. Wittmann, K. Pelle, Z. Noszticzius and L. Sciascia, *J. Phys. Chem. A*, 2007, **111**, 7805–7812.

[113] M. J. Rosen, in *Surfactants and Interfacial Phenomena*, John Wiley & Sons, Inc., 2004, pp. 208–242.

[114] M. H. Najar, A. A. Dar and G. M. Rather, *International Journal of Chemical Kinetics*, 2010, **42**, 659–668.

[115] A. Kaminaga, V. K. Vanag and I. R. Epstein, *J. Chem. Phys.*, 2005, **122**, 174706.

[116] S. P. Moulik, *Curr. Sci.*, 1996, **71**, 368–376.

[117] R. E. Stark, P. D. Leff, S. G. Milheim and A. Kropf, *The Journal of Physical Chemistry*, 1984, **88**, 6063–6067.

[118] M. E. Haque, A. R. Das, A. K. Rakshit and S. P. Moulik, *Langmuir*, 1996, **12**, 4084–4089.

[119] S. S. Rawat, S. Mukherjee and A. Chattopadhyay, *The Journal of Physical Chemistry B*, 1997, **101**, 1922–1929.

[120] M. Yoshimoto, H. Shirahama, S. Kurosawa and M. Naito, *The Journal of Chemical Physics*, 2004, **120**, 7067.

[121] Y. Hara and R. Yoshida, *The Journal of Chemical Physics*, 2008, **128**, 224904.

[122] A. Chattopadhyay and K. Harikumar, *FEBS Letters*, 1996, **391**, 199–202.

[123] A. Cifuentes, J. L. Bernal and J. C. Diez-Masa, *Analytical Chemistry*, 1997, **69**, 4271–4274.

[124] H. Maeda, S. Muroi and R. Kakehashi, *The Journal of Physical Chemistry B*, 1997, **101**, 7378–7382.

[125] J. Dey, N. Sultana and K. Ismail, *Journal of Molecular Liquids*, 2015, **207**, 107–111.

[126] M. K. Franchini and J. Carstensen, *Journal of Pharmaceutical Sciences*, 1996, **85**, 220–227.

[127] J. A. Angelo, *Robotics: A Reference Guide to the New Technology*, Libraries Unlimited, 2007.

[128] D. Trivedi, C. D. Rahn, W. M. Kier and I. D. Walker, *Applied Bionics and Biomechanics*, 2008, **5**, 99–117.

[129] C. Laschi and M. Cianchetti, *Front. Bioeng. Biotechnol.*, 2014, **2**, 1–4.

[130] F. Ilievski, A. D. Mazzeo, R. F. Shepherd, X. Chen and G. M. Whitesides, *Angew. Chem.*, 2011, **123**, 1930–1935.

[131] N. Lu and D.-H. Kim, *Soft Robotics*, 2013, **1**, 53–62.

[132] D. Rus and M. T. Tolley, *Nature*, 2015, **521**, 467–475.

[133] Y. Hara, H. Mayama and K. Morishima, *J. Phys. Chem. B*, 2014, **118**, 2576–2581.

[134] T. Patino, R. Mestre and S. Sánchez, *Lab on a Chip*, 2016, **16**, 3626–3630.

[135] S. Maeda, Y. Hara, R. Yoshida and S. Hashimoto, *Angewandte Chemie*, 2008, **120**, 6792–6795.

[136] T. Arimura and M. Mukai, *Chem. Commun.*, 2014, **50**, 5861–5863.

[137] Y. Zhang, N. Zhou, S. Akella, Y. Kuang, D. Kim, A. Schwartz, M. Bezpalko, B. M. Foxman, S. Fraden, I. R. Epstein and B. Xu, *Angewandte Chemie International Edition*, 2013, **52**, 11494–11498.

[138] Y. Zhang, N. Zhou, N. Li, M. Sun, D. Kim, S. Fraden, I. R. Epstein and B. Xu, *J. Am. Chem. Soc.*, 2014, **136**, 7341–7347.

[139] M. Piovanelli, T. Fujie, B. Mazzolai and L. Beccai, 2012 4th IEEE RAS EMBS International Conference on Biomedical Robotics and Biomechatronics (BioRob), 2012, pp. 612–616.

[140] Y. Hara, M. Saiki, T. Suzuki and K. Kikuchi, *Chem. Lett.*, 2014, **43**, 938–940.

[141] O. Kuksenok and A. C. Balazs, *Scientific Reports*, 2015, **5**, 9569.

[142] N. Kozer and G. Schreiber, *Journal of Molecular Biology*, 2004, **336**, 763–774.

[143] A. P. Minton, *J. Biol. Chem.*, 2001, **276**, 10577–10580.

[144] J. Petrlova, S. Hilt, M. Budamagunta, J. Domingo-Espín, J. Voss and J. Lagerstedt, *Biopolymers*, 2016, 683–692.

[145] A. Berezhkovskii and A. Szabo, *Journal of Physical Chemistry B*, 2016, **120**, 5998–6002.

[146] S. Jun and A. Yethiraj, *Biophysical Journal*, 2009, **96**, 1333–1340.

[147] Y. Hara, K. Fujimoto and H. Mayama, *J. Phys. Chem. B*, 2014, **118**, 608–612.

[148] K. Miyakawa, F. Sakamoto, R. Yoshida, E. Kokufuta and T. Yamaguchi, *Phys. Rev. E*, 2000, **62**, 793–798.

[149] T. Masuda, A. Terasaki, A. M. Akimoto, K. Nagase, T. Okano and R. Yoshida, *RSC Adv.*, 2014, **5**, 5781–5787.

[150] D. Suzuki and R. Yoshida, *J. Phys. Chem. B*, 2008, **112**, 12618–12624.

[151] T. Yamaguchi, L. Kuhnert, Z. Nagy-Ungvarai, S. C. Mueller and B. Hess, *J. Phys. Chem.*, 1991, **95**, 5831–5837.

[152] J.-C. P. Gabriel, C. Sanchez and P. Davidson, *J. Phys. Chem.*, 1996, **100**, 11139–11143.

[153] E. Rosellini, C. Cristallini, N. Barbani, G. Vozzi and P. Giusti, *J. Biomed. Mater. Res.*, 2009, **91A**, 447–453.

[154] J. E. Eastoe, *Biochem J*, 1955, **61**, 589–600.

[155] P. M. Wood and J. Ross, *The Journal of Chemical Physics*, 1985, **82**, 1924.

[156] T. Pal, *J. Chem. Educ.*, 1994, **71**, 679.

[157] H. Firouzabadi, N. Iranpoor and A. Ghaderi, 2011, **9**, 865–871.

[158] J. Hagman, N. Lorén and A.-M. Hermansson, *Biomacromolecules*, 2010, **11**, 3359–3366.

[159] B. Amsden, *Macromolecules*, 1998, **31**, 8382–8395.

[160] L. Friedman and E. O. Kraemer, *J. Am. Chem. Soc.*, 1930, **52**, 1295–1304.

[161] I. Pezron, M. Djabourov and J. Leblond, *Polymer*, 1991, **32**, 3201–3210.

[162] J. S. Varghese, N. Chellappa and N. N. Fathima, *Colloids and Surfaces B: Biointerfaces*, 2014, **113**, 346–351.

[163] M. Qian, M. Liu and J. W. Eaton, *Biochemical and Biophysical Research Communications*, 1998, **250**, 385–389.

[164] W. Sun and M. W. Griffiths, *International Journal of Food Microbiology*, 2000, **61**, 17–25.

[165] S. Rosalam and R. England, *Enzyme and Microbial Technology*, 2006, **39**, 197–207.

[166] N. Muntean, G. Szabó, M. Wittmann, T. Lawson, J. Fülöp, Z. Noszticzius and L. Onel, *The Journal of Physical Chemistry A*, 2009, **113**, 9102–9108.

[167] M. Deneux, R. Meilleur and R. L. Benoit, *Canadian Journal of Chemistry*, 1968, **46**, 1383–1388.

[168] P. De Kepper, I. R. Epstein and K. Kustin, *J. Am. Chem. Soc.*, 1981, **103**, 2133–2134.

[169] G. Beni and J. Wang, in *Robots and Biological Systems: Towards a New Bionics?*, ed. P. Dario, G. Sandini and P. Aebischer, Springer Berlin Heidelberg, 1993, pp. 703–712.

[170] S. Mirjalili, S. M. Mirjalili and A. Lewis, *Advances in Engineering Software*, 2014, **69**, 46–61.

[171] W. M. Spears, *Evolutionary algorithms: the role of mutation and recombination*, Springer, Berlin ; New York, 2000.

[172] W. B. Langdon, *Foundations of genetic programming*, Springer, Berlin ; New York, 2002.

[173] Y. Sun, S. K. Halgamuge, M. Kirley and M. A. Munoz, 7th International Conference on Information and Automation for Sustainability, 2014, pp. 1–6.

[174] O. Erdem, E. Ceyhan and Y. Varli, *SSRN Electronic Journal*, 2014.

[175] L. Shampine and M. Reichelt, *SIAM J. Sci. Comput.*, 1997, **18**, 1–22.

[176] D. C. Hanselman, *Mastering MATLAB*, Pearson, Upper Saddle River, 2012.

[177] R. Glaser and M. Jost, *The Journal of Physical Chemistry A*, 2012, **116**, 8352–8365.

[178] M. Kitsak and D. Krioukov, *Phys. Rev. E*, 2011, **84**, 026114.

[179] J.-C. Delvenne, M. T. Schaub, S. N. Yaliraki and M. Barahona, *arXiv:1308.1605 [physics.soc-ph]*, 2013.

[180] M. Cheetham, *Ph.D. thesis*, University of Southampton, 2004.

[181] B. A. Grzybowski, K. J. M. Bishop, B. Kowalczyk and C. E. Wilmer, *Nat Chem*, 2009, **1**, 31–36.

[182] A. Fernández-Ramos, J. A. Miller, S. J. Klippenstein and D. G. Truhlar, *Chemical Reviews*, 2006, **106**, 4518–4584.

[183] C. N. Hinshelwood, *Proceedings of the Royal Society of London. Series A, Containing Papers of a Mathematical and Physical Character*, 1926, **113**, 230–233.

[184] W. L. Hase, *Acc. Chem. Res.*, 1998, **31**, 659–665.

[185] A. Gibbons, *Algorithmic graph theory*, Cambridge University Press, Cambridge [Cambridgeshire] ; New York, 1985.

[186] P. Shannon, A. Markiel, O. Ozier, N. S. Baliga, J. T. Wang, D. Ramage, N. Amin, B. Schwikowski and T. Ideker, *Genome Res.*, 2003, **13**, 2498–2504.

[187] P. Csermely, T. Korcsmáros, H. J. M. Kiss, G. London and R. Nussinov, *Pharmacology & Therapeutics*, 2013, **138**, 333–408.

[188] M. n. Serrano, M. Boguñá and F. Sagués, *Mol. BioSyst.*, 2012, **8**, 843–850.

[189] M. Winlaw, H. DeSterck and G. Sanders, *An in-Depth Analysis of the Chung-Lu Model*, Lawrence Livermore National Lab. (LLNL), Livermore, CA (United States) Technical Report LLNL–TR-678729, 2015.

[190] A. Bonato, D. R. D'Angelo, E. R. Elenberg, D. F. Gleich and Y. Hou, *arXiv:1608.00646 [physics]*, 2016.

[191] J. J. Tyson and B. Novák, *Annual Review of Physical Chemistry*, 2010, **61**, 219–240.

[192] T. Fink, E. Barillot and S. Ahnert, *submitted*, 2006.

[193] R. Milo, *Science*, 2002, **298**, 824–827.

[194] N. Guelzim, S. Bottani, P. Bourgine and F. Képès, *Nature Genetics*, 2002, **31**, 60–63.

[195] m. N. Yaveroglu, S. Fitzhugh, M. Kurant, A. Markopoulou, C. Butts and N. Pržulj, *ergm.graphlets: A Package for ERG Modeling Based on Graphlet Statistics*, 2014, `https://www.jstatsoft.org/article/view/v065i12`.

[196] R. Milo, *Science*, 2004, **303**, 1538–1542.

Appendices

Appendix A

Algorithms

Algorithm A.1: Visualisation function designed to produce the ternary behaviour diagrams or time series maps.

```
function data = TERNARY_DIAGRAM

%% 3D plot and the production of 4 graphs
global metric

% Create a dialog box to select the desired metric:
% Intensity - absorbance spectrum for dataset
% Amplitude -  peak to peak amplitude of each wave
% https://en.wikipedia.org/wiki/Amplitude#Peak-to-
   peak_amplitude
% peaks - counts the number of peaks present in the spectrum
% freq - frequency of waves on a rolling basis; uses 1/time
   for each
% oscillation

% Where there are the options of p and pp these denote the
   first and second
% derivatives
% I_s is to have just the spectrum

list = {'Intensity', 'Amplitude', 'peaks','freq'};
[metric, v]= listdlg('PromptString','Select a metric to
   display',...
```

```
20      'SelectionMode','Single',...
21      'ListString', list);
22  switch metric
23      case 1
24          list = {'All', 'I_s', 'I_p','I_pp'};
25          [metric, v] = listdlg('PromptString','Select a
                metric to display',...
26              'SelectionMode', 'single', 'ListString',...
27              list);
28          metric = list{1,metric};
29          if strcmp(metric,'All')
30              metric = 'Intensity';
31          end
32      case 2
33          list = {'All', 'Am', 'Am_p','Am_pp'};
34          [metric, v] = listdlg('PromptString','Select a
                metric to display',...
35              'SelectionMode', 'single', 'ListString',...
36              list);
37          metric = list{1,metric};
38          if strcmp(metric,'All')
39              metric = 'Amplitude';
40          end
41      case {3,4}
42          metric = list{1,metric};
43  end
44
45  clearvars list v
46
47  % Create a cell array to contain the data from the output of
        the maxmin.m
48  % function
49
50  data = num2cell(zeros(30,1));
51  for i = 1:length(data)
52      data{i,1} = maxmin(metric);
53  end
54
55  % Create an array of the experimental conditions
56
57  experimental = zeros(30,4);
```

```
58
59 % Make sure that these values are  correct for each analysis
       , in this case
60 % 1 is malonic acid, 2 is sodium bromate, 3 is sulfuric acid
       and 4 is
61 % ferroin
62
63 experimental(:,3) = 0.5;
64 experimental(:,4) = 0.002;
65 for i = 1:6:length(experimental)
66     switch i
67         case (1*6)-5
68             experimental(i:i+5,1) = 0.05;
69             experimental(i:i+5,2) = [0.05; 0.1; 0.2; 0.3;
                   0.4; 0.5];
70         case (2*6)-5
71             experimental(i:i+5,1) = 0.1;
72             experimental(i:i+5,2) = [0.05; 0.1; 0.2; 0.3;
                   0.4; 0.5];
73         case (3*6)-5
74             experimental(i:i+5,1) = 0.15;
75             experimental(i:i+5,2) = [0.05; 0.1; 0.2; 0.3;
                   0.4; 0.5];
76         case (4*6)-5
77             experimental(i:i+5,1) = 0.2;
78             experimental(i:i+5,2) = [0.05; 0.1; 0.2; 0.3;
                   0.4; 0.5];
79         case (5*6)-5
80             experimental(i:i+5,1) = 0.25;
81             experimental(i:i+5,2) = [0.05; 0.1; 0.2; 0.3;
                   0.4; 0.5];
82             % case (6*6)-5
83             %     experimental(i:i+5,1) = 0.5;
84             %     experimental(i:i+5,2) = [0.05; 0.1; 0.2;
                   0.3; 0.4; 0.5];
85     end
86 end
87
88 % Convert the values for each concentration to a molar
       fraction
89
```

```
90 experimental(:,1) = experimental(:,1)./(experimental(:,1)+
      experimental(:,2)+experimental(:,3)+experimental(:,4));
91 experimental(:,2) = experimental(:,2)./(experimental(:,1)+
      experimental(:,2)+experimental(:,3)+experimental(:,4));
92 experimental(:,3) = experimental(:,3)./(experimental(:,1)+
      experimental(:,2)+experimental(:,3)+experimental(:,4));
93
94 A = experimental(:, 1);
95 B = experimental(:, 2);
96 C = experimental(:,3);
97
98 clearvars experimental
99
100 % Switch used to produce the graphical output assigned in
      maxmin.m
101 % These sections require the ternplot package from the
      MATLAB file exchange
102 % http://www.mathworks.com/matlabcentral/fileexchange/2299-
      alchemyst-ternplot
103
104 switch metric
105     % Generates triangular (ternary) plots with number of
          detected peaks
106     case 'peaks'
107         data = cell2mat(data);
108         f = figure;
109         ax = axes('Units','pixels');
110         set (f, 'Units', 'normalized', 'Position',
              [0,0,1,1]);
111         subplot(2, 2, 1)
112         ternplot(A, B, C, '.r');
113         ternlabel('% MA', '% BrO_{3}^{-}', '% H_{2}SO_{4}');
114         subplot(2, 2, 2)
115         ternpcolor(A, B, C, data); ternlabel('% MA', '% BrO_
              {3}^{-}', '% H_{2}SO_{4}');
116         shading interp
117         subplot(2, 2, 3)
118         terncontour(A, B, C, data); ternlabel('% MA', '%
              BrO_{3}^{-}', '% H_{2}SO_{4}');
119         subplot(2, 2, 4)
120         ternsurf(A, B, C, data);
```

```
121
122         % Create pop-up menu to select visual result (not
                necessary but can
123         % aid understanding)
124         popup = uicontrol('Style', 'popup',...
125             'String', {'parula','jet','hsv','hot','cool','
                    gray'},...
126             'Position', [20 340 100 50],...
127             'Callback', @setmap);
128
129     case {'Intensity', 'Amplitude'}
130         % Generates scatter plots for the absorbance
                spectrum or the peak
131         % to peak amplitude depending on the option selected
132
133         f = figure;
134         if length(data{1,1}) > 3;
135             if strcmp(metric,'Amplitude')
136                 x = data{1,1}{1,4}(:,1);
137             else
138                 x = data{1,1}{1,4}{1,1}(:,1);
139             end
140         else
141             x = data{1,1}{1,2}(:,1);
142         end
143         if strcmp(metric,'Amplitude')
144             opt = '.';
145             lab1 = 'Amplitude';
146         else
147             opt = '';
148             lab1 = 'Absorbance';
149         end
150
151         subplot(3,1,1),
152         h = plot(x,data{1,1}{1,1}(:,1),opt);
153         xlabel('Time/s'); ylabel(lab1);
154         subplot(3,1,2),
155         h1 = plot(x,data{1,1}{1,2}(:,1),opt);
156         xlabel('Time/s'); ylabel('First derivative');
157         subplot(3,1,3),
158         h2 = plot(x,data{1,1}{1,3}(:,1),opt);
```

```
159         xlabel('Time/s'); ylabel('Second derivative');
160         print('-clipboard', '-dbitmap')
161
162         % Create a slider so that all of the data / plots
               can be cycled
163         % through in a single figure window
164
165         b = uicontrol('Parent',f,'Style','slider','Callback'
               ,@sld_func,...
166             'SliderStep',[0.033 1],'Position'
                   ,[81,54,419,23],...
167             'value',1, 'min',1, 'max',length(data));
168         bgcolor = 'white';
169         bl1 = uicontrol('Parent',f,'Style','text','Position'
               ,[50,54,23,23],...
170             'String','1','BackgroundColor',bgcolor);
171         bl2 = uicontrol('Parent',f,'Style','text','Position'
               ,[500,54,23,23],...
172             'String',sprintf('%d',length(data)),'
                   BackgroundColor',bgcolor);
173         bl3 = uicontrol('Parent',f,'Style','text','Position'
               ,[240,25,100,23],...
174             'String','Dataset' ,'BackgroundColor',bgcolor);
175
176     case 'freq'
177         f = figure;
178         h = plot(data{1,1}{1,2}(:,1),data{1,1}{1,1}(1,:));
179
180         b = uicontrol('Parent',f,'Style','slider','Callback'
               ,@sld_func,...
181             'SliderStep',[0.027 1],'Position'
                   ,[81,54,419,23],...
182             'value',1, 'min',1, 'max',length(data));
183         bgcolor = f.Color;
184         bl1 = uicontrol('Parent',f,'Style','text','Position'
               ,[50,54,23,23],...
185             'String','1','BackgroundColor',bgcolor);
186         bl2 = uicontrol('Parent',f,'Style','text','Position'
               ,[500,54,23,23],...
187             'String',sprintf('%d',length(data)),'
                   BackgroundColor',bgcolor);
```

```
188         bl3 = uicontrol('Parent',f,'Style','text','Position'
                ,[240,25,100,23],...
189             'String','Dataset' ,'BackgroundColor',bgcolor);
190
191         set(h,'LineStyle','none','Marker','.')
192         %                   print('-clipboard', '-dbitmap')
193     otherwise
194         f = figure;
195         ax = axes('Parent',f,'position',[0.13 0.39  0.77
                0.54]);
196         h = plot(ax,data{1,1});
197         b = uicontrol('Parent',f,'Style','slider','Callback'
                ,@sld_func,...
198             'SliderStep',[0.027 1],'Position'
                    ,[81,54,419,23],...
199             'value',1, 'min',1, 'max',length(data));
200         bgcolor = f.Color;
201         bl1 = uicontrol('Parent',f,'Style','text','Position'
                ,[50,54,23,23],...
202             'String','1','BackgroundColor',bgcolor);
203         bl2 = uicontrol('Parent',f,'Style','text','Position'
                ,[500,54,23,23],...
204             'String',sprintf('%d',length(data)),'
                    BackgroundColor',bgcolor);
205         bl3 = uicontrol('Parent',f,'Style','text','Position'
                ,[240,25,100,23],...
206             'String','Dataset' ,'BackgroundColor',bgcolor);
207
208         switch metric
209             case 'I_s'
210                 axis([0 1200 0 5])
211                 label_1 = xlabel('Time, t / s');
212                 label_2 = ylabel('Absorbance');
213             case 'I_p'
214                 axis([0 1200 -2 2])
215                 label_1 = xlabel('Time, t / s');
216                 label_2 = ylabel('$\frac{dAbsorbance}{dt}$')
                        ;
217             case 'I_pp'
218                 axis([0 1200 -3 3])
219                 label_1 = xlabel('Time, t / s');
```

```
220                 label_2 = ylabel('$\frac{d^{2}Absorbance}{dt
                        ^{2}}$');
221         end
222         set(label_1,'Interpreter','LaTex');
223         set(label_2,'Interpreter','LaTex');
224 end
225
226     % The following function sets up the slider produced on
            the plots above
227     function sld_func(hObj, event)
228         if exist('h1','var') == 1
229             switch metric
230                 case 'Intensity'
231                     set(h,'YData', data{round(get(hObj,'
                            Value')),1}{1,1}(:,1));
232                     set(h1,'YData', data{round(get(hObj,'
                            Value')),1}{1,2}(:,1));
233                     set(h2,'YData', data{round(get(hObj,'
                            Value')),1}{1,3}(:,1));
234                     set(h,'XData', data{round(get(hObj,'
                            Value')),1}{1,4}{1,1}(:,1));
235                     set(h1,'XData', data{round(get(hObj,'
                            Value')),1}{1,4}{1,1}(:,1));
236                     set(h2,'XData', data{round(get(hObj,'
                            Value')),1}{1,4}{1,1}(:,1));
237                 case 'Amplitude'
238                     set(h,'YData', data{round(get(hObj,'
                            Value')),1}{1,1}(:,1));
239                     set(h1,'YData', data{round(get(hObj,'
                            Value')),1}{1,2}(:,1));
240                     set(h2,'YData', data{round(get(hObj,'
                            Value')),1}{1,3}(:,1));
241                     set(h,'XData', data{round(get(hObj,'
                            Value')),1}{1,4}(:,1));
242                     set(h1,'XData', data{round(get(hObj,'
                            Value')),1}{1,4}(:,1));
243                     set(h2,'XData', data{round(get(hObj,'
                            Value')),1}{1,4}(:,1));
244                 case 'freq'
245                     set(h,'YData',data{round(get(hObj, '
                            Value')),1}{1,1}(1,:));
```

```
246                         set(h,'XData', data{round(get(hObj,'
                               Value')),1}{1,2}(1,:));
247                     otherwise
248                         set(h,'YData', data{round(get(hObj,'
                               Value')),1});
249                 end
250             end
251         end
252 end
```

ALGORITHM A.2: Spiral picking algorithm for identifying and tracking spirals with time.

```
1
2  % load directory
3  % directory = dir('[redacted]
       [redacted]');
4  clearvars
5  directory = dir('[redacted]
       [redacted]');
6
7  for i = 1:length(directory)
8      names{i,1} = directory(i).name;
9  end
10 [names, index] = sort_nat(names);
11
12 clearvars directory
13
14 for k = 1:4:length(names)
15     %pic = imread(fullfile[redacted]
           [redacted]',names{k}));
16     pic = imread(fullfile[redacted]
           [redacted]',names{k}));
17     pic = adapthisteq(pic(:,:,2));
18     bz_imshow(pic); shg;
19     num_input = input(sprintf('%i / %i How many spirals are
           present? ',k,length(names)));
20     clearvars c_info
21     for j = 1:num_input
22 %disp(sprintf('%i',j))
```

```
23          for i = 1:15
24              shg
25              dcm_obj = datacursormode(1);
26              set(dcm_obj,'DisplayStyle','window',...
27                  'SnapToDataVertex','off','Enable','on')
28              waitforbuttonpress
29              c_info{i,j} = getCursorInfo(dcm_obj);
30          end
31           disp('Next spiral');
32      end
33      for j = 1:num_input
34          for i = 1:size(c_info,1)
35              positions{i,j} = c_info{i,j}.Position;
36          end
37      end
38      for i = 1:num_input
39          [image{k}.SPIRALS.a(i),...
40              image{k}.SPIRALS.b(i),...
41              image{k}.SPIRALS.X_cen(i),...
42              image{k}.SPIRALS.Y_cen(i),...
43              image{k}.SPIRALS.rfit{i},...
44              image{k}.SPIRALS.th{i},...
45              image{k}.SPIRALS.sep{i}] = fit_logspiral(pic,
                    cell2mat(positions(:,i)));
46          %save('[redacted]
                [redacted]','image');
47      save('[redacted]
            [redacted]','image');
48      end
49      close all
50
51  end
52
53
54  high = find(~cellfun(@isempty,image), 1, 'last' );
55  image(high+1:length(names)) = {[]};
56  clearvars high
57
58  for i = 1:length(image)
59      % Check to see if the cells are empty within the matrix
            above and
```

```
60      % ignore if they are
61      emptyCells = cellfun(@isempty,image);
62      if emptyCells(i) == 1
63          continue
64      else
65          % For however many spirals there are check the
               number of spirals
66          % there are in future images
67          for j = 1:length(image{1,i}.SPIRALS.X_cen)
68              for s = 1:length(image) - i
69                  if emptyCells(i+s) == 1
70                      continue
71                  else
72                      % Calculate the distance between each
                           spiral in current
73                      % image and all other spiral centres in
                           future images,
74                      % stored as dist2
75                      for k = 1:length(image{1,i+s}.SPIRALS.
                           X_cen)
76                          dist2(j,k,s,i) = sqrt(((image{1,i}.
                               SPIRALS.X_cen(j)-image{1,i+s}.
                               SPIRALS.X_cen(k))^2) + ((image{1,
                               i}.SPIRALS.Y_cen(j)-image{1,i+s}.
                               SPIRALS.Y_cen(k))^2));
77
78                          for m = 1:find(dist2(:,1,s,i)>0, 1,
                               'last')
79                              if length(find(dist2(m,:,s,i) ==
                                   min(dist2(m,dist2(m,:,s,i)
                                   >0,s,i)))) == 1
80                                  minimal(m,s,i) = find(dist2(
                                       m,:,s,i) == min(dist2(m,
                                       dist2(m,:,s,i)>0,s,i)));
81                              else
82                                  minimal(m,s,i) = 1;
83                              end
84                          end
85                      end
86                  end
87              end
```

```
88          end
89      end
90  end
91  for i = 1:length(image)
92      if emptyCells(i) == 1
93          mean_seps(i) = 0;
94  std_steps(i) = 0;
95      else
96          mean_seps(i) = mean(cell2mat(image{i}.SPIRALS.sep));
97  std_steps(i) = std(cell2mat(image{i}.SPIRALS.sep));
98      end
99  end
100 %save('[redacted]');
101 save('[redacted]');
102
103 %
104 % figure()
105 % s = 144;
106 % pic2 = imread(fullfile('[redacted]',names{s}));
107 %     pic2 = adapthisteq(pic2(:,:,2));
108 % imshow(pic2);
109 % hold on
110 % for p = 1:i
111 %     plot(image{s}.SPIRALS.rfit{p}.*cos(image{s}.SPIRALS.th
    {p})+image{s}.SPIRALS.X_cen(p),image{s}.SPIRALS.rfit{p}.*
    sin(image{s}.SPIRALS.th{p})+image{s}.SPIRALS.Y_cen(p),'g
    ',...
112 %         image{s}.SPIRALS.X_cen(p),image{s}.SPIRALS.Y_cen(p
    ),'b+');
113 % end
114
115 % for i = 1:692
116 % if emptyCells(710+i) == 1
117 % continue
118 % else
119 % r = minimal(1,i,710);
120 % XCEN(i+1) = image{i+710}.SPIRALS.X_cen([r]);
121 % YCEN(i+1) = image{i+710}.SPIRALS.Y_cen([r]);
```

```
% end
% end
% close all;
% pic = imread(fullfile[redacted]
    [redacted]',names{1150}));
% pic = adapthisteq(pic(:,:,2));
% bz_imshow(pic); shg;
% hold on
% plot(XCEN,YCEN,'.')
```

ALGORITHM A.3: Pre-processing of images to mask background. This ensured only the waves in the petri dish contributed to image statistics.

```
% Malonic acid concentration gives filename
file = {'ZA' 'ZB' 'ZC' 'ZD' 'ZE' 'YA' 'YB' 'YC' 'YD' 'YE'};
%bromate concentrations
conc = {'005' '010' '020' '030' '040' '050'};

c1 = [1309 1270 1274 1246 1321 1230 1281 1250 1345 1309];
r1 = [70 126 82 146 126 186 154 142 102 146];
r2 = [1197 1257 1201 1309 1249 1305 1273 1281 1201 1253];
r3 = [2333 2369 2321 2424 2373 2420 2353 2369 2369 2385];

% cropping files
for i = 1:length(file)
    for k = 1:length(conc)
        mkdir(sprintf[redacted]
            [redacted]',file{i},conc{k}));
    end
    x = dir(sprintf('[redacted]
        [redacted]',file{i}));
    for j = 1:length(x)
        pic = imread(fullfile(sprintf[redacted]
            [redacted]',file{i}),x(j).name)
            );
        for k = 1:length(conc)
            switch k
                case 1
```

```
22                      imwrite(pic(r3(i):end,1:c1(i),:),
                            sprintf('[redacted]',
                            file{i},conc{k},conc{k},j),'jpg');
23                  case 2
24                      imwrite(pic(r3(i):end,c1(i)+1:end,:),
                            sprintf('[redacted]',
                            file{i},conc{k},conc{k},j),'jpg');
25                  case 3
26                      imwrite(pic(r2(i):r3(i)-1,1:c1(i),:),
                            sprintf('[redacted]',
                            file{i},conc{k},conc{k},j),'jpg');
27                  case 4
28                      imwrite(pic(r2(i):r3(i)-1,c1(i)+1:end,:)
                            , sprintf('[redacted]',
                            file{i},conc{k},conc{k},j),'jpg');
29                  case 5
30                      imwrite(pic(r1(i):r2(i)-1,1:c1(i),:),
                            sprintf('[redacted]',
                            file{i},conc{k},conc{k},j),'jpg');
31                  case 6
32                      imwrite(pic(r1(i):r2(i)-1,c1(i)+1:end,:)
                            , sprintf('[redacted]',
                            file{i},conc{k},conc{k},j),'jpg');
33              end
34          end
35      end
36  end
37
38
39  % Set the time values for each experiment
40  for i = 1:length(file)
41      x = dir(sprintf('[redacted]',file{i}));
42      for j = 1:length(x)
43          times(j,i) = datetime(x(j).date);
```

```
44      end
45      dt = diff(times); dt.Format = 's';
46      times_absolute(1,i) = dt(1,i)-dt(1,i);
47      for k = 2:size(dt,1)
48          times_absolute(k,i) = times_absolute(k-1,i) + dt(k
               -1,i);
49      end
50      times_absolute.Format = 'm';
51  end
52
53  % Input the centres of each image. Columns are each malonic
       acid
54  % concentration while rows are each bromate concentration.
55
56  cx = [  633 664 724 661 699 651 734 683 688 722;
57      615 753 636 630 579 677 638 702 561 635;
58      669 611 710 655 703 646 666 680 730 724;
59      632 681 733 672 624 675 627 717 597 609;
60      698 590 657 656 718 649 696 668 708 620;
61      628 685 726 597 645 566 620 617 637 587];
62
63  cy = [  540 573 536 555 507 536 513 594 528 541;
64  590 551 553 517 549 542 626 514 578 535;
65  556 567 588 564 512 551 521 554 522 541;
66  573 557 550 577 611 579 558 524 610 597;
67  537 555 533 561 528 524 526 536 527 574;
68  571 547 603 525 600 550 591 568 574 576];
69
70  r=455;
71
72
73  for i = 1:length(file)
74      for m = 1:length(conc)
75  mkdir(sprintf('[redacted]
       ',file{i},conc{m}));
76          filenames = dir(sprintf('[redacted]
                [redacted]',file{i},conc{m},
               conc{m}));
77          for j = 1:length(filenames)
```

```
78              A = imread(sprintf('[redacted]',file{i},conc{m},
                    filenames(j).name));
79              ix = size(A,2); iy = size(A,1);
80              [x,y]=meshgrid(-(cx(m,i)-1):(ix-cx(m,i)),-(cy(m,
                    i)-1):(iy-cy(m,i)));
81              c_mask=((x.^2+y.^2)<=r^2);
82              A_copy = A;
83              for k = 1:iy
84                  for l = 1:ix
85                      if c_mask(k,l) == 0
86                          A_copy(k,l,:) = 0;
87                      end
88                  end
89              end
90              imwrite(A_copy,sprintf('[redacted]',file{i},filenames(j).
                    name));
91          end
92      end
93  end
94  for i = 1:length(file)
95      for m = 1:length(conc)
96          ent_files{m,i} = dir(sprintf('[redacted]',file{i},
                conc{m}));
97          ent_files_names{m,i} = {ent_files{m,i}.name};
98          [sort_ent{m,i},index] = sort_nat(ent_files_names{m,i
                });
99      end
100 end
101 for i = 1:length(file)
102     for m = 1:length(conc)
103         for j = 1:length(sort_ent{m,i})
104
105             P = imread(sprintf('[redacted]',file{i},sort_ent{m,i}{
                    j}));
106             p = imhist(rgb2gray(P));
107             p = p./numel(P);
108             L = length(p);
```

```
109                 [v, mu] = statmoments(p, 3);
110                 % Average gray level
111                 Texture{m}.values{j,i}(1) = mu(1);
112                 % Standard deviation.
113                 Texture{m}.values{j,i}(2) = mu(2).^0.5;
114                 % Smoothness.
115                 % First normalize the variance to [0 1] by
                        dividing it by (L-1)^2.
116                 varn = mu(2)/(L - 1)^2;
117                 Texture{m}.values{j,i}(3) = 1 - 1/(1 + varn);
118                 % Third moment (normalized by (L - 1)^2 also).
119                 Texture{m}.values{j,i}(4) = mu(3)/(L - 1)^2;
120                 % Uniformity.
121                 Texture{m}.values{j,i}(5) = sum(p.^2);
122                 % Entropy.
123                 Texture{m}.values{j,i}(6) = -sum(p.*(log2(p +
                        eps)));
124                 %Entropy{m}.Ent_vals(j,i) = entropy(imread(
                        sprintf('[redacted]
                        [redacted]',file{i},sort_ent{m,i}{
                        j})));
125             end
126         end
127     end
```

Appendix B

Constants of the Exponential Chirp

The modelling of the stirred system as an oscillating chirp signal gives a

$$f(t) = f_i \eta^t \tag{B.1}$$

f_i is the initial frequency of the oscillation and η controls the rate at which the oscillation reaches its final frequency,f_Ω, at time, t_Ω.

$$k = \left(\frac{f_\Omega}{f_i}\right)^{\frac{1}{\Omega}} \tag{B.2}$$

In the time domain the wave would have the form of the sinusoidal function given by Equation B.3

$$x(t) = A(t) \sin\left[2\pi f_i \left(\frac{\eta^t - 1}{\ln \eta}\right) + \phi_0\right] + x_0 \tag{B.3}$$

Table B.1 gives the value of η, t_Ω (the length of the frequency sweep), f_i and f_Ω for a range of initial conditions of the iron-catalysed Belousov-Zhabotinsky reaction.

$[H_2SO_4]$	$[BrO_3-]$	[MA]	η	T_Ω	f_i	f_Ω
0.250	0.050	0.250	0.9972	1093.4	0.3084	0.0141
0.250	0.100	0.050	0.9997	996.1	0.2163	0.1625
0.250	0.100	0.100	0.9992	637.7	0.2677	0.1597
0.250	0.100	0.150	1.0016	870.1	0.0674	0.2713
0.250	0.100	0.200	1.0229	83.3	0.0497	0.3274
0.250	0.100	0.250	0.9985	1136.8	0.0891	0.0169
0.250	0.200	0.050	0.9973	1140.3	0.2652	0.0123
0.250	0.200	0.050	0.9970	1144.5	0.2972	0.0096
0.250	0.200	0.100	1.0017	124.6	0.0817	0.1009
0.250	0.200	0.100	1.0003	1173.9	0.1385	0.1858
0.250	0.200	0.150	0.9995	809.2	0.2887	0.1965
0.250	0.200	0.150	0.9994	996.1	0.2554	0.1440
0.250	0.200	0.200	0.9972	1092.7	0.2708	0.0128
0.250	0.300	0.050	0.9978	1161.3	0.2760	0.0225
0.250	0.300	0.050	0.9992	1174.6	0.0419	0.0169
0.250	0.300	0.050	0.9981	1148.7	0.1816	0.0211
0.250	0.300	0.050	0.9990	1169.7	0.0651	0.0194
0.250	0.300	0.150	0.9985	1152.9	0.1280	0.0217
0.250	0.300	0.150	0.9983	1156.4	0.0976	0.0138
0.250	0.300	0.150	0.9978	1162.0	0.2094	0.0164
0.250	0.300	0.150	0.9981	1119.3	0.1204	0.0149
0.250	0.400	0.050	0.9994	1158.5	0.2768	0.1360
0.250	0.400	0.050	0.9989	1173.9	0.1265	0.0333
0.250	0.400	0.050	0.9998	924.7	0.0387	0.0323
0.250	0.400	0.050	0.9978	1190.7	0.3564	0.0261
0.250	0.400	0.100	0.9988	1160.6	0.1146	0.0270

0.250	0.400	0.150	0.9988	1171.8	0.1184	0.0294
0.250	0.400	0.150	0.9977	926.1	0.2402	0.0275
0.250	0.400	0.200	0.9979	1197.0	0.3666	0.0292
0.250	0.500	0.050	0.9977	1176.7	0.4728	0.0309
0.250	0.500	0.050	0.9979	1068.2	0.3545	0.0371
0.250	0.500	0.050	0.9995	1160.6	0.0608	0.0359
0.250	0.500	0.050	0.9996	1194.9	0.2220	0.1458
0.250	0.500	0.100	0.9989	674.1	0.0770	0.0376
0.250	0.500	0.100	0.9992	1169.7	0.1260	0.0476
0.250	0.500	0.100	0.9992	1175.3	0.1335	0.0541
0.250	0.500	0.150	0.9988	1180.9	0.2002	0.0474
0.250	0.500	0.200	0.9979	935.2	0.2831	0.0404
0.250	0.500	0.200	0.9986	1152.2	0.3106	0.0608
0.500	0.100	0.050	0.9982	1175.3	0.1868	0.0230
0.500	0.200	0.100	0.9997	1162.0	0.0561	0.0400
0.500	0.300	0.150	0.9982	263.9	0.1858	0.1145
0.500	0.300	0.150	0.9987	821.8	0.1989	0.0673
0.500	0.400	0.200	0.9976	772.1	0.3714	0.0579
0.500	0.500	0.250	0.9983	1194.9	0.6999	0.0902
0.800	0.050	0.050	0.9994	1072.4	0.0149	0.0080
0.800	0.050	0.050	1.0008	1169.7	0.0348	0.0921
0.800	0.050	0.050	1.0002	1118.6	0.0183	0.0221
0.800	0.050	0.050	0.9975	1141.0	0.3873	0.0214
0.800	0.050	0.100	1.0000	1054.2	0.0151	0.0145
0.800	0.050	0.150	0.9978	1180.2	0.3512	0.0273
0.800	0.050	0.200	0.9995	1178.8	0.0662	0.0372
0.800	0.050	0.250	0.9983	1137.5	0.1814	0.0272

0.800	0.100	0.050	0.9992	1181.6	0.1288	0.0478
0.800	0.100	0.050	0.9998	1033.9	0.2043	0.1715
0.800	0.100	0.050	0.9984	1192.1	0.3026	0.0426
0.800	0.100	0.100	0.9985	1185.8	0.3553	0.0596
0.800	0.100	0.150	0.9991	1192.8	0.1858	0.0646
0.800	0.100	0.200	0.9988	1190.7	0.2402	0.0562
0.800	0.100	0.250	0.9984	1190.0	0.3714	0.0563
0.800	0.200	0.050	0.9992	1190.7	0.3061	0.1145
0.800	0.200	0.050	0.9991	1195.6	0.4155	0.1460
0.800	0.200	0.050	0.9989	1190.0	0.2910	0.0753
0.800	0.200	0.100	0.9979	856.8	0.6602	0.1122
0.800	0.200	0.100	0.9988	892.5	0.3326	0.1122
0.800	0.200	0.100	0.9999	738.5	0.2038	0.1913
0.800	0.200	0.150	0.9988	868.0	0.3238	0.1168
0.800	0.200	0.200	0.9988	1189.3	0.2946	0.0701
0.800	0.200	0.250	0.9984	638.4	0.3836	0.1339
0.800	0.200	0.250	0.9979	939.4	0.4630	0.0672
0.800	0.300	0.050	0.9987	787.5	0.4111	0.1453
0.800	0.300	0.050	0.9988	1190.0	0.4233	0.0989
0.800	0.300	0.100	0.9983	1195.6	0.6205	0.0799
0.800	0.300	0.150	0.9988	1196.3	0.5808	0.1396
0.800	0.300	0.200	0.9989	880.6	0.4508	0.1786
0.800	0.300	0.250	0.9980	1180.2	0.6614	0.0649
0.800	0.400	0.050	0.9992	807.1	0.5026	0.2738
0.800	0.400	0.050	1.0000	1196.3	0.4630	0.4881
0.800	0.400	0.050	0.9988	1194.9	0.6205	0.1436
0.800	0.400	0.100	0.9997	1195.6	0.3598	0.2421

0.800	0.400	0.150	0.9988	642.6	0.5820	0.2619
0.800	0.400	0.200	0.9992	1161.3	0.2601	0.0988
0.800	0.400	0.250	0.9990	1194.2	0.4630	0.1452
0.800	0.500	0.050	0.9996	1194.9	0.3873	0.2265
0.800	0.500	0.100	1.0000	1195.6	0.4034	0.3869
0.800	0.500	0.150	0.9997	1194.2	0.3819	0.2545
0.800	0.500	0.200	0.9995	1192.1	0.3317	0.1849
0.800	0.500	0.250	0.9993	1195.6	0.5010	0.2126

TABLE B.1: Constants of the exponential chirp across a range of initial conditions.

Appendix C

Fundamental Frequencies

[H+]	[BrO3]	[MA]	f_0 / s^{-1}	t_p / s
0.25	0.05	0.1	0.0075	133.3444
0.25	0.05	0.1	0.0083	120.01
0.25	0.05	0.1	0.0075	133.3444
0.25	0.05	0.1	0.0075	133.3444
0.25	0.05	0.15	0.0075	133.3444
0.25	0.05	0.25	0.0175	57.1476
0.25	0.1	0.05	0.0075	133.3444
0.25	0.1	0.05	0.0092	109.1
0.25	0.1	0.1	0.0083	120.01
0.25	0.1	0.1	0.0178	56.3048
0.25	0.1	0.15	0.0083	120.01
0.25	0.1	0.2	0.0075	133.3444
0.25	0.1	0.25	0.0233	42.8607
0.25	0.2	0.05	0.0108	92.3154
0.25	0.2	0.05	0.01	100.0083
0.25	0.2	0.1	0.0083	120.01
0.25	0.2	0.1	0.0208	48.004

0.25	0.2	0.15	0.0125	80.0067
0.25	0.2	0.15	0.0075	133.3444
0.25	0.2	0.2	0.0183	54.55
0.25	0.3	0.05	0.0258	38.7129
0.25	0.3	0.05	0.0175	57.1476
0.25	0.3	0.05	0.0208	48.004
0.25	0.3	0.05	0.02	50.0042
0.25	0.3	0.15	0.0175	57.1476
0.25	0.3	0.15	0.015	66.6722
0.25	0.3	0.15	0.02	50.0042
0.25	0.3	0.15	0.0133	75.0063
0.25	0.4	0.05	0.0408	24.4918
0.25	0.4	0.05	0.0308	32.4351
0.25	0.4	0.05	0.0292	34.2886
0.25	0.4	0.05	0.0275	36.3667
0.25	0.4	0.1	0.0375	26.6689
0.25	0.4	0.15	0.0325	30.7718
0.25	0.4	0.15	0.0333	30.0025
0.25	0.4	0.2	0.0408	24.4918
0.25	0.5	0.05	0.0317	31.5816
0.25	0.5	0.05	0.0383	26.0891
0.25	0.5	0.05	0.0425	23.5314
0.25	0.5	0.05	0.04	25.0021
0.25	0.5	0.1	0.0583	17.1443
0.25	0.5	0.1	0.0592	16.9028
0.25	0.5	0.1	0.0542	18.4631
0.25	0.5	0.15	0.0467	21.4304

0.25	0.5	0.2	0.0558	17.9119
0.25	0.5	0.2	0.065	15.3859
0.5	0.1	0.05	0.02	50.0042
0.5	0.2	0.1	0.0592	16.9028
0.5	0.3	0.15	0.0075	133.3444
0.5	0.3	0.15	0.0992	10.0849
0.5	0.4	0.2	0.115	8.6964
0.5	0.5	0.25	0.1292	7.7426
0.8	0.05	0.05	0.01	100.0083
0.8	0.05	0.05	0.0258	38.7129
0.8	0.05	0.05	0.0208	48.004
0.8	0.05	0.05	0.02	50.0042
0.8	0.05	0.1	0.0192	52.1783
0.8	0.05	0.15	0.0283	35.2971
0.8	0.05	0.2	0.0375	26.6689
0.8	0.05	0.25	0.0275	36.3667
0.8	0.1	0.05	0.05	20.0017
0.8	0.1	0.05	0.0092	109.1
0.8	0.1	0.05	0.0542	18.4631
0.8	0.1	0.1	0.0583	17.1443
0.8	0.1	0.15	0.0725	13.7943
0.8	0.1	0.2	0.0583	17.1443
0.8	0.1	0.25	0.0642	15.5857
0.8	0.2	0.05	0.01	100.0083
0.8	0.2	0.05	0.1125	8.8896
0.8	0.2	0.05	0.0783	12.767
0.8	0.2	0.1	0.1183	8.4514

0.8	0.2	0.1	0.1167	8.5721
0.8	0.2	0.1	0.0075	133.3444
0.8	0.2	0.15	0.0075	133.3444
0.8	0.2	0.2	0.1217	8.2199
0.8	0.2	0.25	0.0075	133.3444
0.8	0.2	0.25	0.13	7.6929
0.8	0.3	0.05	0.1383	7.2295
0.8	0.3	0.05	0.1042	9.6008
0.8	0.3	0.1	0.0075	133.3444
0.8	0.3	0.15	0.1508	6.6304
0.8	0.3	0.2	0.01	100.0083
0.8	0.3	0.25	0.1658	6.0307
0.8	0.4	0.05	0.1979	5.054
0.8	0.4	0.05	0.2366	4.2257
0.8	0.4	0.05	0.1342	7.454
0.8	0.4	0.1	0.0083	120.01
0.8	0.4	0.15	0.0083	120.01
0.8	0.4	0.2	0.0092	109.1
0.8	0.4	0.25	0.0075	133.3444
0.8	0.5	0.05	0.2783	3.5931
0.8	0.5	0.1	0.0167	60.005
0.8	0.5	0.15	0.0075	133.3444
0.8	0.5	0.2	0.195	5.1286
0.8	0.5	0.25	0.01	100.0083

TABLE C.1: Fundamental frequencies of oscillations as determined by Fourier Transform. Some low frequencies are observed under high acid conditions as a result of the threshold used for detection.

Appendix D

Spiral Wave Parameters

$[H_2SO_4]$ / M	[MA] / M	$[NaBrO_3]$ / M	$\alpha \times 10^3$ / min^{-1}	$\bar{\lambda}_0$ / cm
0.80	0.05	0.05	1.06	0.28
		0.10	0.86	0.21
	0.10	0.05	0.77	0.24
		0.10	1.48	0.12
		0.20	0.80	0.11
	0.15	0.05	1.81	0.22
		0.10	1.62	0.16
	0.20	0.05	1.67	0.25
		0.10	1.72	0.14
		0.20	0.76	0.12
		0.30	0.79	0.10
	0.25	0.05	0.56	0.30
		0.10	0.73	0.26
		0.20	1.65	0.07
		0.30	0.63	0.12
	0.05	0.05	1.41	0.17
	0.10	0.05	1.38	0.15

	0.10	1.91	0.07
0.15	0.05	1.20	0.15
	0.10	2.06	0.06
	0.20	1.06	0.07
0.20	0.05	1.74	0.12
	0.10	1.77	0.04
0.25	0.05	4.76	0.19
	0.10	0.64	0.15
	0.20	2.04	0.02

TABLE D.1: Spiral wave parameters across a range of initial conditions for the iron-catalysed BZ reaction. In all cases [ferroin] = 0.002 M

Appendix E

Equations of the Marburg-Budapest-Missoula Model

Below are presented the equations of the MBM model. Where the reactions are reversible the use of $\rightleftharpoons$ or $\rightleftharpoons$ as opposed to $\rightleftharpoons$ denotes that the difference between the forward and reverse rate constants spans more than 3 orders of magnitude in the corresponding direction. Note that the reactions are divided into the following subsystems: inorganic reactions (R1 - R10), reactions in the BrMA subsystem (R11 - R26) and reactions in the MA subsystem (R27 - R48).

The following abbreviations are used:

(Br)MA = (Bromo)malonic acid

(Br)TA = (Bromo)tartronic acid

OA = Oxalic acid

MOA = Mesoxalic acid

ETA = Ethanetetracarboxylic acid

EETA = Ethenetetracarboxylic acid

BrEETRA = Bromoethenetricarboxylic acid

EEHTRA = ethenehydroxytricarboxylic acid

Reaction Number	**Reaction**
R1	$Br^- + HOBr + H^+ \rightleftharpoons Br_2 + H_2O$
R2	$Br^- + HBrO_2 + H^+ \rightleftharpoons 2\,HOBr$
R3	$Br^- + {BrO_3}^- + 2\,H^+ \rightleftharpoons HOBr + HBrO_2$
R4	$HBrO_2 + H^+ \rightleftharpoons {H_2BrO_2}^+$
R5	$HBrO_2 + {H_2BrO_2}^+ \longrightarrow HOBr + {BrO_3}^- + 2\,H^+$
R6	$HBrO_2 + {BrO_3}^- + H^+ \rightleftharpoons Br_2O_4 + H_2O$
R7	$Br_2O_4 \rightleftharpoons 2\,{BrO_2}^\bullet$
R8	$Ce(III) + {BrO_2}^\bullet + H^+ \rightleftharpoons Ce(IV) + HBrO_2$
R9	$2\,{BrO_3}^- + 2\,H^+ \longrightarrow 2\,HBrO_2 + O_2\uparrow$
R10	${BrO_2}^\bullet \longrightarrow \frac{1}{2}Br_2 + O_2\uparrow$
R11	$BrMA + Ce(IV) \rightleftharpoons {BrMA}^\bullet + Ce(III) + H^+$
R12	$2\,{BrMA}^\bullet \longrightarrow BrEETRA + Br^- + H^+ + CO_2\uparrow$
R13	$BrMA \rightleftharpoons BrMA\,(enol)$
R14	$BrMA\,(enol) + Br_2 \longrightarrow Br_2MA + Br^- + H^+$
R15	$BrMA\,(enol) + HOBr \longrightarrow Br_2MA + H_2O$
R16	${BrMA}^\bullet + {BrO_2}^\bullet \longrightarrow BrMABrO_2$
R17	$BrMABrO_2 \longrightarrow OA + HOBr + Br^- + H^+ + CO_2\uparrow$
R18	$BrMABrO_2 \longrightarrow BrTA + HBrO_2$
R19	$BrTA \longrightarrow Br^- + MOA + H^+$
R20	$MOA + Ce(IV) + H_2O \longrightarrow OA + Ce(III) + {COOH}^\bullet + H^+$
R21	$OA + Ce(IV) \longrightarrow {COOH}^\bullet + Ce(III) + H^+ + CO_2\uparrow$
R22	$2\,{COOH}^\bullet \longrightarrow OA$
R23	${COOH}^\bullet + Ce(IV) \longrightarrow Ce(III) + H^+ + CO_2\uparrow$
R24	${COOH}^\bullet + BrMA \longrightarrow {MA}^\bullet + Br^- + H^+ + CO_2\uparrow$
R25	${COOH}^\bullet + {BrMA}^\bullet \longrightarrow BrMA + CO_2\uparrow$
R26	${COOH}^\bullet + {BrO_2}^\bullet \longrightarrow HBrO_2 + CO_2\uparrow$

R27	$MA + Ce(IV) \rightleftharpoons MA^{\bullet} + Ce(III) + H^{+}$
R28	$2\,MA^{\bullet} \longrightarrow ETA$
R29	$MA \rightleftharpoons MA\,(enol)$
R30	$MA\,(enol) + Br_2 \longrightarrow BrMA + Br^{-} + H^{+}$
R31	$MA\,(enol) + HOBr \longrightarrow BrMA + H_2O$
R32	$MA^{\bullet} + BrO_2^{\bullet} \longrightarrow MABrO_2$
R33	$MABrO_2 \longrightarrow MOA + HOBr$
R34	$MABrO_2 \longrightarrow TA + HBrO_2$
R35	$MA^{\bullet} + BrMA^{\bullet} \longrightarrow Br^{-} + EETA + H^{+}$
R36	$MA^{\bullet} + COOH^{\bullet} \longrightarrow MA + CO_2\uparrow$
R37	$TA + Ce(IV) \rightleftharpoons TA^{\bullet} + Ce(III) + H^{+}$
R38	$2\,TA^{\bullet} \longrightarrow EEHTRA + H_2O + CO_2\uparrow$
R39	$TA \rightleftharpoons TA\,(enol)$
R40	$TA\,(enol) + Br_2 \longrightarrow BrTA + Br^{-} + H^{+}$
R41	$TA\,(enol) + HOBr \longrightarrow BrTA + H_2O$
R42	$TA^{\bullet} + MA^{\bullet} \longrightarrow EETA + H_2O$
R43	$TA^{\bullet} + BrMA^{\bullet} \longrightarrow BrEETRA + H_2O + CO_2\uparrow$
R44	$TA^{\bullet} + COOH^{\bullet} \longrightarrow TA + CO_2\uparrow$
R45	$TA^{\bullet} + BrO_2^{\bullet} \longrightarrow TABrO_2$
R46	$TABrO_2 \longrightarrow MOA + HBrO_2$
R47	$TA + BrO_3^{-} \longrightarrow HBrO_2 + MOA$
R48	$MA^{\bullet} + BrO_3^{-} + H^{+} \longrightarrow BrO_2^{\bullet} + TA$

Table E.1

Appendix F

Rate Constant Optimisation Results

Contained in this appendix are the results of the grey wolf optimiser experiments. These show how far the rate constants produced by the optimisation algorithm differed from the literature value for the cerium(IV)-catalysed Belousov-Zhabotinsky reaction according to Hegedűs *et al.*. Experiments were undertaken for three optimisation ranges and are reported in the table below as such from left to right: $k \pm 0.1k$, $k \pm 0.5k$ and $k \pm k$.

k	Literature value	Optimised	% Difference	Optimised	% Difference	Optimised	% Difference
R1.f	8000000000	7865489625	-1.68137969	8905537070	11.3192134	1633534062	-79.580824
R1.b	110	100.2905715	-8.826753221	59.46353798	-45.942238	79.91064034	-27.353963
R2.f	2900000	3021449.974	4.187930125	2341076.577	-19.273221	2.54E+05	-91.243958
R2.b	2.00E-05	2.09E-05	4.452702381	1.94E-05	-2.7624836	3.21E-05	60.7013867
R3.f	0.6	0.587160049	-2.139991789	0.570082497	-4.9862505	0.7387248	23.1207999
R3.b	3.2	3.496588178	9.268380556	4.251031545	32.8447358	1.728040106	-45.998747
R4.f	2000000	2034590.403	1.729520128	1659564.586	-17.021771	3751349.946	87.5674973
R4.b	100000000	90929666.67	-9.070333325	128238704.9	28.2387049	52641213.11	-47.358787
R5.f	170000	157367.3147	-7.430991342	95139.74552	-44.035444	57332.79663	-66.274826
R6.f	48	52.8	10	35.32112375	-26.414326	24.972211	-47.97456
R6.b	3200	3143.291957	-1.772126347	3481.079693	8.78374039	4479.215162	39.9754738
R7.f	75000	71665.80846	-4.44558872	87393.08463	16.5241128	41052.66862	-45.263109
R7.b	1400000000	1347487348	-3.750903688	1504153557	7.43953978	1050291012	-24.979213
R8.f	60000	60621.58021	1.035967012	32636.93886	-45.605102	108173.999	80.2899983

R8.b	13000	13127.42202	0.980169378	8674.679131	-33.271699	13701.40784	5.39544493
R9.f	6.00E-10	6.11E-10	1.915435638	3.00E-10	-50	1.03E-09	71.1086558
R10.f	0.06	0.057677507	-3.870822203	0.07701684	28.3614006	0.044530749	-25.782085
R11.f	0.1	0.096084612	-3.915387646	0.06246374	-37.53626	0.029654455	-70.345545
R11.b	400	392.5164663	-1.87088342	579.2059384	44.8014846	532.9327999	33.2332
R12.f	1000000000	927875286.7	-7.212471326	695353701.1	-30.46463	828387781.8	-17.161222
R13.f	0.012	0.011737648	-2.186262619	0.012228409	1.9034051	0.011613721	-3.2189926
R13.b	800	797.2228049	-0.347149393	668.6244809	-16.42194	32.24783431	-95.969021
R14.f	3500000	3481679.055	-0.523455559	4565025.776	30.4293079	1103969.371	-68.458018
R15.f	1100000	1210000	10	666791.408	-39.382599	1024961.782	-6.8216562
R16.f	2000000000	2103300999	5.165049934	3000000000	50	1857497503	-7.1251248
R17.f	0.62	0.58673793	-5.364849931	0.812928531	31.1175051	1.175184382	89.5458681
R18.f	0.46	0.447438264	-2.730812264	0.434645516	-5.5118444	0.803495534	74.6729422
R19.f	1.5	1.620071416	8.004761056	1.026130956	-31.59127	1.932693869	28.8462579
R20.f	7000	7241.064398	3.443777118	5997.308699	-14.324161	3818.806868	-45.445616
R21.f	28	26.93199307	-3.814310463	28.91264621	3.25945075	35.30995057	26.1069663
R22.f	5000000000	4767285837	-4.654283261	6139265742	22.7853148	469998911.6	-90.600022

R23.f	10000000	10580472.86	5.804728585	13635240.26	36.3524026	3484963.988	-65.15036
R24.f	10000000	9439189.396	-5.608106045	5000000	-50	2206417.163	-77.935828
R25.f	3000000000	3162782266	5.426075537	1601110780	-46.629641	4648334250	54.944475
R26.f	5000000000	4746235358	-5.075292839	2699009142	-46.019817	1664734066	-66.705319
R27.f	0.23	0.230339543	0.147627555	0.28045499	21.9369521	0.231194907	0.51952475
R27.b	22000	21440.65664	-2.542469803	23571.60473	7.14365786	819.1820877	-96.276445
R28.f	3200000000	3254169471	1.692795966	2239965076	-30.001091	4541870237	41.9334449
R29.f	0.0026	0.002413951	-7.155747051	0.002851236	9.66291171	0.003336776	28.3375267
R29.b	180	166.6264429	-7.429753949	231.8594078	28.8107821	110.4564875	-38.635285
R30.f	2000000	2171186.689	8.559334437	2340574.586	17.0287293	650644.805	-67.46776
R31.f	670000	705141.9749	5.245070881	600898.2534	-10.313694	63076.79256	-90.585553
R32.f	5000000000	5175507827	3.510156532	3605698801	-27.886024	1276179029	-74.476419
R33.f	0.55	0.605	10	0.428660211	-22.06178	0.474247741	-13.773138
R34.f	1	1.093693194	9.369319388	0.584393581	-41.560642	0.946024072	-5.3975928
R35.f	2000000000	2073829687	3.691484366	1347486232	-32.625688	0	-100
R36.f	4000000000	3851396930	-3.715076753	2101355514	-47.466112	99247641.24	-97.518809
R37.f	0.66	0.658716539	-0.194463808	0.447539019	-32.191058	0.080102602	-87.863242

R37.b	17000	17353.46872	2.079227763	22309.45225	31.2320721	12366.66317	-27.254923
R38.f	1000000000	1031653741	3.165374149	965704413.7	-3.4295586	412742121.9	-58.725788
R39.f	2.30E-05	2.30E-05	0.116762444	1.26E-05	-45.17599	2.45E-05	6.44362292
R39.b	1.5	1.550342433	3.356162208	1.794795309	19.6530206	0.876799275	-41.546715
R40.f	300000	284098.1228	-5.300625721	407621.2723	35.8737574	505845.5025	68.6151675
R41.f	200000	209374.7298	4.68736489	166046.7584	-16.976621	242023.9667	21.0119833
R42.f	1000000000	1096052845	9.605284456	1414021085	41.4021085	184691377.2	-81.530862
R43.f	1000000000	951003334.3	-4.899666567	803962697.7	-19.60373	464572100.5	-53.54279
R44.f	3000000000	3112255775	3.741859164	1583056324	-47.231456	997855136	-66.738162
R45.f	2000000000	2056078428	2.803921393	1108829484	-44.558526	81270600.56	-95.93647
R46.f	0.1	0.096811358	-3.188641618	0.11897239	18.9723903	0.059147725	-40.852275
R47.f	5.00E-05	4.58E-05	-8.373404348	2.59E-05	-48.174612	1.64E-05	-67.254684
R48.f	160	176	10	95.97121093	-40.017993	213.7809908	33.6131193